2011-12-13

Modeling Solid Propellant Ignition Events

Daniel A. Smyth
Brigham Young University - Provo

MODELING SOLID PROPELLANT IGNITION EVENTS

Daniel Austin Smyth

A dissertation submitted to the faculty of
Brigham Young University
in partial fulfillment of the requirements for the degree of

Doctor of Philosophy

David O. Lignell, Chair
Merril W. Beckstead
Thomas H. Fletcher
Larry L. Baxter
William C. Hecker
William G. Pitt

Department of Chemical Engineering

Brigham Young University

December 2011

ABSTRACT

Modeling Solid Propellant Ignition Events

Daniel Austin Smyth
Department of Chemical Engineering, BYU
Doctor of Philosophy

This dissertation documents the building of computational propellant/ingredient models toward predicting AP/HTPB/Al cookoff events. Two computer codes were used to complete this work; a steady-state code and a transient ignition code.

Numerous levels of verification resulted in a robust set of codes to which several propellant/ingredient models were applied. To validate the final cookoff predictions, several levels of validation were completed, including the comparison of model predictions to experimental data for: AP steady-state combustion, fine-AP/HTPB steady-state combustion, AP laser ignition, fine-AP/HTPB laser ignition, AP/HTPB/Al ignition, and AP/HTPB/Al cookoff.

A previous AP steady-state model was updated, and then a new AP steady-state model was developed, to predict steady-state combustion. Burning rate, temperature sensitivity, surface temperature, melt-layer thickness, surface species at low pressure and high initial temperature, final flame temperature, final species fractions, and laser-augmented burning rate were all predicted accurately by the new model. AP ignition predictions gave accurate times to ignition for the limited experimental data available.

A previous fine-AP/HTPB steady-state model was improved to predict a melt layer consistent with observation and avoid numerical divergence in the ignition code. The current fine-AP/HTPB model predicts burning rate, surface temperature, final flame temperature, and final species fractions for several different propellant formulations with decent success. Results indicate that the modeled condensed-phase decomposition should be exothermic, instead of endothermic, as currently formulated. Changing the model in this way would allow for accurate predictions of temperature sensitivity, laser-augmented burning rate, and surface temperature trends. AP/HTPB ignition predictions bounded the data across a wide range of heat fluxes.

The AP/HTPB/Al model was based upon the kinetics of the AP/HTPB model, with the inclusion of aluminum being inert in both the solid and gas phases. AP/HTPB/Al ignition predictions bound the data for all but one source. AP/HTPB/Al cookoff predictions were accurate when compared to the limited data, being slightly low (shorter time) in general. Comparisons of AP/HTPB/Al ignition and cookoff data showed that the experimental data might be igniting earlier than expected.

Keywords: Daniel Austin Smyth, solid propellant, model, steady state, combustion, ammonium perchlorate, AP, hydroxy-terminated poly-butadiene, HTPB, aluminum, ignition, cookoff

ACKNOWLEDGMENTS

It's difficult to look back on such a long period of time and try to remember just how many influences I've had during this time of my life. Major players will be easy to recall, while others will likely be forgotten. It took me a long time to finally decide to even write this page (it's optional after all) because I didn't want to forget anyone that had helped me. In the end, I've decided that this is literally an impossible task. Still, I'm going to try my best at getting everyone and everything down here. I'll more than likely fail, but I guess it's the attempt that counts.

First, I think I need to thank my adviser and teacher during these last nine years: Dr. Merrill Beckstead. I have no idea why he decided to even take me on as a graduate student in the first place. Maybe he didn't have a choice. I'm sure there have been times along the way that he's wished he hadn't been given that last graduate student; that he'd been able to finish his illustrious career on the high note of my predecessors and not have to deal with the frustration of the kid that just wouldn't take anything for granted. I've learned a lot from him and always tried to take everything that I could from what he taught and apply it in a way that made sense to me. I know our conclusions didn't always agree. I guess that's part of science though: looking at everything we can and then making a determination from what we've seen. Regardless of the outcome, I know that I'd never have been able to stand a chance at accomplishing the things I did during this period of research without the knowledge and understanding that came from him on a regular basis.

Second I need to thank my current adviser on this end of things, Dr. David Lignell. I don't think it's too far of a long shot to say that I wouldn't have been able to finish my research had it not been for him. After Dr. Beckstead's retirement, Dr. Lignell got up and swung for me

when it seemed like no one else wanted to. He's not only given me the chance to finish the job I set out to do, but helped to widen my view of combustion and simulation modeling as a whole.

Third goes to Dr. Tom Fletcher. He's the one that helped me to even earn the right to be accepted to graduate school. He helped me to find a way to do what I wanted to do: to learn enough that I could be a go-to person when asking difficult technical questions. The lessons that I've leared during graduate school have made that possible. I wouldn't have even been able to get my foot in the door without him.

Fourth, though first in matters pertaining to the heart, I need to thank my wife and the unending support that she's given me. Long hours away and longer nights alone have seemed to be the norm for us, not only during these years of graduate school, but also during my undergraduate years when I was trying to learn everything I could in the time that I had available to me. I can never thank her enough for her patience and love and understanding; for her support of me and the goals and dreams that I had during this time. I will forever be grateful to her and to my three kids—Kaylee, Parker and Brenna—that prayed continually for my safety, health, and success. It's literally impossible to get too far down on life and its hardships when you have such a wonderful family to come home to every night.

I'm thankful for my office mates and fellow partners in "research" crime: Karl Meredith, Ephraim Washburn, Scott Felt, Matt Gross, Matt Tanner, Karthik Pudduppakkam, Mike Hawkins, Johnathan Wierschke, Liz Monson, Derek Harris, and Guangyuan Sun. Countless hours of brainstorming and trouble-shooting and debugging were spent in their company. Many ah-ha moments and critical developments came as a result of their friendship. Jed Campbell passed along a critical piece of advice to me (several times over several years) concerning

Designs of Experiment, and I can't thank him enough for continuing to bother me until I gave in and just did it. That's a lesson that I won't soon forget.

Many others provided non-technical and moral support during the tough times. My parents and other family members played a very important role in keeping my spirits high. Friends from my community and those from church. Friends from home, like Jeremy Brown, who was always there to share and brighten my day and help me remember who I was. My thanks go to all of them, but most importantly to Laren Robison, who never gave up on me and was, even until the week before he passed away, telling me to keep fighting because I was going to make it. The most difficult thing I ever did in graduate school was not quit, and it was people like Laren that helped me make it all the way here.

Lastly I need to thank my Heavenly Father and his son, Jesus Christ, for making me the person that I am—for teaching me and guiding me down life's path in such a way that I could learn those things that make me me. The strength and perspective that I've gained from keeping them within my world-view has made everything worthwhile.

TABLE OF CONTENTS

LIST OF FIGURES

LIST OF TABLES

NOMENCLATURE

ROMAN

A – area, rate constant pre-exponential

AF – area fraction

C – heat capacity

E – energy

H – enthalpy, heat

K – absorption parameter

P – pressure

Q – heat

R – universal gas constant

T – temperature

V – diffusion velocity

W – molecular weight

X – Cartesian dimension

Y – species mass fraction

b – rate equation constant

c – specific heat capacity

d – diameter

h – specific enthalpy

m – mass burning

n – rate equation pressure exponent

q – heat

r – rate, radial distance

t – time

u – velocity

x – Cartesian distance

GREEK

ρ – density

λ – thermal conductivity

τ – temperature gradient

ω – specific reaction

φ—fraction (void or solid)

μ – viscosity

Φ – conserved quantity

π – Pi

SUBSCRIPTS

Al – aluminum

CM – continuous medium

a – activation

abs – absorb

b – burning

c – cross section, condensed phase

eff – effective

f – formation

g – gas

init – initial conditions

l – liquid

p – constant pressure

rxn – reaction

s – solid, sphere

tr – transition

SUPERSCRIPTS

$\overline{\quad}$ – average

$\dot{}$ – rate

$'''$ – volumetric

The man who does not read good books has no advantage over the man who can't read them.
-- Mark Twain

CHAPTER 1: INTRODUCTION

In 1996, the federal government signed a treaty to prohibit the testing of nuclear weapons. This led scientists and researchers to turn to computer simulation for testing large-scale weapons and bombs. In an effort to encourage research in this area, the United States Department of Energy created the Accelerated Strategic Computing Initiative (ASCI) program. Within this program, the Center for the Simulation of Accidental Fires and Explosions (C-SAFE) was formed at the University of Utah. C-SAFE's goal was to provide state-of-the-art, science-based tools for the numerical modeling of fires and explosions within the realm of highly flammable materials. One of the specific problems included the transient response of a high explosive (HE) confined within a heated container. The response of this system is referred to as a cookoff event. Cookoff systems are defined as being "slow" or "fast" dependent upon the level of heat applied to them.

Slow cookoff occurs when the container and HE warm slowly (3-4 K/hr[1]). Heat fluxes are small and frequently result in the entire system rising slowly and essentially uniformly in temperature. Ignition in these systems usually occurs in the solid phase after hours or days. At ignition, most of the HE reacts due to its elevated temperature and resultant high chemical reactivity. Thus, slow-cookoff explosion events are very violent and frequently transition to detonation.

Fast cookoff occurs when the container and HE are heated at a relatively rapid rate (100 K/hr[1]). The container, which is usually metal, transfers the heat to the propellant quickly due its high thermal conductivity. Typical values of thermal conductivity for HE materials are much lower, and thus heat transfer slows considerably at the surface of the HE material. This results in a fast temperature rise near the surface of the HE, and thus increased level of reactivity within only a thin outer layer of the HE. Fast-cookoff ignition events typically occur in the gas phase within minutes. Since only a small layer of HE is thermally active at the point of ignition, these events are much less violent than slow cookoff and result instead in the simple mechanical failure of the container. Transition to detonation is still possible, as determined by the level of confinement provided by the container.

The HE material used for C-SAFE experiments and modeling was PBX, which is 95% HMX and 5% mixed binder. The experiments use cylindrical HMX samples placed in capped metal containers with potentially significant but unknown contact resistances between the HMX and container. A fast-cookoff system, similar to that of the C-SAFE experiments, is simplistically displayed in Figure 1, as suggested by Raun *et al.*[2].

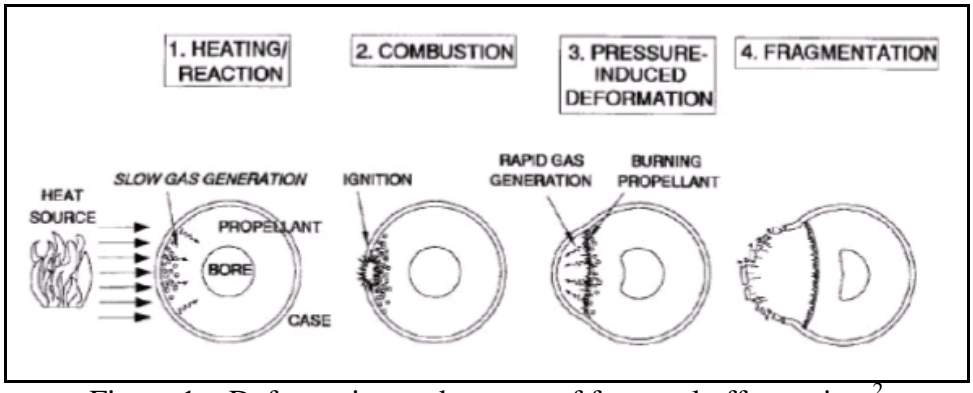

Figure 1 – Deformation and rupture of fast-cookoff container[2]

There are four main stages in the fast-cookoff scenario. The first includes an initial heat up period, during which the HE is thermally stable. The second phase occurs when the HE reaches a temperature at which it begins to decompose appreciably and fill the container's void space with decomposed gases. The third phase begins once the outer surface of the HE reaches a sufficiently high temperature that it begins to melt, evaporate (if applicable), and react more vigorously. The fourth and final phase occurs when the contained gases begin to react to a significant degree, prompting a sharp ignition event. Ignition causes the container pressure to increase rapidly until the container bursts from the resulting strain.

The fast cookoff system was studied and modeled by Meredith and Beckstead[3] as part of the C-SAFE work. Their model predicted time to ignition for HMX very well as it varies with applied heat flux. Further investigation needed to be conducted, however, as their model was only applied to a single ingredient. A typical propellant of interest to the fast-cookoff environment is the mixture of ammonium perchlorate and hydroxyl-terminated polybutadiene binder, (AP/HTPB), both with and without an aluminum additive. These types of propellants are used extensively in missiles, rockets, and explosives.

AP/HTPB composite propellants, instead of being milled and then inserted into a container, are usually poured into the container while at a slightly elevated temperature. The propellant then cools and sets. This process results in good thermal contact between the propellant and outer casing. Systems using these types of propellants have fewer gaps between the propellant and casing than present in an HMX cookoff system. The thermal expansion of the metal container is much greater than either propellant however, and this results in similar voids within both systems.

The development of accurate propellant cookoff models can come only through validation of their predictions against experimental data. It is often the case that there is little cookoff data to compare model predictions against due to the expense of large-scale experimentation. A cookoff model should optimally be general enough that it accurately predicts data from experiments conducted under various conditions, such as steady-state combustion and laser-driven ignition events, and cookoff events.

The ultimate goal of the current work was to predict accurately the time to ignition for cookoff events associated with test articles containing an AP/HTPB/Al propellant. To accomplish this goal, the task of verifying the two codes used to make these calculations and validating several propellant models used within those codes was of primary interest. To accomplish this, each component piece of the codes and models was tested and improved, where necessary. Steady-state combustion played a foundational role for predicting laser-driven ignition events, which in turn played a foundational role for predicting cookoff events. Since there were considerable amounts of data found for AP deflagration, the AP model was first validated so that it could play a foundational role for the AP/HTPB model, which in turn played a foundational role for the AP/HTPB/Al model. Each piece of this work built upon that which had come before, in the hopes that the final simulations, for which little experimental data were available, might be as accurate as possible.

This dissertation first addresses the work that has been previously accomplished in pertinent research areas through a literature review in Chapter 2. Chapter 3 outlines the specific objectives of this work. Chapter 4 presents the work involved in verifying and validating the steady-state propellant/ingredient models and computer codes of interest, including the comparison of past and current steady-state propellant/ingredient models to pertinent data, and

will also present HMX ignition results from the updated ignition code. Chapter 5 contains the ignition and cookoff results for each of the propellants/ingredients of interest: AP, AP/HTPB, and AP/HTPB/Al. Modeling simulations will be compared to available experimental data. Chapter 6 contains summaries of this work and suggests possible directions for future research.

Get your facts first, and then you can distort 'em as much as you please.
-- Mark Twain

CHAPTER 2: HISTORICAL PERSPECTIVE

Although extremely useful, solid propellants are quite destructive if not handled very carefully. As such, a large amount of work has been directed toward trying to understand how these materials behave in general, as well as within particular systems of interest. The concepts and propellant ingredients that are of greatest importance to this work are discussed in this chapter.

2.1 STEADY-STATE PROPELLANT/INGREDIENT MODELING

Steady-state combustion involves a large majority of the most important processes that occur during transient combustion. Steady-state experimental and theoretical results relevant to the current work appear in this section.

A general description of monopropellant combustion[4] (not drawn to scale) is depicted in Figure 2 that includes the three regions of interest described by models: the unreactive solid phase, the reactive foam-layer, and the gas phase.

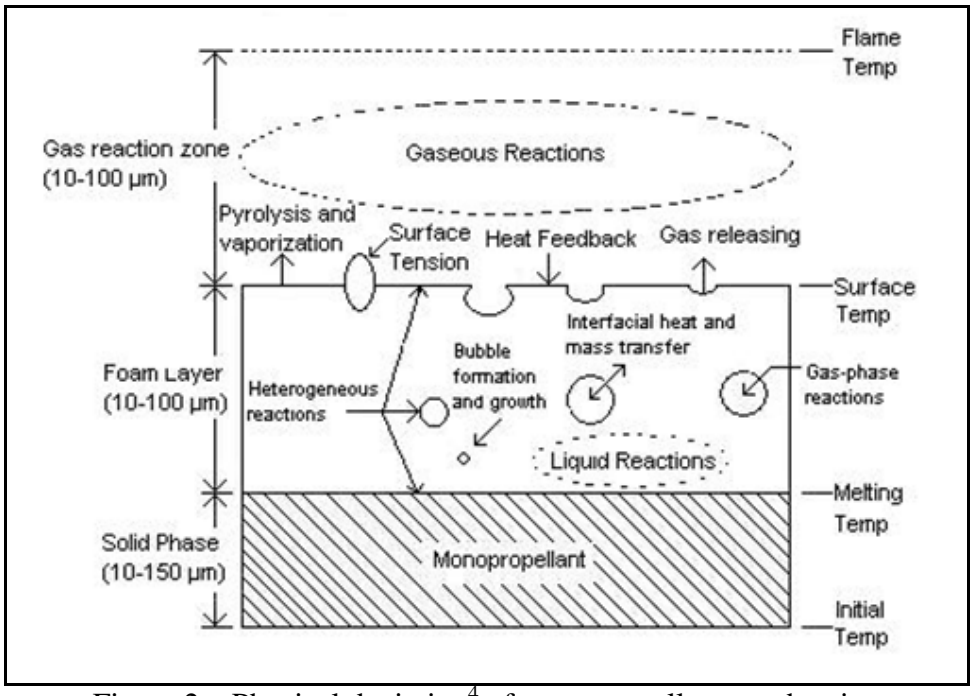

Figure 2 – Physical depiction[4] of monopropellant combustion

The solid phase includes the pristine, unreacted material. As the temperature rises from the initial temperature to the melting temperature, decomposition reactions are typically assumed to be negligible in this region.

The second region consists of a foamy layer and is frequently referred to as the "condensed phase". This zone typically extends from the location of the melting point to the surface and contains an intermixed liquid and gas phase. Decomposing gases are trapped as bubbles within the liquid that grow in size due to decomposition, and possibly evaporation. There are frequently complicated mechanisms of heat transfer, bubble growth, and bubble velocity that occur as part of this process. Additionally, there are some propellants/ingredients that contain a liquid-in-gas layer (droplets entrained by extant gases) as observed by Hanson-Parr and Parr for HMX[5]. This can sometimes lead to difficulties in describing the actual "burning surface" or "surface temperature" of a model within a numerical code. Typically, it is assumed

that there are no gas-phase reactions that occur within the condensed phase, although gas-phase "bubble reactions" will infrequently be included as part of a condensed-phase description[6,7]. Reactions within the condensed phase are typically considered to be global or semi-global in nature, as we know very little of what is actually happening in this region. Modern condensed-phase reaction mechanisms contain relatively few reactions (on the order of ten, but sometimes as few as one) and involve similar numbers of species[6-8].

In the gas phase region, the species evolved by the decomposing condensed phase react toward final products and a final flame temperature while interacting with the condensed phase through the following mechanisms:

1) the evolution rate of decomposed species from the condensed phase,;
2) the temperature of gases leaving the condensed phase;
3) conductively heating the surface of the condensed phase to due flame proximity.

Modern reaction mechanisms used to describe gas-phase chemistry contain tens to hundreds of species and involve hundreds of reactions[9].

Early combustion models for propellants/ingredients were global in nature and only contained rudimentary descriptions of kinetic processes. These models relied mostly on the solution of the energy equation and were solved in a single dimension. Results from these models showed that simply matching burning rate predictions to data was not enough to validate a given model. An example of these early global models[10-13] that describes the combustion of various propellants/ingredients was the BDP model[14], which presented equations for solving the thermal development of a combusting material. This model proposed that there is a limited amount of energy available to the system with known beginning (initial) and ending (equilibrium) conditions. The evolution of heat within the model could be described in a variety of ways—with endothermic condensed phases followed by exothermic gas phases, or exothermic

condensed phases followed by exothermic gas phases—with the possible models being able to accurately predict burning rate data regardless of the balance between the two. The important restriction in determining the evolution of heat was that the initial and final conditions be correct. More rigorous predictions of temperature sensitivity (change in burning rate for a propellant/ingredient with a higher initial temperature—defined in Appendix A) and laser-augmented burning rate can validate this kind of model to a greater extent, giving more confidence in their accuracy. It is these predictions that require a more accurate description of how a propellant/ingredient responds to a given application of heat. Understanding these phenomena is the driving force for making these models more closely approximate reality.

As the science of modeling continued to develop and computing power multiplied, complex gas-phase descriptions were coupled to simple condensed-phase models to try and describe the combustion process of propellants/ingredients in greater detail. For these detailed models, comparisons have been made between model predictions[15] and observed temperature and species profiles above the burning surface. In making such improvements, it became additionally important to match equilibrium species fractions as part of the final model conditions.

The BYU steady-state propellant/ingredient models were developed through the use of the Phase3[16] computer program, which is named after the three regions of such a model illustrated in Figure 2. The most recent version of a gas-phase reaction mechanism for modeling a large set of monopropellants and homogenous mixtures was developed at BYU by Puduppakkam[15] (for HMX[8,16], RDX[16], GAP[15], BTTN[15]) and later expanded by Gross (to include AP and ADN[17]). It contained 106 species and 611 reactions and is referred to as BYU's "universal" mechanism. The number of species involved in a gas-phase mechanism, which

affects the number of conservation equations in the solution process, and the non-linearity of those reactions will typically dictate the length of time required for calculation. As such, robust numerical techniques have been used within Phase3 to quickly and accurately solve the necessary system of conservation equations. Phase3 uses a modified version of PREMIX[18] in the burner-stabilized mode for the gas phase solution and a modified version of DVODE[19] for the condensed phase.

In the solid-phase region of Phase3, the heat equation is included by implication, according to Equation 1, and not included as part of the simulation calculations.

$$\rho_s c_p r_b \frac{\partial T}{\partial x} - \lambda_s \frac{\partial^2 T}{\partial x^2} = 0 \tag{1}$$

The liquid-gas foamy region includes the solution of the temperature, void fraction, and species equations, while satisfying continuity through the assumptions that,

1) the momentum of the liquid is equal to the momentum of the gas ($\rho_g u_g = \rho_l u_l$);
2) the temperature of the gas and liquid within a discretized distance are equivalent;
3) the velocity of the liquid, u_l, is equal to the burning rate of the propellant.

The equations describing the condensed-phase region comprise Equations 2 through 6.

$$\frac{\partial}{\partial x}\left(\lambda A_c \tau\right) = \dot{m}\overline{C_p}\tau + A_c \sum_{k=1}^{NumSpec} \dot{\omega}_k H_k \tag{2}$$

$$\frac{\partial T}{\partial x} = \tau \tag{3}$$

$$\frac{\partial\left(1-\phi\right)}{\partial x} = \frac{1}{\rho_l u_l} \sum_{k=1}^{NumLiqSpec} \dot{\omega}_k \tag{4}$$

$$\frac{\partial}{\partial x}\left[\left(1-\phi\right)\rho_l u_l Y_{l,k}\right] = \dot{\omega}_k \ , k = 1...NumSpec \tag{5}$$

$$\frac{\partial}{\partial x}\left[\phi\rho_g u_g Y_{g,k}\right] = \dot{\omega}_k \ , k = 1...NumSpec \tag{6}$$

The second-order temperature equation has been split into two first-order equations for ease of solution. The void fraction is calculated based on the global condensed-phase decomposition reaction(s), and the gas and liquid species are solved separately. (i.e.: all gas-phase species in the condensed phase sum to one, and all condensed-phase species sum to one.)

The equations describing the gas phase are given by Equations 7 through 10.

$$\dot{m} = \rho A_c u \tag{7}$$

$$\rho = \frac{P\overline{W}}{RT} \tag{8}$$

$$\dot{m}\frac{\partial T}{\partial x} - \frac{1}{\overline{C_p}}\frac{\partial}{\partial x}\left(\lambda A_c \frac{\partial T}{\partial x}\right) + \frac{A_c}{\overline{C_p}}\sum_{k=1}^{NumSpec}\rho Y_k V_k C_{p,k}\frac{\partial T}{\partial x} + \frac{A_c}{\overline{C_p}}\sum_{k=1}^{NumSpec}\dot{\omega}_k h_k W_k = 0 \tag{9}$$

$$\dot{m}\frac{\partial Y_k}{\partial x} + \frac{\partial}{\partial x}\left(\rho A_c Y_k V_k\right) - A_c\dot{\omega}_k W_k = 0 \ , k = 1...NumSpec \tag{10}$$

2.1.1 Ammonium Perchlorate

Ammonium perchlorate (NH_4ClO_4 or AP) is the most widely used propellant ingredient in current production. It has been used for decades in applications ranging from the large space shuttle booster to relatively small fighter-jet missiles. AP exhibits some of the most interesting and complicated decomposition characteristics seen within the entire family of traditional propellant ingredients.

At ambient conditions, AP is a crystalline salt with an orthorhombic structure that changes to cubic at 513 K. It is a stable compound and can be grown into large crystals that are centimeters in size or crushed and ground into particles that are microns in size. When AP deflagrates, the resulting gases are very rich in oxygen (~30% O_2, final products), and thus it is

typically mixed with very fuel-rich binders, resulting in excellent propellants. Additionally, varying the size of AP particles within a propellant allows a unique method of control over the propellant burning rate. Propellants formulated with fine AP burn more quickly, while those that include coarse AP burn more slowly.

Years of study and research have been focused toward trying to understand the details of AP decomposition and deflagration both as a monopropellant and when it's contained within a matrix of heterogeneous propellant.

2.1.1.1 LOW-TEMPERATURE DECOMPOSITION

At relatively low temperature, samples of AP undergo partial decomposition, a phenomenon that is unique to this ingredient. In these experiments, AP crystals are heated at either a very low rate or in an oven of constant temperature, typically ranging from 480 to 600 K. Approximately 30% of every sample will decompose, at which time the decomposition rate slows considerably. Vyazovkin and Wight[20] have published a review of twenty different studies of this phenomenon. The works included were conducted at low pressures (from vacuum to atmospheric) and over a wide range of temperatures (from 475 to 750 K) using a variety of data collection techniques. Decomposition ranged from 30% to 100% and activation energies from 70 to 260 kJ/mol were reported. The temperature range included the solid-phase temperature transition at 513 K, and therefore the data included the orthorhombic phase, the cubic phase, and partially-decomposed variants of each.

Numerous other publications have tried to determine the decomposition pathways of AP and the activation energies of these processes[21-25] with similar results and significant data scatter. The trends that have been observed suggest that the decomposition of both orthorhombic and

cubic AP initially proceed from pristine conditions to a state of partial decomposition (~30%), at which time the rate drops appreciably but continues to completion.

Small-diameter AP particles have also been shown, however, to have partial decomposition values that are significantly less than the ~30% observed in large crystals. Beherens and Minier[24] collected decomposition data at 0.3 psi, reporting 25% partial decomposition for 200 micron particles and 13% for 20 micron particles. Kraeutle *et al.*[26] also saw this phenomenon to a limited extent in their work. Although no direct relationship between AP particle size and extent of decomposition was given by Kraeutle, it was noted that under some conditions samples of ground AP would decompose in the range of 25-35% before slowing, and that AP ground to 3 microns didn't decompose to any appreciable extent. It is not understood why this occurs, but it does seem as if there is some kind of limiting phenomenon that leads to the gradual disappearance of the low-temperature decomposition pathway as AP crystal size decreases and the level of decomposition approaches ~30%.

2.1.1.2 STEADY-STATE WORK

Ammonium perchlorate can self-deflagrate above pressures of ~18 atm (300 psi). Below this pressure, AP will not burn without assistance of some sort, be that through the addition of heat, a kinetic catalyst, or additional fuel source. This pressure-deflagration limit (PDL) varies with initial temperature as noted by Watt and Peterson[27]. At pressures higher than the PDL, AP exhibits some very non-linear burning behavior, which has been divided into four suggested pressure zones by Boggs[28], as shown in Figure 3 alongside data from Atwood *et al.*[29].

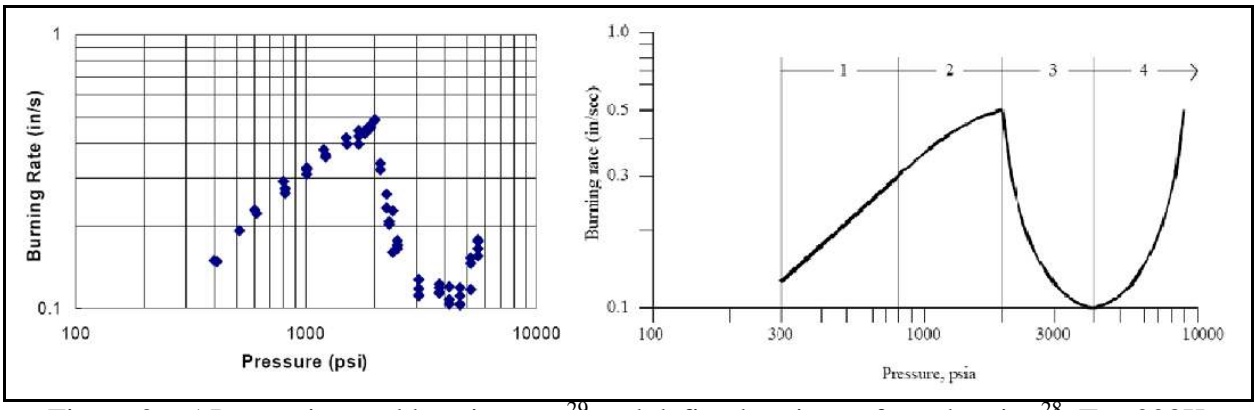

Figure 3 – AP experimental burning rate[29] and defined regions of combustion[28], T_{init} 298K

The first region, which begins at the PDL and continues to ~54 atm (800 psi), can be described by a simple burning rate relationship, $r_b \sim bP^n$, where P is the pressure of the system and b and n are fitting parameters. Examination of the condensed phase from samples quenched at steady-state burning in this pressure region (using techniques such as SEM) shows three distinct structures of AP: the original orthorhombic crystal at the base of the sample, a layer of unreacted cubic AP, and a thin film (1-5 microns[28]) of melted AP that is frothy and full of decomposed gases.

SEM data from samples burned in the second pressure region, between 54 and 136 atm (800 and 2000 psi), show the gradual disappearance of the melt layer and exposure of the cubic-AP layer. The surface of the crystal in this region resembles a thumbprint with solid-phase ridges and reaction-dominated valleys covering the entire surface. The ridges increase in height as pressure increases. The burning rate in this region increases less rapidly than in region one but holds to the same general description of burning rate: $r_b \sim bP^n$, with $n_{RegII} < n_{RegI}$.

The third and fourth regions, at pressures greater than 136 atm (2000 psi), exhibit combustion that is incredibly erratic and unstable. Over this pressure range, the burning rate drops drastically by nearly 80% and then rises again at a much steeper rate of change. Composite

propellants formulated with a fraction of AP, however, do not show this type of distinct behavior at these pressures, and therefore accurately describing AP combustion in these regions is of little practical importance.

Accurate experimental measurements of AP properties have been very difficult to obtain. Thermocouples embedded in the solid crystal break at the 513 K phase transition as the structure changes from orthorhombic to cubic. This has made it virtually impossible to determine the melt temperature and/or surface temperature of a burning sample of AP through traditional means. Additionally, the PDL at ~18 atm has made it difficult to obtain temperature and/or species profile data within the gas-phase region above the burning surface, since these measurements are usually collected at pressures less than 1 atm due to the very steep gradients of temperature and species found during deflagration at high pressure. Current technology has not found a way to yet resolve these steep gradients typically found at high pressure.

Other methods of detection, however, have been used to determine these important physical parameters for AP. Beckstead and Hightower[30] inferred the surface temperature for a deflagrating AP crystal at pressures from 18 to 68 atm (300 to 1000 psi) to be somewhere between 800 and 875 K through a thermal analysis of the measured depth of the cubic-phase layer of quenched samples. They utilized the phase-transition temperature, experimentally-observed thermal conductivity, and the assumption that the relationships governing thermal conductivity in the cubic and melt phases were identical. Cordes[31] estimated the melting temperature of AP to be between 845 and 885 K, by comparing the melting temperatures of similarly structured crystals. High-pressure compression data for crystalline AP under non-combustive conditions have been extrapolated to pressures of interest by Foltz and Maienshein[32] that suggest the onset of the crystalline melt could be as low as 600 to 675 K.

Ermolin *et al.*[33] collected data at 0.6 atm from samples of AP preheated to 530 K to try and resolve the species leaving the surface during deflagration. The low pressure allowed for a longer gas-phase reaction zone and showed that decomposing gases were predominantly final product species. Korobeinichev[34] modeled this system with a gas-phase reaction mechanism proposed by Ermolin *et al.*[35] and reported that to predict the experimental species profiles collected at 0.6 atm, the condensed-phase decomposition products of his model needed to be approximately 20-30% final products (HCl, Cl_2, N_2, N_2O, NO, etc) and 70-80% sublimation products (NH_3, ClO_4) and intermediates (ClO_2, ClOH). Behrens and Minier[24] found decomposition products from AP crystals heated to temperatures between 433 and 483 K that are qualitatively consistent with Korobeinichev's result.

Several AP burning rate models have been previously developed[10-14] based on global kinetics and containing a wide array of inputs. Price *et al.*[36,37] compared their model and results to the Beckstead-Derr-Price (BDP) model, the Guirao-Williams (GW) model, and the Manellis-Strunnin (MS) model. The inputs between them vary significantly, the most pertinent to this work being the condensed-phase heat release. BDP and GW assumed 30% sublimation, resulting in an overall exothermic condensed phase. The MS model assumed 100% sublimation. Price *et al.*[37] used a condensed phase that varies from ~30% to ~80% sublimation, shifting the condensed phase from exothermic to endothermic over the pressure range of 400 to 1500 psi. More recently, new models have been developed for AP that include detailed kinetic mechanisms for the gas-phase[17,38-43]. These models have only been applied to the two low-pressure regions of practical interest (less than 136 atm).

An AP model by Jing[41] made use of the Phase3 computer code and was of interest to the current work. A five-step global kinetic mechanism was proposed to describe the condensed-

phase decomposition and predict steady-state surface species. His condensed-phase mechanism is shown in Table 1.

Table 1 – AP condensed-phase decomposition reactions from Jing[41]

Reaction	**A [s^{-1}]**	**E_a [cal/mol]**
$4AP_c \rightarrow 3.25HCl+5.875H_2O+4.146O_2 +1.833N_2O+0.375Cl_2+0.33NH_3$	N/A	N/A
$AP_c \rightarrow NH_3+HClO_4$	$4.0 \cdot 10^{12}$	28,000
$AP_c \rightarrow H_2O+O_2+HCl+HNO$	$1.0 \cdot 10^{8}$	22,000
$AP_c \rightarrow 2H_2O+Cl+NO_2$	$5.0 \cdot 10^{7}$	22,000
$AP_c \rightarrow ClO_3+NH_3+OH$	$1.0 \cdot 10^{9}$	22,000

The first reaction accounted for 30% of the solid decomposition and was assumed to run to completion before the onset of melting. This reaction took the place of the bubble reactions of the earlier Beckstead and Tanaka[44] model. The remaining four condensed-phase reactions described the completion of condensed-phase decomposition, though greater than 99% of this remaining decomposition moved through the endothermic, sublimation reaction (reaction 2 in Table 1). A gas-phase kinetic mechanism by Ermolin[45,46] containing 30 species and 79 reactions was used. Thermodynamic properties used in Jing's model are listed in Table 2. The model accurately predicted burning rate from 20 to 100 atm and final flame temperature. Temperature sensitivity predictions were within the upper range of the data.

Table 2 – AP properties used in the Jing[41] AP model

Property	**Value**		
Chemical Structure	NH_4ClO_4		
$\Delta H_{f,298}$[47], [kcal/mol]	-70.7		
Molecular Weight, [gm/mol]	117.5		
Phase	Orthorhombic	Cubic	Liquid
Density[47], [gm/cm^3]	--	--	1.76
ΔH_{tr}[42], [kcal/mol]	--	2.5	7.0
Temperature range, [K]	< 513	513 – 815	> 815
Heat capacity[47], [cal/gm/K]	$C_p(T[K]) = 0.14 + T \cdot 0.41 \cdot 10^{-3}$ (T < 513)		
	$C_p(T[K]) = 0.16 + T \cdot 0.41 \cdot 10^{-3}$ (513 < T < 815)		
	$C_p = 0.49$ (T > 815)		
Thermal cond[48], [cal/cm/K/sec]	$\lambda(T[K]) = 9.95 \cdot 10^{-4} - T \cdot 3.75 \cdot 10^{-7}$		

The recent work of Gross[17] is most applicable to the current work. This was a steady-state model built upon the work of Jing[41] that used a single condensed-phase decomposition reaction, as given in Table 3.

Table 3 – AP condensed-phase decomposition reaction from Gross[17]

Reaction	**A [s^{-1}]**	**E_a [cal/mol]**
$10AP_c \rightarrow 7O_2+13H_2O+3N_2+4NH_3+HCl+HClO_4+Cl_2+3ClO_3+3Cl$	$3.0 \cdot 10^{10}$	28,000

Thermodynamic properties for Gross's condensed phase were identical to those used by Jing in Table 2. The gas-phase kinetic mechanism of Puduppakkam[15] was modified to work for AP by expanding it to include 106 species and 611 reactions. The expansion of the Puduppakkam mechanism included adding several new reactions for NOCl, HCl, and several nitrogen-hydrogen species from an ADN mechanism originally proposed by Liau *et al.*[49] and later modified by Korobeinichev *et al.*[50]. To achieve correct final nitrogen species concentrations

in the gas phase, and after trying several different approaches, Gross decided to increase the pre-exponential rate factor for the reaction:

$$NO = N_2 + O_2 \tag{11}$$

by 6 orders of magnitude. In his work as well as in those that came before him at BYU, a very large amount of NO was predicted to still be present in the final species fractions of several different propellants/ingredients. In this case, Gross surmised that something was lacking in the final gas-phase mechanism used for AP, and that this deficiency probably involved inadequately describing the nitrogen-chlorine chemistry. Increasing the pre-exponential rate factor of the NO-elimination reaction forced the model to predict equilibrium conditions for NO, N_2, and O_2 as well as final flame temperature, which had previously been low by ~30 K. Gross's final model[17] was able to accurately predict burning rate from 20 to 100 atm (300 to 1500 psi) as shown in Figure 4 with data from Boggs[28] and Atwood[29], temperature sensitivity, final flame temperature, and final species fractions.

Predicted surface species fractions of the Gross model were closer than the Jing model to those found by Ermolin *et al*.[33]. The heat release in the condensed phase for Gross's AP model (-42 cal/gm, exothermic) was also more consistent with other BYU monopropellant models, which have condensed-phase heat releases ranging from +50 cal/gm, endothermic, to -150 cal/gm, exothermic. The Jing model had a condensed-phase heat release that was +175 cal/gm, endothermic. The melt layer thickness predicted by Gross's model at 18 atm was 0.07 microns and increased with increasing pressure. Both the value and trend of these predictions are contrary to experimental data, which show that in the region from 18 to 68 atm (300 to 1000 psi), the thickness of the AP melt layer is on the order of 1-5 microns[28], the cubic layer in the range of 10-30 microns[30], and that each of them decrease with increasing pressure.

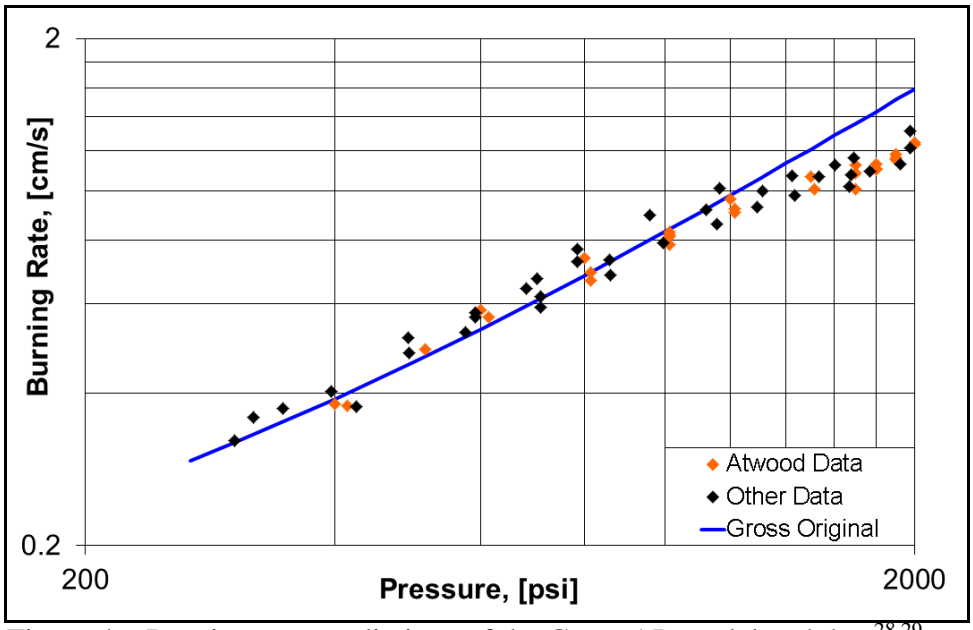

Figure 4 – Burning rate predictions of the Gross AP model and data[28,29], T_{init} 298K

Two examples of more recent models for AP include those by Ramakrishna *et al.*[51] and Rahman *et al.*[52] The first focused upon accurately predicting the PDL and related the condensed-phase heat release to the thickness of the melt layer, which was predicted to be 1-3 microns across a pressure of 20 to 100 atm and disappear at the PDL according to a heat loss model formulated to make accurate predictions. Burning rate predictions were accurate in both of these works but temperature sensitivity predictions, which are necessary to properly validate a propellant/ingredient model, were quite high. Both works used an exothermic condensed phase.

2.1.2 AP/HTPB

Most of the current research for AP/HTPB models have considered a homogeneous condensed phase and premixed conditions in the gas phase. Beckstead[53] published a review on the combustion mechanisms of typical AP- and HMX-based propellants. He assumed that for large AP particles, a multi-flame model can be used to describe the overall burning rate. This

description collapses to a single flame at low to moderate pressures if the particles are of sufficiently small size and the gaseous products evolving from the surface of the propellant approach premixed conditions.

Ermolin *et al.*[54] developed a kinetic mechanism from their experimental data to describe the combustion of AP/PB (polybutadiene) propellants, which had 35 species, 58 reactions, and was based on Ermolin's earlier work with AP. Ermolin[55] calculated kinetic parameters for the gas-phase mechanism assuming simple bi-molecular reaction steps for the AP/PB system.

Chorpening *et al.*[56] sought to gain understanding into the deflagration of thin AP/HTPB sandwiches with a layer of HTPB binder between two layers of AP. They varied the binder thickness and looked at the flame structure, burning rate, and UV-active species in the gas phase. They also conducted numerical calculations of the gas phase that included a global mechanism of 5 species and 2 reactions. Knott and Brewster[57] improved the model developed by Chorpening *et al.*[56] to more appropriately model AP/HTPB sandwiches. It was a fully coupled, periodic, steady-state model that allowed for a free surface, solid phase boundary condition, and included simplified chemical kinetics for the gas and condensed phases.

Jeppson *et al*[7]. developed a model for the steady-state, one-dimensional combustion of an AP/HTPB propellant composed of fine AP, which was also of interest to the current work. They assumed premixed conditions at the gas-phase inlet, and used a 44-species, 157-reaction gas-phase mechanism in conjunction with a semi-global, ten-step, condensed-phase mechanism. Their condensed-phase mechanism is presented in Table 4.

Table 4 – AP/HTPB condensed-phase decomposition mechanism from Jeppson[7]

Reaction	**A [mol, cm^{-3}, s^{-1}]**	**E_a [cal/mol]**
$HTPB1200_c \rightarrow 2HTPB590_c+2OH$	$1.0\cdot10^{10}$	11,300
$HTPB590_c \rightarrow 10C_4H_6+3CH_4$	$2.0\cdot10^{11}$	12,500
$HTPB590_c+10AP_c \rightarrow 15CO+10C_2H_4+3H_2O+8HCN+10ClO_2+2NO+29H_2$	$3.0\cdot10^{11}$	14,500
$HTPB590_c+10AP_c \rightarrow 14CO_2+10C_2H_2+9HCN+10ClOH+NO_2+36H_2+H$	$3.0\cdot10^{11}$	15,000
$HTPB590_c+20HClO_4 \rightarrow 8CO+24CO_2+24H_2O+20HCl+5C_2H_2+CH_4+5H_2$	$1.0\cdot10^{12}$	15,000
$AP_c \rightarrow NH_3+HClO_4$	$4.0\cdot10^{12}$	28,000
$AP_c \rightarrow H_2O+O_2+HCl+HNO$	$1.0\cdot10^{8}$	22,000
$AP_c \rightarrow 2H_2O+Cl+NO_2$	$5.0\cdot10^{7}$	22,000
$AP_c \rightarrow ClO_3+NH_3+OH$	$1.0\cdot10^{9}$	22,000
$4AP_c \rightarrow 3.25HCl+5.875H_2O+4.146O_2+1.833N_2O+0.375Cl_2+0.33NH_3$	N/A	N/A

The tenth step of his condensed phase mechanism is a pre-melt step in which 13% of the initial AP mass decomposes (as observed by Behrens and Minier[24] for 20 micron AP particles) through a low-temperature decomposition pathway identical to Jing[41]. Thermodynamic properties for AP in Jeppson's model were identical to those used by Jing and can be found in Table 2. Thermodynamic properties for HTPB used in Jeppson's model are given in Table 5.

Table 5 – HTPB properties used in the Jeppson[7] AP/HTPB model

Property		
Chemical Structure	$(C_4H_6)_{40}(OH)_2$	
$\Delta H_{f,298}$[58], [kcal/mol]	-170	
Molecular Weight[59], [gm/mol]	1212	
Phase	Solid (< 523K)	Liquid (> 523K)
Density[47], [gm/cm^3]	0.88	0.88
ΔH_{tr}[60], [kcal/mol]	--	2.0
Heat capacity[47,60], [cal/gm/K]	$C_p(T[K]) = 0.25 + T\cdot0.85\cdot10^{-3}$ (T < 523)	
	$C_p(T[K]) = 0.19 + T\cdot0.62\cdot10^{-3}$ (T > 523)	
Thermal conductivity[47], [cal/cm/K/sec]	$\lambda(T[K]) = 4.4\cdot10^{-4} + T\cdot1.3\cdot10^{-7}$	

Burning rate versus pressure predictions from Jeppson's AP/HTPB model[7], given in Figure 5, showed good comparison to Foster's data[61] from 7 to 35 atm for an AP/HTPB propellant with 20 micron AP particles.

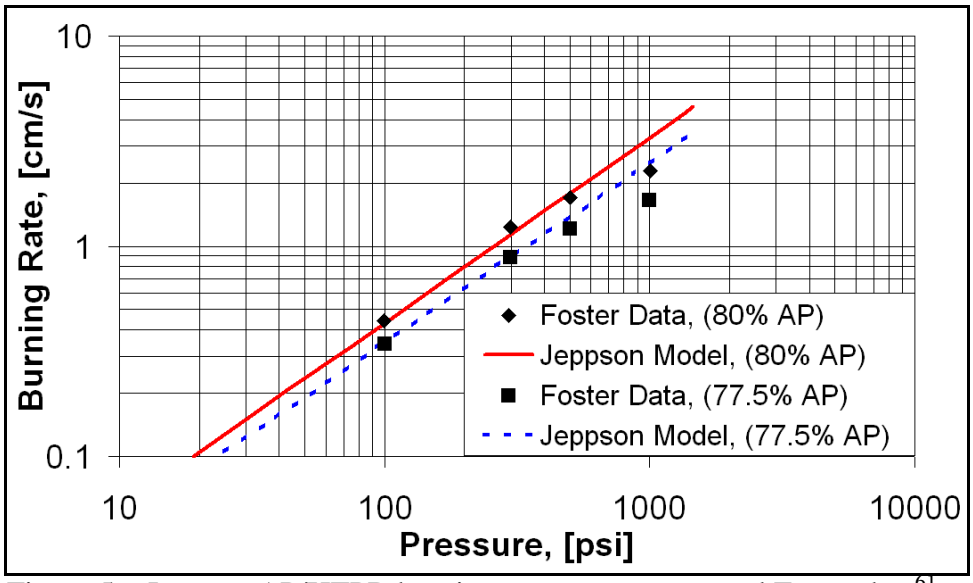

Figure 5 – Jeppson AP/HTPB burning rate vs. pressure and Foster data[61], T_{init} 298K

Above 35 atm, the model over-predicted burning rate, suggesting that the premixed assumption was no longer valid for 20 micron[24] AP particles at those pressures. This divergence from the premixed assumption is typically associated with significantly hotter diffusion flames being present near the surface above the solid interfaces of AP and HTPB. These diffusion flames are present for large diameter AP and at high pressures. The limits over which a premixed model can be assumed to be valid are not well-defined, but they are more likely to be correct for very small diameter AP and/or at relatively low pressure.

Jeppson's model[7] predicted experimental[29,61] burning rates for an AP/HTPB propellant at 20.4 atm and an initial temperature of 298 K, with formulations ranging from 77 to 100% AP. Final flame calculations were also made and are given in Figure 6.

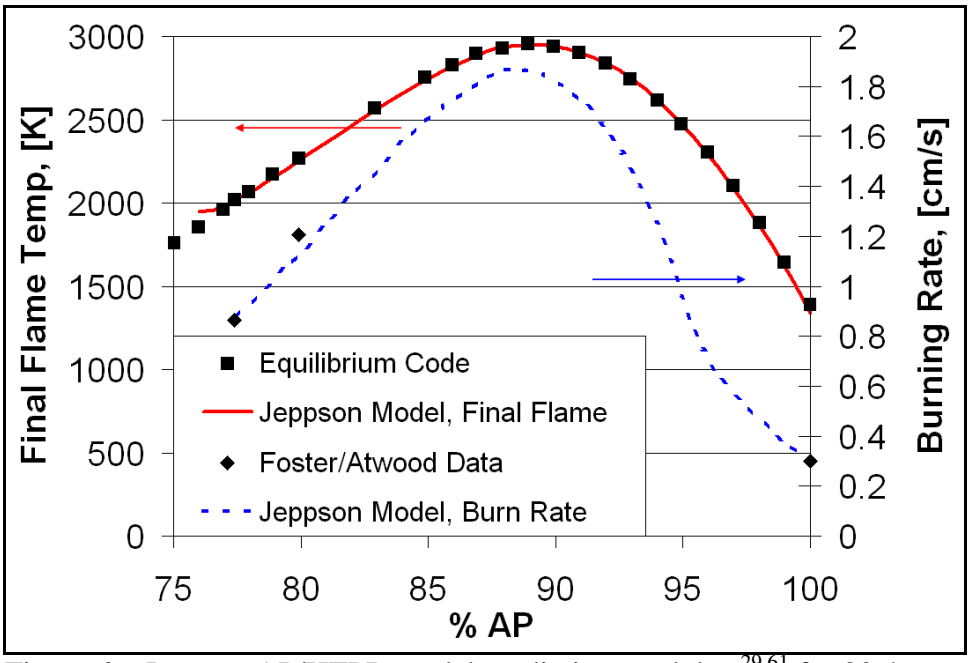

Figure 6 – Jeppson AP/HTPB model predictions and data[29,61] for 20.4 atm, T_{init} 298K

Model predictions below 77% AP began to diverge from experimental data and were thus excluded from reported results. It was assumed that a lack of carbon in the gas-phase mechanism accounted for the divergence of the model's predictions.

Further work on BYU's AP/HTPB model was completed by Tanner[62] to try and increase the compositional range over which Jeppson's[7] AP/HTPB model could be applied. The final model was significantly different than Jeppson's, with a different mechanism in both the gas (Gross's[17] version of BYU's universal mechanism) and condensed phase (individual decomposition reactions for several, specified propellant formulations). Tanner's work focused

on developing the compositional range between 60% and 80% AP and included the three-reaction, condensed-phase decomposition mechansim presented in Table 6.

Table 6 – AP/HTPB condensed-phase decomposition reactions from Tanner[62]

Reaction	A [mol, cm^{-3}, s^{-1}]	E_a [cal/mol]
$10AP_c \rightarrow 7O_2+13H_2O+3N_2+4NH_3+HCl+HClO_4+Cl_2+3ClO_3+3Cl$	$3.0 \cdot 10^9$	28,000
$HTPB \rightarrow 20C_4H_6+6CH_4+2OH$	$1.0 \cdot 10^{10}$	12,500
Formulation-specific AP/HTPB reaction, listed in Table 7	$1.4 \cdot 10^{11}$	11,000

The AP reaction used was from Gross's AP model, though the kinetic pre-factor was decreased by an order of magnitude, from $3 \cdot 10^{10}$ to $3 \cdot 10^9$ s^{-1}, and the melt temperature was decreased from 815 K to 800 K. No reasoning was given for either of these changes. Tanner's HTPB decomposition reaction is a combination of Jeppson's[7] two HTPB decomposition reactions. The third decomposition reaction used by Tanner to describe the condensed-phase reaction between AP and HTPB was determined by the formulation of the propellant. Each of these AP/HTPB reactions was based upon the decomposition products he expected would be present for a propellant with that composition, but not based explicitly upon any observed data. Additionally, the species evolved from these condensed-phase reactions, when compared across several formulations, were structured to follow the trends he expected as well. Thus, as the mixture became more fuel-rich by reducing the amount of AP in the formulation, species like CO and H_2 were increased, while those like H_2O and CO_2 were decreased. The kinetic parameters for each of these AP/HTPB decomposition reactions were identical to one another so as to maintain consistency within the model. The proposed decomposition reactions for each of the six separate formulations of the AP/HTPB propellant in Tanner's model are given in Table 7, with the listed

species for each propellant formulation being divided into reactants and products and the reaction parameters for all reactions being listed at the top of the table.

Table 7 – Specific AP/HTPB condensed-phase decomposition reactions by Tanner[62]

Reaction parameters for all reactions:																	$A = 7.0 \cdot 10^{10}$, [mol, cm^{-3}, s^{-1}]	E_a = 11,000, [cal/mol]
	Reactants		Products															
% AP	$HTPB_s$	AP_s	C_4H_6	CO	H_2O	HCN	N_2	H_2	CO_2	ClOH	HCl	CH_4	C_2H_2	NH_3	$HClO_4$	C_s		
79.90	2	82	22	4	88	20	8	12	12	32	4	0	24	46	46	0		
77.73	2	72	24	6	78	16	8	14	10	28	4	0	22	40	40	0		
75.03	2	62	26	8	68	12	8	16	8	24	4	0	20	34	34	0		
71.59	2	52	28	12	37	8	5	30	4	15	2	0	18	34	35	0		
65.97	2	40	27	11	25	3	4	39	1	10	1	0	16	29	29	17		
59.25	2	30	20	4	0	0	0	69	0	0	0	1	15	30	30	57		

Tanner's model was compared to Foster's burning rate data[63] for three formulations: 75, 77.5, and 80% AP. This comparison is given in Figure 7. No comparison of temperature sensitivity predictions to data was reported.

Using the high AP formulation data, Tanner fit his model at lower formulations through an extrapolation of the final flame temperature predicted by equilibrium. Tanner's final model predictions fit both the actual (filled) and extrapolated (hollow) points, presented in Figure 7, quite well.

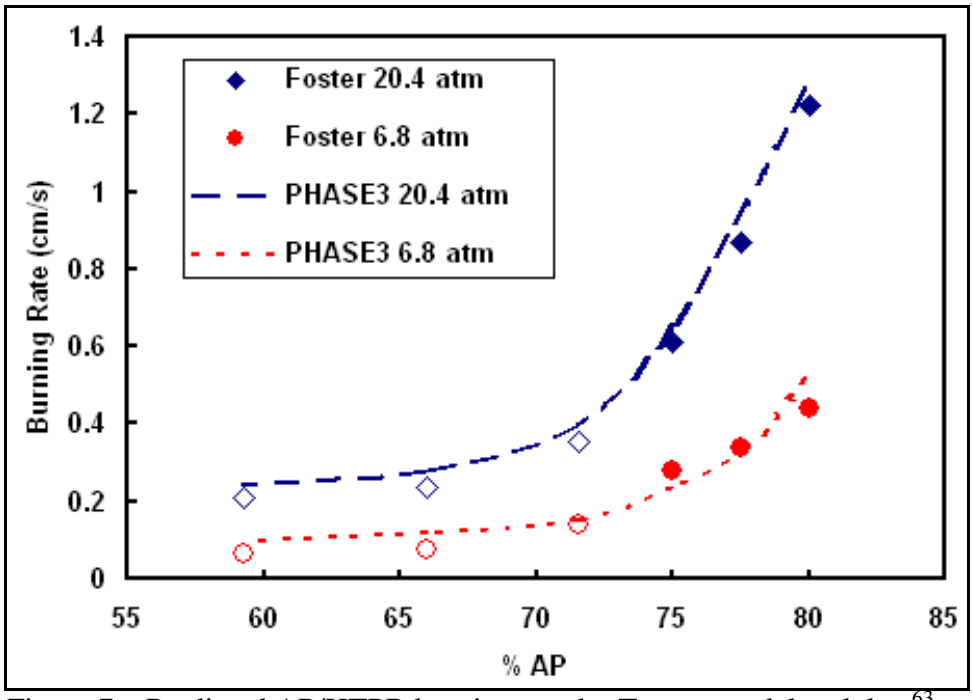

Figure 7 – Predicted AP/HTPB burning rate by Tanner model and data[63] for 6.8 and 20.4 atm

Final flame temperature and species fractions were also predicted very well, but the final gas-phase mechanism included one artificial reaction that was introduced and tuned to allow the final species fractions and final flame temperature to match equilibrium. This reaction is given by Equation 12.

$$HCN \rightarrow H + CN \tag{12}$$

In addition to his work with AP/HTPB, Tanner also attempted to model an aluminized AP/HTPB propellant. To do this, inert aluminum was added to both the solid- and gas-phase mechanisms with the thermal properties of the metal included as a function of temperature, as given by the JANNAF tables[64]. No aluminum reactions were included in either phase. Comparisons to final flame temperature and species were poor. Tanner stated that this discrepancy was possibly due to the fact that the aluminum was essentially acting as a large heat-

sink within the two phases, since no chemical reactions for aluminum were included in the model. No temperature sensitivity predictions were reported for the aluminized propellant model.

Although aluminum will not be included in any of the steady-state modeling associated with the current work, the properties of aluminum are introduced here because transient ignition predictions for an AP/HTPB/Al propellant will be included in the presented results of the current work. They are presented in Table 8.

Table 8 – Aluminum properties used by Tanner[62] and the current AP/HTPB model

Property		
Chemical Structure	Al	
$\Delta H_{f,298}$, [kcal/mol]	0.0	
Molecular Weight, [gm/mol]	26.98	
Phase	Solid (< 933K)	Liquid (> 933K)
Density[64], [gm/cm^3]	2.7745	2.5546
ΔH_{tr}[64], [kcal/mol]	--	2.5583
Heat capacity[64], [cal/gm/K]	$C_p(T[K]) = 0.144 + T \cdot 1.58 \cdot 10^{-4}$ (T < 933) $C_p(T[K]) = 0.281$ (T > 933)	
Thermal conductivity[64], [cal/cm/K/sec]	$\lambda(T[K]) = 0.651 - T \cdot 1.62 \cdot 10^{-4}$	

2.2 IGNITION

Ignition events can occur through various means, but most often develop as a result of the transient heating of an HE material by radiative, convective, or conductive means. Experimental data are collected by applying heat to an HE material and observing the time at which a light appears or the time at which complete combustion can still be attained after removal of the applied heat. The results of such experimentation are usually plotted[65] in a manner similar to that shown in Figure 8, for time to ignition versus energy flux. The actual positions and trends of the lines, however, are dependent upon many factors.

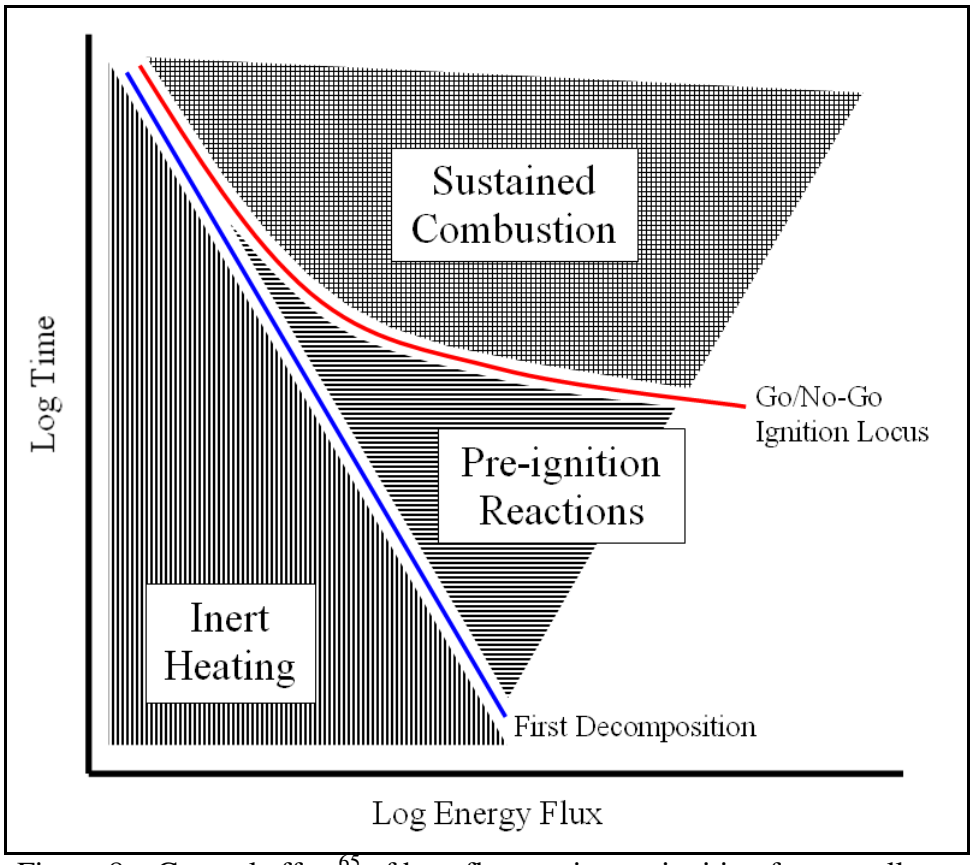

Figure 8 – General effect[65] of heat flux on time to ignition for propellants

In these experiments, a sample of propellant/ingredient is exposed to a heat source of particular value. The applied energy flux first results in a period of inert heating of the sample, which is followed by the beginning of decomposition reactions (first decomposition, FD) that are usually endothermic or mildly exothermic in nature. The condensed-phase pre-ignition reactions that follow, frequently, but not always, lead to light-producing reactions (first light, FL, sometimes referred to as ignition in older references) above the surface of the sample. Eventually, the sample will contain a sufficient amount of heat-producing reaction in the condensed and gas phases to allow the sample to transition to steady-state burning when the energy flux is removed. The point in time at which this transition can occur, without resulting in extinguishment, is referred to as the go/no-go point. Experimentalists report go/no-go times as

the time at which 50% of the experimental samples successfully transition to steady-state burning after removal of the energy flux. Samples heated longer than the go/no-go time can transition to steady state (go), whereas samples heated for less time will extinguish (no-go). Go/no-go times typically shorten as pressure increases. This effect is significant below about 5 atm of pressure[66] and is bound at very high pressures by the time to first decomposition, or first light, since inert heating is essentially independent of pressure.

2.2.1 *MODELING AND EXPERIMENTAL WORK*

Both Vilyunov and Zarko[67], and Hermance[66] published comprehensive reviews on the ignition of the solid and condensed phases of various materials from both experimental and theoretical viewpoints. Studies including both experimental and modeling work have helped us better understand the details of the ignition process. Previous ignition models have varied in complexity ranging from those including only very few equations of conservation and global kinetics through those that solve a large number of conservation equations and include very detailed kinetic mechanisms. A few of these models are discussed here.

Early work focused only upon the condensed phase. Vilyunov *et al.*[68] performed a statistical analysis of their solid-phase model and found that thermal conductivity, initial temperature, and kinetics had the greatest influence on time to ignition. Vilyunov and Zarko[67] extended work done by Zeldovich concerning radiative ignition based only on the condensed-phase solution with respect to one-dimension and time. They defined an expression that related time to ignition that was primarily affected by the imposed heat flux.

Dik *et al.*[69] calculated temperature profiles within a condensed substance that was heated to ignition through an inert, opaque shield. Knyazeva and Dik[70] conducted experimental and

modeling work to better refine an analytical model accounting for sub-optimal contact between a condensed substance and a thermal shield. Zarko[71] compiled a summary review on irradiative ignition and developed a model based only on the condensed phase. He proposed that ignition had occurred only if the initiation of rapid exothermic reaction within the condensed material had begun and if the fuel could transition to a steady-burning state.

Further work included the simulation of both the condensed and gas phases in an ignition system. Significant work towards understanding the ignition transients within various types of rocket motors was conducted during the early 1990's[72-77]. Gheris and Price[74] used a code that coupled the condensed and gas phases to predict motor performance during ignition. Dik and Selikhovkin[78] developed a simple ignition model that tracked the maximum temperature through the condensed and gas phases using a single value of heat flux at the surface. They had to assume a value for surface temperature as a function of time to close the equations. Knyazeva and Zarko[79,80] developed a one-dimensional, unsteady, numerical model for the purpose of determining the ignition criteria of homogenous, condensed substances. They reported that if an external irradiative source, of magnitude greater than 37% of the un-augmented steady-state heat flux, was applied to the energetic material, then the resultant ignition of the propellant would be unstable and could extinguish upon termination of the radiative flux. This result is contrary to the behavior typically seen in experimental data as described by Figure 8, since there is no extinguishment region at prositions above the go/no-go line. Their results could be applicable if the time over which the energy flux is removed is taken into account within a given model, and the kinetic assumptions of that model are accurate.

Huang *et al.*[81] developed a four-phase model to predict the ignition capability of nitramine-based propellants that were subjected to the impingement of a hot fragment of foreign

material (solid phase, liquid phase, gas phase, and hot solid fragment). They focused on reactions occurring in the solid and liquid phases of the HE material. Yang and Liau[82], Liau and Yang[83], and later Liau *et al.*[84] presented work on a time-accurate RDX model that used detailed kinetics to predict laser-induced ignition events. Their model solved the mass, energy, and species conservation equations for both gas and condensed phases using a detailed 45-species gas-phase mechanism. The gas and condensed phases were coupled through an iterative process that converged on values of surface temperature and burning rate.

Atwood *et al.*[85] has conducted a series of laboratory experiments on ignition data for RDX to use as inputs to a transient combustion model that predicted the burning rate of HE ingredients. Parr and Hanson-Parr[86] collected experimental data on the ignition/extinction of RDX. In these studies, ignition occurred at a point in the gas phase away from the surface, and then the flame sheet snapped back to a position close to the surface, quickly transitioning into laser-augmented steady-state combustion. The removal of the laser determined the go/no-go data presented.

Several sources of ignition data for AP/HTPB propellants and AP were available for validation of model predictions. Atwood *et al.*[65,87] have reported time-to-ignition data for neat AP at 34 atm (500 psi) at two levels of laser heat flux. Initial sample temperatures of 298 K and 373 K are included in their results. They note that the time of apparent first-decomposition for AP coincides with the go/no-go point within the uncertainty of their measurements, which is not explicitly reported. This behavior is different from that observed for HMX and AP/HTPB propellants, where the condensed phase melts and begins to react well before the go/no-go point.

Atwood *et al.*[65,88] have presented time to first decomposition and time to ignition (go/no-go) for AP/HTPB propellants with formulations of 80% and 84% AP[65] and a non-specified AP

formulation[88] that is likely similar to the same formulation. It has been observed[89,90] that significant decomposition begins to occur in AP-based propellants after the 513 K phase change of AP. Time to first-light and time to ignition for an AP/HTPB/Al propellant with 20% aluminum was also included in their results[65].

Shannon[91] presented a large array of time to ignition data for AP/CTPB propellants that varied several parameters. He used an arc-image furnace to ignite the samples and looked at how times to ignition varied with respect to applied heat, pressure, binder type, and additives. Sofue and Iwama[92] also presented ignition data for an AP/CTPB propellant (75% AP, 22% CTPB, 3% additives) at sub-atmospheric and atmospheric pressures. In addition to varying pressure, they changed the composition of the surrounding gas to ascertain its effects upon time to ignition and reported go/no-go times for Ar < N_2 < He at 160 torr. This trend is consistent with the idea that gases with a higher thermal diffusivity will allow for increased conduction of heat away from the surface of the propellant and thus lead to longer times to ignition.

Ahmad and Russell[93] studied an AP/HTPB propellant of unspecified formulation (with a small amount of nitramine) and measured ignition transients. They presented go/no-go times using an Ar-ion laser (varying the wavelength from 250-800 nm) for energy fluxes of 25 to 125 W/cm^2, reporting that approximately 90% of the incident energy was absorbed by the composite propellant regardless of laser wavelength.

Cain and Brewster[94] reported times to ignition for an AP/HTPB propellant with 75% fine AP (2 micron). They studied the effects of adding up to 1% carbon upon the results, and also showed that time to first light and time to go/no-go for this formulation of propellant diverge at sufficiently high heat fluxes (~150 W/cm^2).

2.2.2 *MEREDITH IGNITION MODEL*

Meredith and Beckstead[95] developed a one-dimensional, time-dependent, numerical model to predict the laser-induced ignition of HMX that was of primary interest to this work. They used a detailed kinetic gas-phase mechanism of 45 species and 231 reactions and a condensed-phase mechanism first proposed by Brill[96] and later modified by Yang and Liau[82], as presented in Table 9, with heat of reaction calculated at the melt temperature of 554.5 K.

Table 9 – HMX condensed-phase decomposition reactions used by Meredith[95]

Condensed-phase reactions	**ΔH_{rxn}, [cal/gm]**	**A, [s^{-1}]**	**E_a, [cal/mol]**
$HMX_c \rightarrow 4CH_2O + 4N_2O$	-233	10^{13}	34,400
$HMX_c \rightarrow 4HCN + 2NO + 2NO_2 + 2H_2O$	+133	$10^{16.5}$	44,100

Thermodynamic properties for Meredith's condensed phase were similar to those used by Davidson[16]. Those that were different are given in Table 10.

Table 10 – HMX properties used in Meredith[95] ignition model

Property	**Value**			
Chemical Structure	$C_4H_8N_8O_8$, $(H_2CNNO_2)_4$			
Density[97], [gm/cm^3]	1.9			
Phase	β	α	δ	Liquid
ΔH_{tr}[98], [kcal/mol]	--	0.45	1.9	11.4
K_{laser} for CP-absorption[99], [cm^{-1}]	5672	4800	1294	1165
Temperature range[98], [K]	< 388	388 - 439	439 - 554	> 554
Heat capacity[47], [cal/gm/K]	$C_p(T[K]) = 0.0497 + T \cdot 6.6 \cdot 10^{-4}$			
Thermal conductivity[47], [cal/cm/K/sec]	$\lambda(T[K]) = 0.0015 - T \cdot 1.15 \cdot 10^{-6}$			
GP absorption cross-sectional area[100], [cm^2/molecule]	CO_2: $2.0 \cdot 10^{-22}$ HMX_g: $5.59 \cdot 10^{-19}$			

Meredith's model solved a transient set of conservation equations for the gas phase, which are presented in Equations 13 through 17.

$$\frac{\partial(\rho)}{\partial t}+\frac{\partial}{\partial x}(\rho u)=0 \tag{13}$$

$$\frac{\partial(\rho u)}{\partial t}+\frac{\partial(\rho u u)}{\partial x}+\frac{\partial P}{\partial x}-\frac{4}{3}\frac{\partial}{\partial x}\left[\mu\frac{\partial u}{\partial x}\right]=0 \tag{14}$$

$$\frac{\partial \rho H}{\partial t}-\frac{\partial P}{\partial t}-u\frac{\partial P}{\partial x}+\frac{\partial \rho u H}{\partial x}-\frac{\partial}{\partial x}\left(\lambda\frac{\partial T}{\partial x}\right)+\sum_{k=1}^{NumSpec}\left(\frac{\partial(\rho Y_k V_k H_k)}{\partial x}\right)-\frac{4}{3}\mu\left(\frac{\partial u}{\partial x}\right)^2-Q_g'''=0 \tag{15}$$

$$\frac{\partial(\rho Y_k)}{\partial t}+\frac{\partial(\rho u Y_k)}{\partial x}+\frac{\partial}{\partial x}(\rho V_k Y_k)-\dot{\omega}_k W_k=0\ ,k=1...NumSpec \tag{16}$$

$$\rho=\frac{P}{RT\sum_{i=1}^{N}\frac{Y_i}{W_i}} \tag{17}$$

The condensed-phase description was based on the work of Erikson[101], which assumed that all gas-phase species beneath the surface were dissolved within the solid (i.e. the gas is trapped within the solid/liquid phase and moves with the same velocity). The equations used to describe the condensed phase are presented in Equations 18 through 20.

$$\frac{\partial\left(r^{\kappa}\rho_c u_c\right)}{\partial r}=0 \tag{18}$$

$$\rho_c C_p\frac{\partial T}{\partial t}+\rho_c u_c C_p\frac{\partial T}{\partial r}-\frac{1}{r^{\kappa}}\frac{\partial}{\partial r}\left(r^{\kappa}\lambda\frac{\partial T}{\partial r}\right)-\sum_{k=1}^{NumSpec}\omega_k W_k h_k-q_s''K_{abs}\exp(K_{abs}r)=0 \tag{19}$$

$$\rho_c\frac{\partial Y_k}{\partial t}+\rho_c u_c\frac{\partial Y_k}{\partial r}=\dot{\omega}_k W_k\ ,k=1...NumSpec \tag{20}$$

The boundary conditions for Meredith's model were:

1) an inlet flow condition at the beginning of the solid phase, which fed pristine HMX at initial conditions into the flow field;

2) temperature, momentum, and species flux conservation at the boundary between the condensed and gas phases (surface);

3) an outflow condition at the end of the gas phase, which allowed for the escape of gases assumed to be no longer changing with respect to temperature, momentum, or composition;

4) an applied heat flux at the surface of the condensed phase for laser-assisted combustion and ignition simulations.

Meredith's condensed-phase code was written in Fortran and used an iterative method of lines to solve the conservations equations of species and temperature. The gas-phase code was written in Ansi C and used the PETSc[102] libraries for solution. The gas-phase code solved the continuity, momentum, energy, and species conservation equations by a non-linear, Newton-like, Krylov sub-space method. Gas-phase properties and reaction rates were calculated using the Chemkin[103] libraries.

Meredith's results are compared to various sources of experimental data in Figure 9.

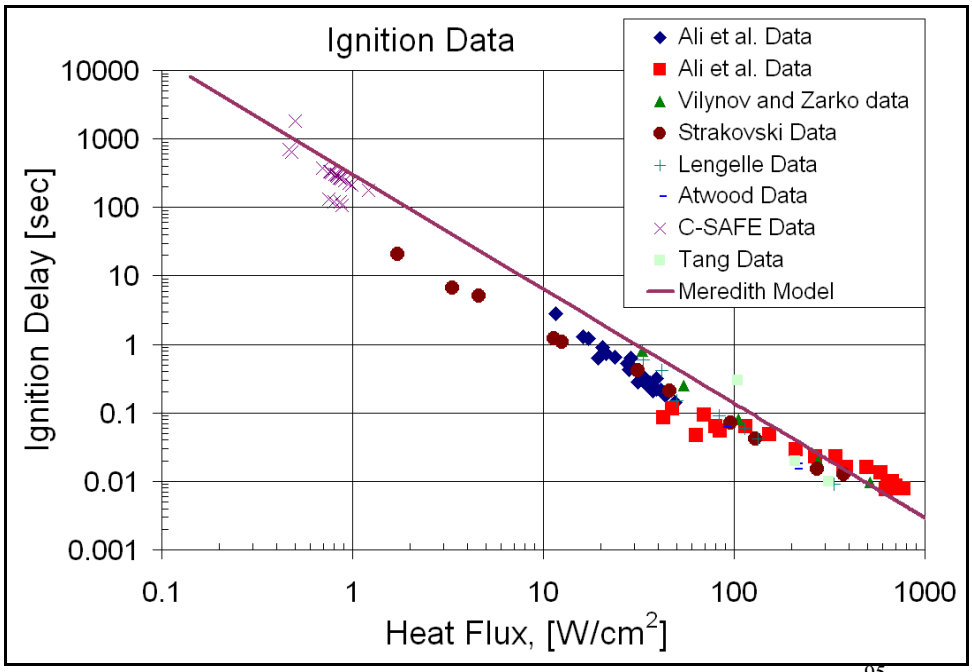

Figure 9 – HMX ignition delay versus heat flux of Meredith model[95] and data, T_{init} 298K

Meredith's ignition model included the ability to model the transition from unsteady to steady-state burning after the removal of the laser heat flux, as shown in Figure 10.

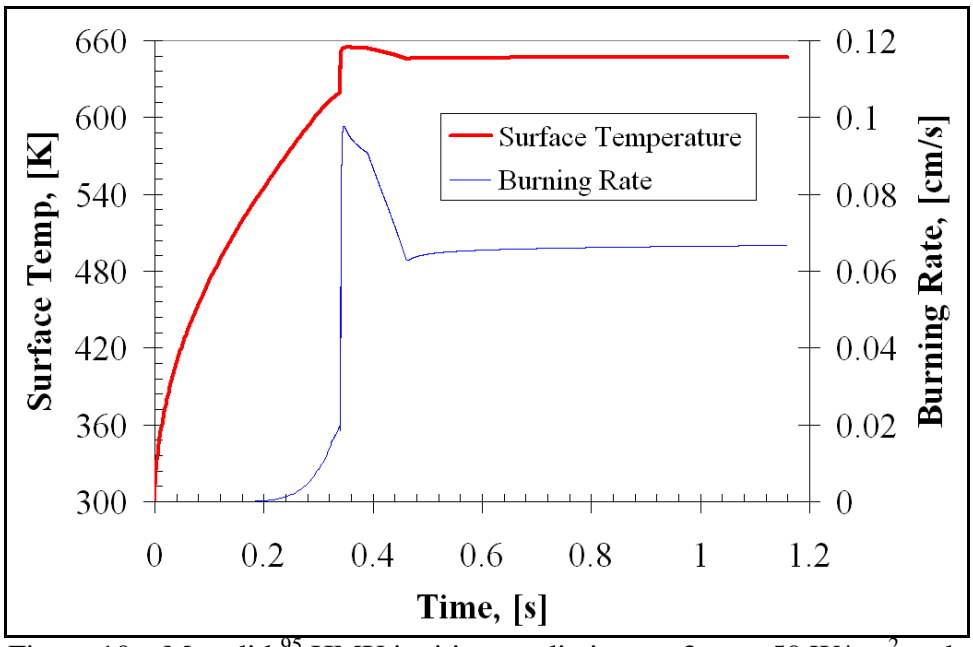

Figure 10 – Meredith[95] HMX ignition predictions at 2 atm, 50 W/cm^2 and transition to steady state

The primary source of ignition validation data comes from experimental time to ignition versus applied heat flux. For these predictions, the laser heat was applied as a boundary condition at the surface of the gas/liquid foamy layer. The model the predicted snap-back effect observed by Ali *et al.*[104], where the gas ignites away from the surface and then propagates back toward the surface (13.0 ms to 13.5 ms in Figure 11), and a dark zone during laser-augmented combustion (33.8 ms in Figure 11).

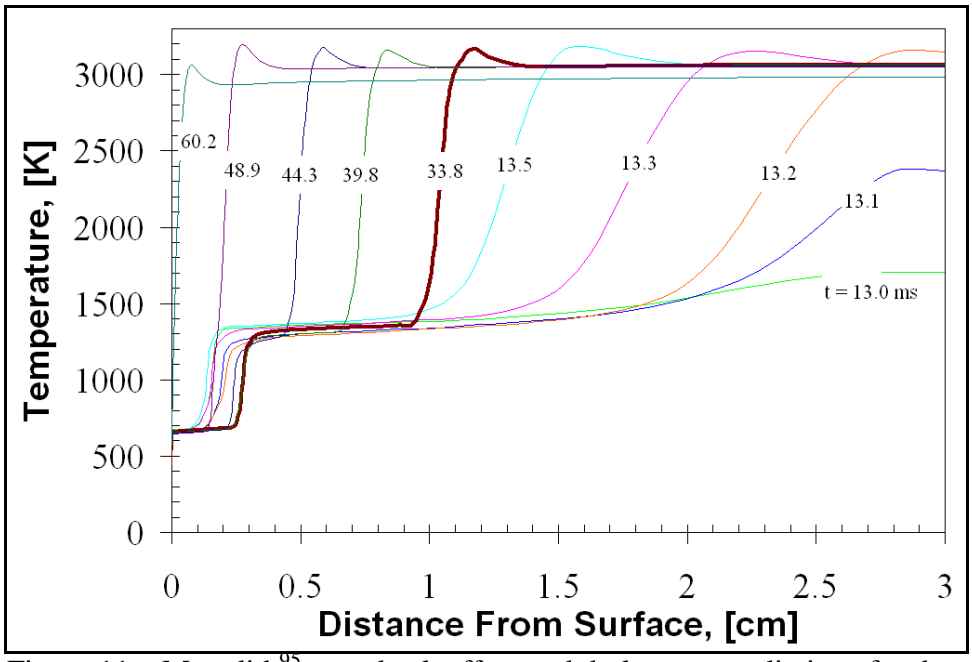

Figure 11 – Meredith[95] snap-back effect and dark-zone predictions for the HMX ignition model, 1 atm, 400 W/cm^2

Steady-state predictions were validated by removing the laser heat flux after ignition was achieved (39.8 ms to 48.9 ms in Figure 11) and running the simulations until all transients had died out (60.2 ms in Figure 11). The model was also very accurate in predicting steady-state burning rate, surface temperature, and melt-layer thickness versus pressure, as well as laser-augmented burning rate and dark zone presence for laser heat-fluxes of less than 200 W/cm^2 at 1 atm.

2.3 COOKOFF

Cookoff can be described as the thermal initiation of a device containing an energetic material. Devices usually considered include ammunition, small rockets, missiles, and bombs. These types of munitions come in many different shapes and sizes. For cookoff experiments, bombs are generally self-contained and require no additional preparation, but the open nozzles of

rockets and missiles are plugged to avoid any impingement of external flames or direct heat to the propellant material within the article as well as confining all decomposed gases. Cookoff has been split into two sub-categories based on the intensity of the heating rate. Systems with a low heating rate are referred to as slow-cookoff systems, and those that are heated relatively quickly are called fast-cookoff systems. The current work was most specifically focused on fast-cookoff; however, this literature review will first include a small amount of discussion concerning slow-cookoff research for completeness.

2.3.1 SLOW COOKOFF

Slow cookoff is characterized by monotonic heating rates of 3-4 K/hr[1] resulting in an almost uniform temperature rise throughout the system, despite the low thermal conductivity of the explosive. When the explosive reaches a sufficiently high temperature, solid-phase decomposition begins. Decomposition occurs throughout the solid, but positions below the surface heat up more quickly than the surface itself, due to the typical radial or spherical geometry of the propellant in the test article. Thus, ignition events usually occur within the solid material. Containment of evolved gases and the advanced level of resulting decomposition within the solid usually lead to very violent and destructive ignition events. Early experimental work and modeling efforts by Creighton[105] studied the "ignition temperature" and time to thermal runaway (point at which heat cannot be conducted away quickly enough to avoid exponential heat growth due to condensed-phase decomposition) in slow-cookoff systems. A similar model was studies by Hobbs *et al.*[106] and Baer *et al.*[107]. They each reported that slow-cookoff predictions showed the initiation of ignition events to occur beneath the surface of the explosive.

2.3.2 FAST COOKOFF

Fast-cookoff heating rates are on the order of 100 K/hr[1] but cover a wide range of values. Externally applied fluxes at these heating rates are on the order of 0.1 to 25 W/cm^2. This level of heating rate coupled with the low thermal conductivity of HE ingredients results in only a very small portion of the energetic material near the outer surface of the solid ever reaching an elevated temperature. Gases evolved from condensed-phase decomposition are trapped and heated within the localized region between the propellant and enclosing case, and the gases eventually ignite. Gas-phase ignition events for these systems cause a rapid increase in pressure and ultimate failure of the container, but are typically much less violent than slow cookoff events.

Early fast-cookoff modeling efforts employed the codes originally developed for slow-cookoff with modified boundary conditions. Baer *et al.*[107] noticed that higher heating rates resulted in the ignition of the system occurring near the heated boundaries, and that such events coincided with the mechanical failure of the containment, as depicted in Figure 1. Erikson and Schmitt[108-110] conducted a series of modeling validations for their code against fast-cookoff experimental data taken by Atwood *et al.*[111] for spherical geometries with relative success. Time to ignition and temperature of reaction were predicted by the Erikson model reasonably well, but it was stated that more efforts needed to be taken to validate the mechanical properties and chemical-reaction mechanisms.

Jing[41] developed two different models to predict fast cookoff. He assumed a zero-dimensional model that did not take into account an actual gas phase, but treated the gas and solid phases to be in the same space and ignored convection within the computational domain. Jing's second model (one-dimensional) included a description of both the condensed and the gas

phases but did not couple the two together due to numerical difficulties. His model showed that the thermal wave became steeper when the incident heat flux was increased. The model's condensed-phase results compared well to an analytical model. No comparisons to experimental data were made, but both his zero- and one-dimensional models matched the predictions of an earlier fast cookoff model by Beckstead and Hendershot[112].

Meredith and Beckstead[3] extended their ignition model to predict HMX cookoff systems. The equations for the gas and condensed phases were identical to those used in their ignition model, as were the kinetic mechanisms and physical properties of HMX. The only differences between their cookoff and ignition models were a coordinate transformation into radial space and the following new boundary conditions:

1) zero inflow at the center of the cylindrical test article;
2) zero outflow at the end of the gas-phase domain;
3) heat flux equality across the boundary of the gas and steel shell;
4) heat flux application at the exterior of the steel shell.

The model most importantly allowed for the coupling of the condensed and gas phases that Jing's[41] cookoff model for HMX could not. The model predicted the pressurization of the container, implemented variable time-stepping and mesh-refinement algorithms, scaled well when used on parallel architectures, and showed the ability to allow for an increasing gap between the HE surface and thermally-expanding steel shell. Meredith's numerical results showed excellent agreement with experimental data[95] over a large range of heat fluxes, as previously shown in Figure 9.

Cirro and Eddings[113] conducted a small number of cookoff experiments to study the thermal boundary layer at the HE surface/container interface. An important observation of these

experiments was the amount of damage done to the cookoff container for varying HE configurations. The experiments performed showed a wide range of violence of explosion—the most benign resulting in pressure bursts of the container and little damage to container, while the most violent transitioned to detonation and left only small quarter-size pieces of the steel container.

An important finding of Meredith's work was the realization that it is the imposed heat flux upon the surface of the propellant that dictates the time to ignition and not the heat flux imposed at the external surface of the container shell. It was also reported that the time to ignition of a fast-cookoff system was strongly dependent upon the width of the modeled air gap between the HE and container. This is of particular interest because the model applied to the external container was one that only calculated the thermal wave through the steel and did not include the direct effects of dynamic pressure loading or thermal expansion upon the radius of the heated shell. Meredith's cookoff model investigated two separate means of approximating the width of the air gap. The first was a constant width air gap. It was found that using values between 0.5 and 1.0 mm resulted in the best prediction of the experimental data. Additionally, a more accurate but entirely empirical method of determining the air gap width that was proposed by Cirro and Eddings[113] was employed in Meredith's model. The results were much the same as when using the constant gap width assumption, as the empirical equation had the air gap width vary from 0.5 to 1.0 mm over the course of the simulation.

Finally, Meredith's cookoff code was coupled to the post-processed, large-scale simulation of a container within a pool fire[3] through the heat flux to the surface of the container. It was noted that applying the predicted heat flux from the fire simulation (which fluctuated greatly with respect to time) to the surface of the container, resulted in essentially the same time

to ignition as a simulation where the average heat flux to the exterior of the container was used. This was attributed to the dampening effect of the steel shell and led to significant simplification of later simulations.

There were a few sources of experimental data found concerning the application of AP/binder/Al propellants to fast cookoff systems. Ford *et al.*[114] used an AP/HTPB/Al propellant cast within the cylindrical portion of a large bullet-shaped test articlet that was placed within a tube filled with flowing hot gases from the combustion of propane. The experimental apparatus was designed to provide a constant heat flux to the cylindrical extermal surface of the test article (radial coordinate system). The wall of the cylindrical test article was 3.175 mm thick 3140 steel. Between the steel wall and the propellant was 0.762 mm of EPDM insulator and 0.762 mm of an HTPB and carbon black liner.

Wilson *et al.*[115] used an AP/PBAN/Al propellant cast into a cylindrical casing that was bolted over a table-hole, end-on. A propane/oxygen torch was placed beneath the table and applied the incident heat flux according to the flame's proximity to the end of the test article (Cartesian coordinate system). At the heated end of the test article was a 12.7 mm thick steel plate. Between this steel plate and the propellant was 2.54 mm of nitrile-butyl rubber insulation and 1.42 mm of an unspecified polymer liner. Their work was initiated to extend the range of heat fluxes to which AP/Binder/Al propellants had been applied in the past. Their data showed times to ignition that were earlier than expected (low surface temperatures), but which were consistent with other sources of data.

Washburn *et al.*[116] inserted an AP/Binder/Al propellant catridge into a cylindrical casing, which was then attached to a plate, end-on, and exposed to radiant heating by a quartz lamp (Cartesian coordinate system). The propellant was bonded by its radial surface to the casing by a

room-temperature vulcanizing (RTV) silicone adhesive. At the end of the heated article was a 1.47 mm thick steel plate. No insulation or liner was used between the propellant and steel plate, though four thermocouples were placed there. Their results showed surface temperatures at ignition that were more consistent with bare propellant data.

The bulk of the work that has been accomplished, as evidenced by the small collection of data presented in this section, has only been collected within the past few years. Understanding the science surrounding the prediction of cookoff events for composite propellants, such as the one at the center of the current research, is very new, but has the propensity to be categorized and better understood by propellant/ingredient modeling of steady-state conditions and bare surface ignition events. Understanding how AP/HTPB/Al propellants respond to cookoff conditions is of vital importance as a majority of the weapons and munitions in production today employ propellants that are very similar in nature and formulation to those investigated by the current work. The current work comprises one of the relatively few efforts in the literature being made to better understand these propellants and how they respond to thermal stimuli so that any possible accidents involving these potentially destructive propellants may be avoided.

Work and play are words used to describe
the same thing under differing conditions.
-- Mark Twain

CHAPTER 3: OBJECTIVES

The primary goal of this work was to model an AP/HTPB/Al cookoff system by making accurate predictions of time to ignition. Propellant ignition models are typically validated by comparing to experimental time to ignition data. The models used to predict these data are based on propellant/ingredient models that have first been validated by comparison to steady-state deflagration data. The current work involved a rigorous attempt to verify and validate the time-to-ignition of cookoff events by investigating each level in the structure of the complete model and code and then identifying wherein they each needed to be improved. In doing so, several updates were made to both the models and the codes that employed those models. The end goal was not only to make meaningful predictions but to have confidence in those predictions as well, or at the very least to define a path by which confidence might be attained. Knowledge and understanding were of primary concern to the current work and provided a singular drive toward its completion.

This project began at the ending point of the work accomplished by Meredith and Beckstead[3,95] and the ignition code developed by them, as well as the ending points of the propellant/ingredient models of Gross[17] and Tanner[62]. Several different sub-projects were accomplished as part of the current work, each of which fell into one of two categories:

1) code improvement;
2) propellant model improvement.

The first of the coding projects was to generalize the ignition code with regard to the simulated propellant/ingredient. When initially written, the ignition code was built for the single propellant ingredient HMX. The condensed-phase portion of the ignition code, which had originally been written in Fortran, also needed to be translated into Ansi-C to make a clean integration between the ignition code and several other external software packages.

The second code-development project involved removing the use of Chemkin in the ignition code. In February of 1997, the open-source Chemkin libraries were licensed to Reaction Design[117]. As part of this process, a restricted license was grandfathered to all those with a current version of Chemkin II or earlier, but the proliferation of the Chemkin II libraries to new sources was restricted. To keep the ignition code free of charge for all users (including industrial contacts that had no previous access to Chemkin II), Chemkin needed to be removed from the code and replaced with a comparable open-source package. Cantera[118] is a C++, open-source, chemistry and thermodynamics package that was available at the initiation of the current work. This set of libraries was developed by Dave Goodwin at Cal Tech. It was able to calculate the thermal properties and reaction rates needed by the ignition code as accurately as Chemkin II, and it had also been shown to make its calculations up to 40% faster.

The steps involving the improvement of the several propellant/ingredient models of interest were structured such that each piece built upon the foundation of the work that had come before it. Thus, the individual propellant/ingredient models were first validated against steady-state data, then compared to laser-augmented data, and last to time-to-ignition data. Building a validation structure in this way provides for a high level of confidence when making predictions for the complicated details of ignition and cookoff at which a limited amount of experimental data has been collected.

The several tasks that needed to be completed were:

1. Re-validate ignition predictions for the HMX model using the improved ignition code
2. Update Gross's steady-state AP model using current literature resources
3. Validate the updated steady-state AP model, making changes if necessary
4. Validate laser-augmented predictions for the AP model
5. Validate ignition predictions for the updated AP model, making changes if necessary
6. Update Tanner's steady-state AP/HTPB model using current literature resources
7. Validate the updated steady-state AP/HTPB model, making changes if necessary
8. Validate laser-augmented predictions for the AP/HTPB model
9. Validate ignition predictions for the updated AP/HTPB model, making changes if necessary
10. Validate ignition predictions for the AP/HTPB/Al model
11. Validate cookoff predictions for AP/HTPB/Al model

Steps two through nine of the above list fit into a validation structure for the new propellant/ingredient models in various modeling configurations that have been included in the current work. This validation structure is succinctly described by Figure 12.

	AP	AP/HTPB	AP/HTPB/AL
Cook	No data	Very little data Qualitative	Validate
Ign	Validate	Validate	Validate
Laser	Validate	Validate	No current model
SS	Update Validate	Validate	No current model

Figure 12 – Proposed validation structure for the current work

Figure 12 lists the most complicated predictions of the current work (cookoff)—for which we have the least data—at the top right, and the most simple (steady-state AP)—for which we have the most data—at the bottom left. Predictions that are lower and to the left in the validation structure are not only simpler but provide a foundation for making predictions with confidence in regions that are higher and to the right.

You can't depend on your eyes when
your imagination is out of focus.
-- Mark Twain

CHAPTER 4: CODE AND MODEL IMPROVEMENTS

The current work included the modification/improvement of two computer codes—the steady-state propellant code, Phase3, and the ignition code developed by Meredith—and the validation of several propellant/ingredient models applied to those codes (HMX, AP, and AP/HTPB). The ultimate goal was to predict the combustion characteristics of these propellants/ingredients under steady-state and laser-augmented conditions within Phase3 so that the models could then be applied toward predicting ignition events, fast cookoff events, and the transient changes that accompany each within the ignition code. Additionally, it was intended that the ignition code be used to validate an AP/HTPB/Al propellant model for ignition and cookoff events. Improvements made to the computer codes and propellant models, which had all been previously developed at BYU, will be discussed in this chapter.

4.1 PHASE3 CODE IMPROVEMENTS

Two major improvements were made to the Phase3 code so that the current work could be completed. The first was to allow for the inclusion of phase transitions within the modeled domain of the condensed-phase. Prior to this work, the only portion of the condensed phase that was explicitly calculated was the melt layer. All temperature-based phase changes and the energy associated with each were accounted for prior to beginning the condensed-phase calculation of the melt layer. Phase changes that had been defined at temperatures above the melt temperature

were not included in the calculations. During the development of the AP model for the current work, the desire arose to compare predicted cubic-layer thickness to experimental data. Condensed-phase calculations were therefore made that included a domain of temperatures lower than the melt temperature. Thus, the method of calculation needed to be changed such that temperature-based phase changes, and the energy associated with each of them, could be accounted for regardless of the temperature at which the condensed-phase calculations began. Additionally, to implement the final version of the current AP model, which will be discussed later, it was necessary that the code also be able to make transitions between individual phases of a propellant ingredient (e.g.: orthorhombic AP, cubic AP, and melted AP) such that different regimes of kinetic decomposition for a single ingredient (AP, in this example) could be described.

The second improvement made to the Phase3 code was to add the ability to model the penetration and absorption of a laser into the condensed-phase domain for a laser-augmented case. Previously, the only option to model laser-augmented combustion within Phase3 was to treat the laser as a boundary condition at the defined surface of the propellant. This assumption, though used rather frequently in modeling efforts is far from accurate for AP, an ingredient that is highly transparent to the wavelength of laser light typically used (~10.6 microns). AP is different in this regard from most other propellants/ingredients, which are essentially opaque to the laser light. This sub-model was fairly difficult to incorporate into the code because the condensed-phase solver employs a shooting-method that calculates the solution profiles from the cold side of the propellant toward the hot, whereas the absorption of the laser has to be calculated from the hot side of the propellant toward the cold. After numerous trials, an iterative method

was developed to converge upon the location of maximum absorption that worked sufficiently well.

4.2 IGNITION CODE IMPROVEMENTS

Several improvements were made to the ignition code over the course of this work. The first involved the replacement of the Chemkin libraries with Cantera. This effort was a straight-forward process, as each call to Chemkin from the initial version of the code had an analogous call to Cantera. A comparison between the two versions of the ignition code was made. Rates and properties returned from Cantera were within less than 1% of those calculated by Chemkin, and required less time to calculate as well. Both Cantera and Petsc, the numerical solver library used by the ignition code, were kept up to date with current releases of the software. As of the completion of the current work, the ignition code was using Cantera 1.8.0 and PETSC 3.1-p7.

Many changes were also made to the condensed-phase portion of the ignition code. The first involved translating the code from Fortran into Ansi C. The decision to do this was made for two reasons: the first, to simplify the integration of Cantera libraries into the code, which was developed in C++; the second, because it was believed that doing so would simplify the development process, which it did to considerable effect. The completion of this work led to an in-depth analysis of the ignition code in general, which led to further correction of a number of issues that the code was exhibiting when the current work was first begun. These issues concerned general convergence, accuracy, memory overflow/overwriting, and the proper integration of external library software packages.

Another change to the condensed-phase portion of the ignition code was to make the condensed-phase equations and assumptions consistent with those of Phase3. Initially, there were

a few major differences between the two, and it was thought that comparisons between the results of each would be more consistent with one another if these differences were removed. As such, calculations for all species profiles within the condensed-phase portion of the ignition code were changed to be calculated separately for liquid- and gas-phase species (e.g.: all liquid-phase species fractions sum to one and all gas-phase species fractions sum to one within the condensed phase). This change necessitated the addition of an accurate void fraction to the calculations of the condensed-phase, which is given in Equation 21.

$$\frac{\partial\left[\rho(1-\Phi)\right]}{\partial t}+\frac{\partial\left[\rho u(1-\Phi)\right]}{\partial x}=\sum_{k=1}^{NumLiqSpec}\dot{\omega}_k \tag{21}$$

This equation was discretized as up-winded, identical in manner to the species mass fraction equations. Additionally, condensed-phase properties, which were originally based only on the solid-phase species, were updated to include the effects of decomposed gases as well. Physical properties for the condensed phase of both codes are now functions of temperature, composition, and void fraction.

Another change made to the condensed-phase portion of the ignition code involved the species convergence and progress of a simulation. Temperature convergence had always been fast and robust, but the species convergence was extremely slow and determined on an absolute basis. When the sum of the change of all species totaled a value that was lower than a defined criterion, the condensed phase was determined to be converged. This criterion is given in Equation 22.

$$\sum_{i=0}^{TotNodes}\sum_{j=1}^{NumSpec}\left(Ynew_{i,j}-Yprev_{i,j}\right)<ConvCrit \tag{22}$$

It is more commonly held that convergence on a relative basis is more robust than an absolute one. The new convergence of species, void fraction and temperature (all represented by Φ) is now determined by Equation 23.

$$\mathrm{Max}\left(\frac{\Phi new_{i,j} - \Phi prev_{i,j}}{\Phi prev_{i,j}}\right) < ConvCrit\ , i = 0 \ldots TotNodes,\ j = 1 \ldots NumSpec \tag{23}$$

The convergence of the condensed phase was also altered so that its effect upon the progression of the simulation would be minimized. Wall-clock calculation time for a given simulation time step is typically dominated by the gas-phase calculations (typically, 90% or more). Originally, any difficulty in the condensed-phase convergence was reduced by decreasing the time step for the entire solution. This resulted in the overall calculation time being increased significantly due to an insignificant contributor to wall-clock time. To avoid this, a multiple time step method was added to the condensed-phase solution code. This allowed for the condensed phase to take multiple time steps for each single time step of the gas phase, and has been implemented so that the number of condensed-phase time steps taken for each gas-phase time step is dictated by the difficulty of the condensed-phase solution.

Additionally, the means of transitioning one condensed-phase species into another, as was mentioned as being implemented into Phase3, was integrated into the condensed-phase portion of the ignition code. This process was significantly more involved for the ignition code than it was for Phase3 due to the nature of the condensed-phase solution for the ignition code. Current implementation transitions “adjacent” ingredient forms (eg. orthorhombic AP and cubic AP at 513 K) across a 10 K window of temperature and across a 2% void-fraction window for adjacent ingredient forms that transition at a particular void fraction. (i.e.: A temperature transition at 513 K is linearly interpolated across a temperature range from 508 to 518 K, and a decomposition transition at a void fraction of 0.3 is linearly interpolated across a void-fraction of

0.29 to 0.31.) Using a temperature window smaller than this (10K) for the current AP model resulted in an oscillatory solution due to the very exothermic initial step of the condensed-phase decomposition. The coding for this transitional ability had to be implemented individually for each ingredient and was accomplished for the HMX, AP, AP/HTPB, and AP/HTPB/Al models. If any future work on other propellants/ingredients needs to use this transitioning capability within the ignition code, either the current coding would have to be generalized in some way or additional code would have to be similarly developed to handle those new propellants/ingredients.

The largest and perhaps most glaring difference between the steady-state and ignition codes was the assumption as to when the effects of condensed-phase reactions were included. In Phase3, condensed-phase reaction rates are not calculated below the melt temperature. This assumption was consistent with numerous other modeling efforts. The ignition code, however, needs a finite reaction rate to be calculated throughout the entire condensed phase due to the mass flow rate of evolved species being important to both the condensed- and gas-phase solutions at each time step.

In Phase3, the calculated reaction rate of condensed-phase components is dependent upon both temperature and void fraction. The melt temperature condition occurs at a single position in the condensed phase and does not change unless the inputs/conditions change. The point at which the melt temperature criterion in the ignition code is met occurs first at, or near, the surface of the propellant/ingredient and then propagates back into the solid as the melt layer develops over time. As such, the rate of decomposition throughout the condensed phase at a given location varies over a large range for a given simulation. Employing a method of solution

where the reactions are "turned on" at a particular temperature, as is the case for the Phase3 code, is difficult because of the numerical instability associated with such a change.

Three means were determined by which this discrepancy between the two codes might be alleviated.

1) ignore the differences, using the reaction parameters from the steady-state model directly,but calculate them at all temperatures;

2) re-fit the condensed-phase kinetic parameters of the model in Phase3 by including the entire condensed phase in the calculations (above the initial temperature instead of just above the melt temperature), and then apply those new kinetic parameters to the ignition code;

3) ramp the reaction rate values gradually within the ignition code, once they are "turned on" at the melt temperature, to try and alleviate any possible numerical instability.

The first of these options was employed by Meredith during the initial development of the HMX ignition/cookoff model. His results showed that this was a decent assumption for HMX, with less than 5% of the simulated propellant decomposing or evaporating prior to an ignition simulation reaching the defined melt temperature. Using this option for the AP model, however, resulted in the ignition code never reaching the defined melt temperature due to sufficiently-high reaction rates being predicted in the orthorhombic and cubic phases, which is inconsistent with what has been observed for AP[28]. This seemed to imply that the difference between the kinetics of orthorhombic/cubic AP and melted AP were probably more than 2-3 orders of magnitude apart, an assumption employed by the Phase3 code due to observations similar to that of Behrens and Bulusu[119] for RDX. Thus, using the method of Meredith in applying the HMX model to the ignition code in a manner different than that employed by Phase3 would not work for AP.

Efforts made as part of the current work to find new kinetic parameters for AP using the second option were also unsuccessful. Thus, the third option was investigated and a logarithmic-

interpolation scheme was ultimately developed as part of the current work for the purpose of minimizing the numerical instability involved in turning on the condensed-phase reactions at a defined temperature. At each time step, the condensed-phase decomposition is checked at each node to see if it has more than doubled since the previous time step. If it has, then the decomposition is ramped for up to 200 time steps from that point, based on the level of disparity between the decomposition at the previous time step and the decomposition predicted for the current step. Ramping the decomposition solution in this way was very successful in predicting minimal sub-melt decomposition while still allowing for numerical convergence of the condensed-phase equations once the melt temperature criterion was reached.

Another problem with the original ignition code was that it was developed specifically for HMX. The code itself contained variables and arrays that were dimensioned and organized for the HMX reaction mechanism and were thus not directly compatible with reaction mechanisms for other ingredients. The code was generalized as part of the current work to allow for different properties and/or reaction mechanisms.

There were a number of issues that dealt with the convergence of the ignition code that were also addressed. For example, the first several time steps of a simulation would typically require a large number of non-linear iterations. The code would also typically diverge if the gas-phase solution for a particular time step took more than five non-linear iterations. Restart cases had frequent difficulty for ignition simulations, with cookoff simulations always diverging. Also, cases defined with a high number of gas-phase nodes or large number of species (as is the case for the current AP/HTPB gas-phase kinetic mechanism), would typically diverge immediately. It was found that two coding errors led to the sum of these oddities.

The first was a discrepancy between the size (in memory) of variables being passed into subroutines (mostly Petsc subroutines, but some within the subroutines of the ignition code itself) that was not being caught by the compiler. This error was corrected as part of the current work. The second issue dealt with an incompatibility between the Cantera and Petsc libraries. The Cantera installation included a partial implementation of the BLAS and LAPACK numerical libraries that was different than the version used to build the Petsc libraries. This was resolved by specifying that the Cantera installation use the version of BLAS and LAPACK that was used when building Petsc. To all appearances, the incompatibilities between these two software packages have been resolved.

Two additional changes were made to the ignition code to allow for the inclusion of aluminum in the modeled propellant. The first deals with the calculation of the thermal conductivity of a propellant when aluminum has been added to the formulation, and the second deals with the reflection of laser light from aluminum particles within the propellant.

The modeled effect of aluminum particles on the thermal conductivity of an AP/HTPB/Al propellant is calculated by applying Maxwell's approximation[120] for the effective thermal conductivity of a sphere surrounded by a continuous medium. The aluminum particles are assumed to be spherical in shape, and the AP/HTPB propellant is assumed to be a continuous phase surrounding the aluminum spheres. Maxwell's approximation is given in Equation 24.

$$k_{eff} = k_{CM}\left(1 + \frac{3\phi_S}{\left(\frac{k_S + 2k_{CM}}{k_S - k_{CM}}\right) - \phi_S}\right) \tag{24}$$

This approximation treats the effect of aluminum upon the thermal conductivity of the propellant as a deviation from the thermal conductivity of the continuous phase, AP/HTPB, and

is dependent upon the volume fraction (but not size) of aluminum in the modeled propellant. The validity of this approximation will be discussed in Chapters 4 and 5, where it has been applied to the current AP/HTPB propellant model.

The second effect that the addition of aluminum has upon a propellant, both modeled and experimentally, is an increased ability to reflect laser light. Since most sources of current ignition experimentation are handled with laser-light, this effect needed to be considered.

The size of aluminum particles used within propellants typically fall into the range of 1-100 microns in diameter, while the wavelength of laser light from a CO_2 laser is 10.6 microns. The similar size between particle diameter and wavelength of light leads to a particle-light interaction referred to as Mie scattering. The determination of how particles and light waves interact under these conditions is a non-trivial, previously-solved problem[121]. Incident light waves interacting with a solid, spherical, aluminum particle can produce one of three effects:

1) reflection, or backscattering;
2) absorption;
3) forward scattering.

The numerical results of a computer program, Bhmie-c[122], which was written using the algorithm of Bohren and Huffman, was applied to the calculations of the current ignition code to determine the extent of each outcome for incident laser-light interacting with the aluminum particles present in the modeled, semi-transparent propellant. No absorption of laser light by the aluminum is considered in the current ignition code.

The reflection sub-model in the ignition code was built upon a three-dimensional analysis of a uniformly-structured propellant and then applied to a modified version of the laser-absorption sub-model. In the current reflection sub-model, the size of a characteristic cube of

propellant is determined by setting the ratio of the volumes of a sphere and a cube (with the sphere assumed to be completely contained by the cube) using the volume fraction and particle diameter of the included aluminum. The single dimension of this characteristic cube is calculated by using Equation 25.

$$X_{cube} = \left(\frac{\pi d_{AL}^{\ 3}}{6\phi_{AL}} \right)^{\frac{1}{3}} \tag{25}$$

This characteristic dimension dictates the coverage of aluminum across a projection of the top of the cube (effective area of aluminum coverage, as viewed by the laser light and calculated by using Equation 26), and also the depth of propellant present before another characteristic cube will be reached by penetrating laser light.

$$AF_{AL} = \frac{\pi d_{AL}^{\ 2}}{4 X_{depth}^{\ 2}} \tag{26}$$

These two dimensions are illustrated in Figure 13.

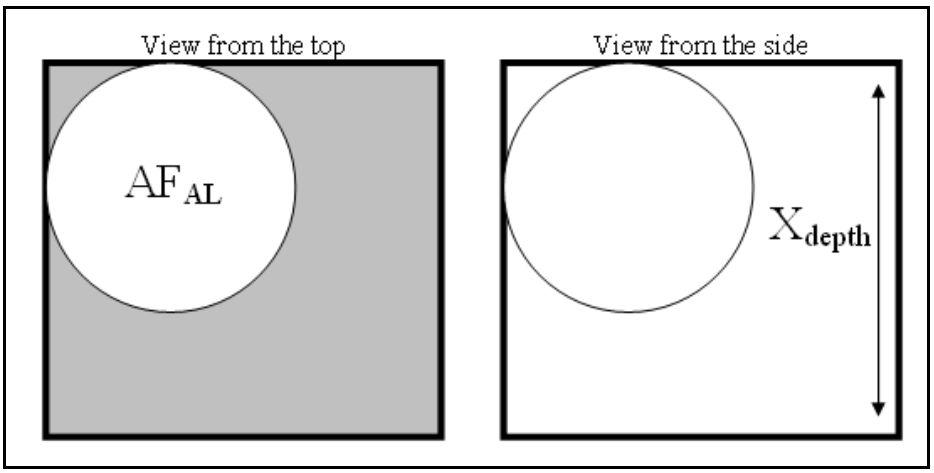

Figure 13 – Characteristic cube used in aluminum-reflection sub-model

Laser light incident upon the area fraction covered by the aluminum spheres is either back-scattered or forward-scattered according to the calculations made by the Mie code. The fraction of back-scattered light at the surface is considered to be reflected away from the propellant and lost. The fraction forward-scattered at the surface is added to the fraction of the laser falling outside the area of aluminum coverage, which sum total is then allowed to penetrate into the propellant. The laser light is absorbed into the propellant according to the current laser-absorption sub-model to a distance of X_{depth}. At this depth within the modeled propellant, a new characteristic cube is reached, and the process is repeated. For successive layers of characteristic cubes, the area fraction of aluminum is assumed to not overlap that of previous layers. Thus, the maximum depth to which the sub-model calculates aluminum reflection is: X_{depth}/AF_{Al}. Light reflected at sub-surface depths is assumed to be absorbed by the propellant as it travels back out of the propellant/ingredient. Since tens of thousands of characteristic boxes make up the modeled surface of a propellant, this approximation is assumed to be valid. An illustration of the complete aluminum-reflection sub-model is given in Figure 14, where the amount of incident laser light for each layer is equal to the sum of reflected and forward-scattered fractions at that level.

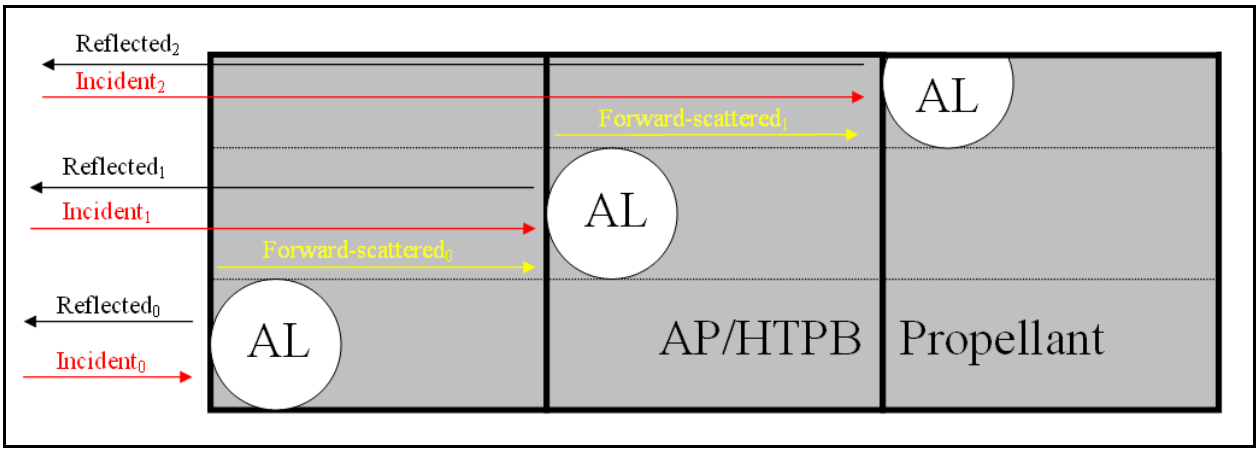

Figure 14 – Physical description of the aluminum-reflection sub-model

Laser light still present as a forward-scattered fraction after the entire cross-sectional area of the top of the characteristic cube is complete was typically a small fraction (< 15%) of the overall incident laser light at the surface of the propellant and was assumed to absorb into the propellant at greater depths without further particle interaction. This is consistent with the assumption that none of the laser light allowed for by the current sub-model that makes it to this depth will be able to back-scatter up to the surface and escape.

This implementation of light scattering due to aluminum particles has only been implemented within the condensed phase equations. Part of the results of the current work suggested that aluminum reflection of particles within the gas phase might be of importance during the transition of an ignition simulation to an augmented steady-state solution. This period of time for relatively high heat fluxes, however, involves the melting, conglomeration, and far-surface ignition of the aluminum particles. None of these effects have been considered by other models in literature to our knowledge, and thus they have not been considered as part of the current work either.

4.3 IMPROVEMENT OF THE STEADY-STATE AP MODEL

The propellant/ingredient model modifications sparked a majority of the updates to the computer codes that have previously been described. Improvements were made to the steady-state AP model with two distinct directions in mind. The first involved the extension of Gross's[17] original model to include updated sources of input from the literature, and the second was a complete re-thinking of the AP model to try and better describe the steady-state data.

The work associated with these two efforts fell beneath the wider goal of validating the AP model for laser-driven ignition events. To make laser-driven ignition predictions with

confidence, the steady-state AP model needed to be able to predict not only steady-state combustion, but laser-augmented combustion as well. Being able to accurately predict the laser-augmented burning rate is important because it is an "ending point" for the transient, laser-augmented simulations in like manner to the final flame temperature being an "ending point" for steady-state simulations. In each case, the ending point is the goal at which simulations need to arrive to be considered a valid description of simulated combustion.

4.3.1 Part 1: Updating and optimizing the Gross model

The main changes to the model inputs used by Gross in part one were to:

1) update the thermal properties of AP based on recent measurements of Parr[123];
2) decrease the melt temperature from 815 K to 735 K to keep cubic-layer thickness predictions consistent with measurements from Beckstead and Hightower[30];
3) update BYU's "universal" gas-phase mechanism for propellants by updating 14 reactions and adding 35 new reactions according to the ab-initio calculations of Lin *et al.*[124,125]. (Listed in Appendix D.)

After the above-outlined changes were made to Gross's model, the pre-exponential of the original condensed-phase reaction needed to be decreased by a factor of 20 to again predict the steady-state burning rate. To better understand the need for this change, the relationship between the condensed-phase pre-exponential and the predicted burning rate is shown in Figure 15 for both the original Gross model and the updated model for a pressure of 68 atm (1000 psi).

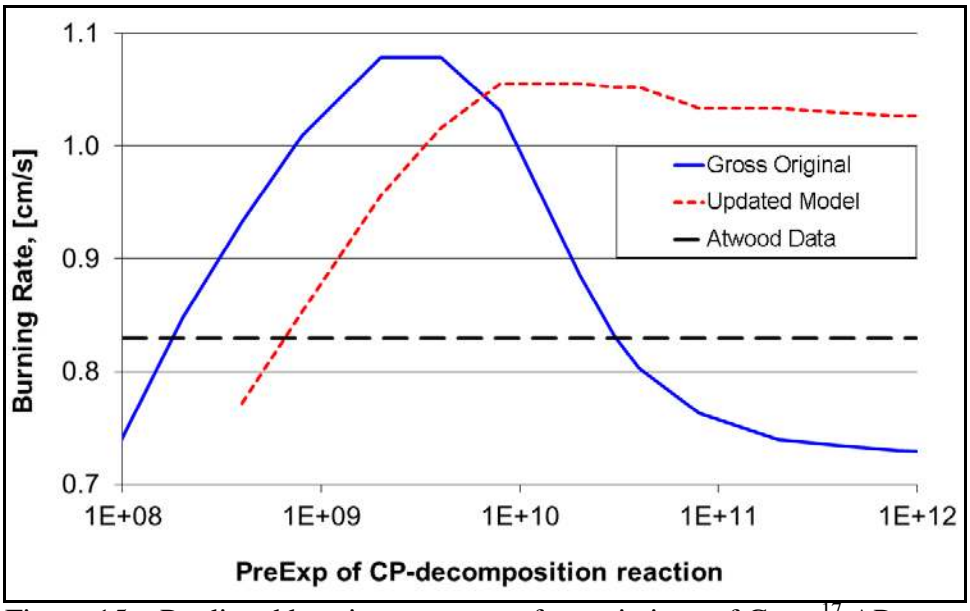

Figure 15 – Predicted burning rate range for variations of Gross[17] AP model and data[29]

Gross's original AP model[17] allowed for accurate burning rate predictions to be achieved at two separate values of condensed-phase pre-exponential rate constant. The updated model, which was completed as part of the current work, only allowed for a single intersection between the model's predictions and experimental data when using Gross's original condensed-phase decomposition reaction. Changing the pre-exponential rate constant for the updated model caused a few large changes to the predictions.

The melt-layer thickness prediction at 18 atm (300 psi) increased from 0.07 microns (original model) to 0.89 microns (updated model). Although this change was in the right direction, 0.89 microns is still less than the 1-5 micron layer that was observed by Boggs[28]. Predicted burning rate versus pressure for the updated model was decent when compared to data[28,29] (Figure 16), but the predicted temperature sensitivity was significantly higher than the data[29,37] (Figure 17).

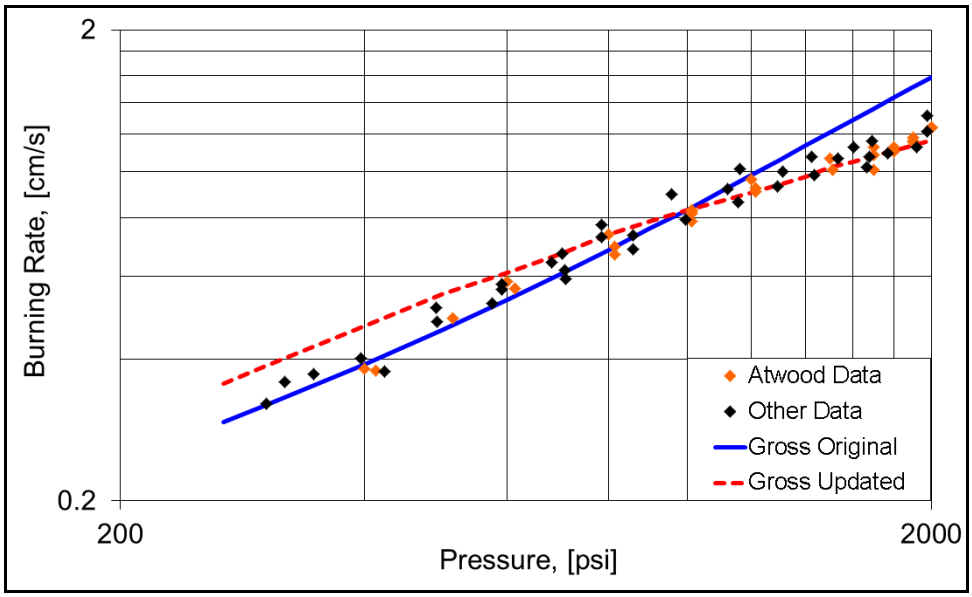

Figure 16 – Predicted burning rate for variations of Gross AP model and data[28,29], T_{init} 298K

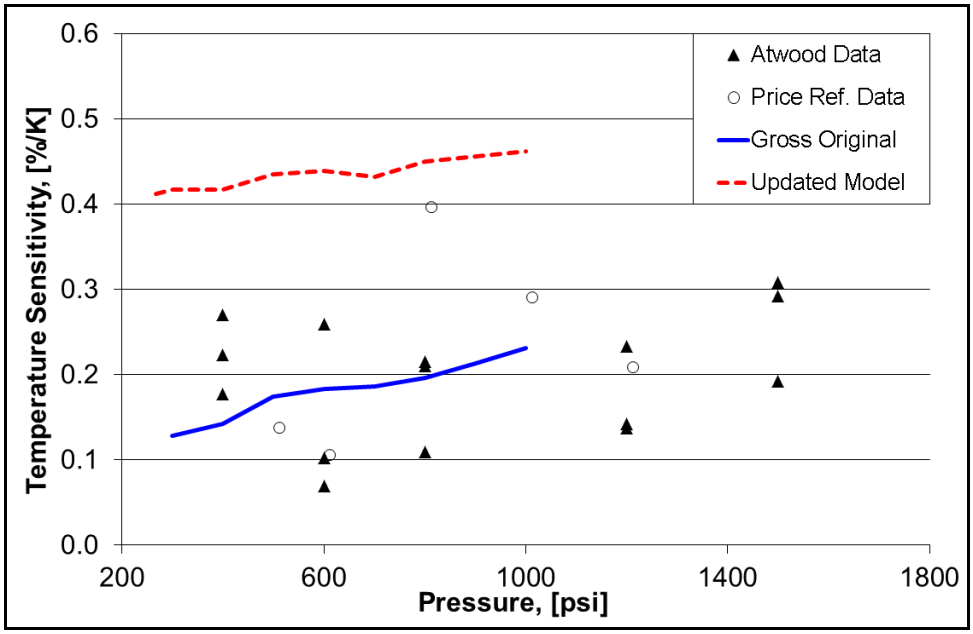

Figure 17 – Predicted temperature sensitivity for variations of Gross AP model and data[29,37]

The increase in predicted temperature sensitivity came as a result of decreasing the condensed-phase reaction pre-exponential. For surface reaction models, the condensed-phase

kinetics do not affect temperature sensitivity predictions. For in-depth condensed-phase reaction models, however, the condensed-phase kinetics cause some variance in the temperature sensitivity predictions. This variation for the original Gross model[17], which was as large as 100%, is shown in Figure 18.

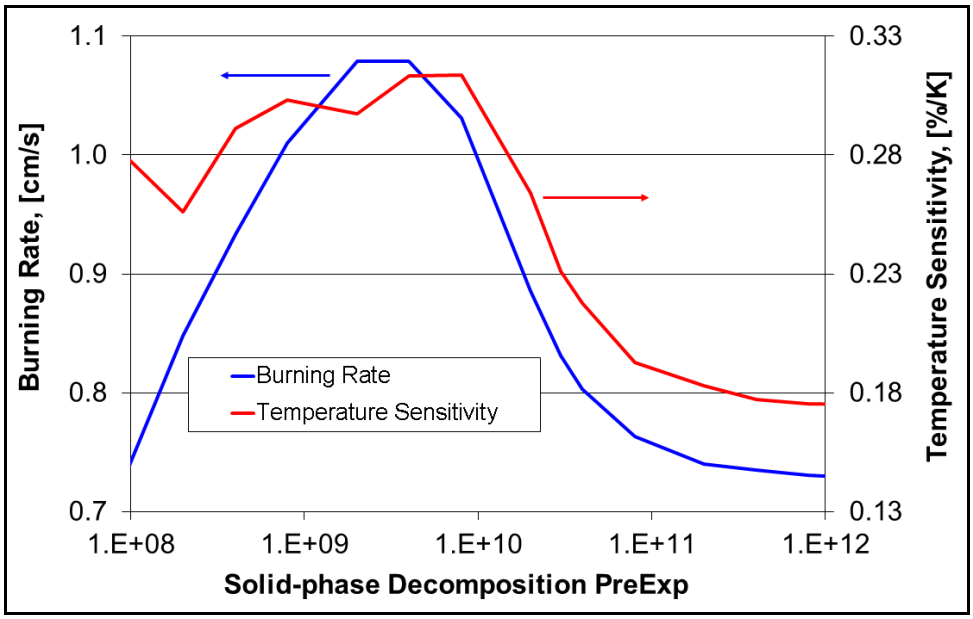

Figure 18 – Variation of predictions for Gross AP model, 68 atm

The shift in temperature sensitivity predictions for the updated AP model was concerning, since the accurate prediction of temperature sensitivity is a main point of validation for all propellant/ingredient models.

Of additional concern was that the predicted laser-augmented burning rates of both Gross's original model and the updated model were too high by ~100% when compared to data[126-129] and differed from each other by less than 3%. Laser-augmented burning rate predictions using Gross's original model are shown in Figure 19.

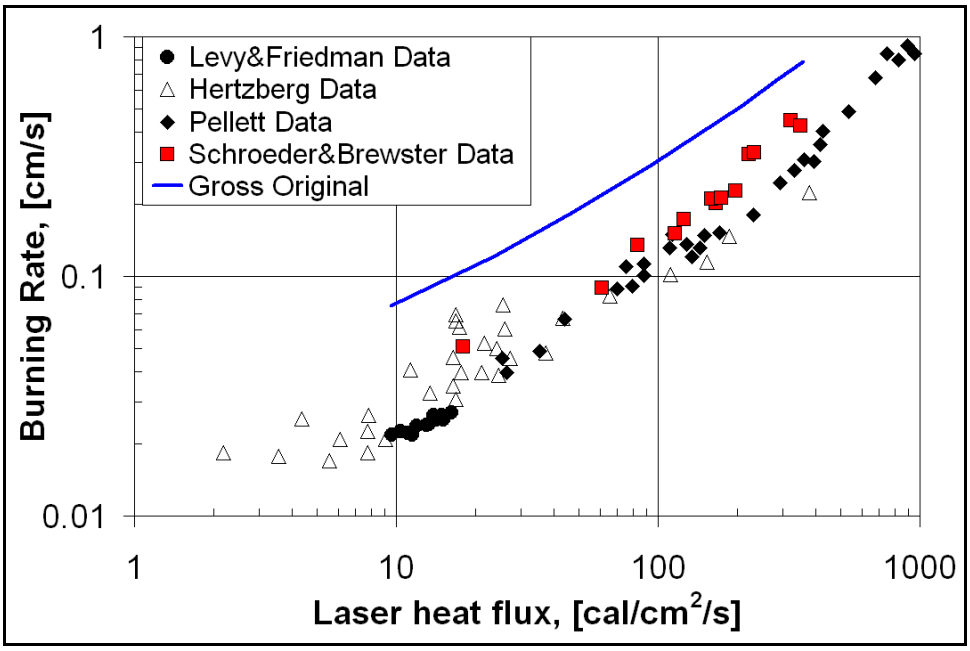

Figure 19 – Predicted laser-augmented burning rate of Gross AP model and data[126-129], 1 atm

Gross's original model was never applied to laser-augmented combustion, and so the discrepancy here is not surprising since making these kinds of predictions was not of primary concern to his work. The fact that laser-augmented predictions from the updated model changed by less than 3% was unexpected. A large parametric study was performed on the condensed-phase inputs to determine what could be done to better predict laser-augmented burning rate. It was found that the only parameter that made a significant impact (> 5%) upon these predictions was the heat release in the condensed phase. This is due to the fact that changing the condensed-phase heat release directly impacts the surface heat flux, and a change in the surface heat flux directly affects the impact of a given level of laser-heat applied at the surface of AP. For example, a laser heat flux value of 100 cal/cm^2/s will more significantly affect a model with a nominal surface heat flux of 50 cal/cm^2/s (200% increase) than it would a model with a nominal surface heat flux of 200 cal/cm^2/s (50% increase).

The predicted final species fractions of the updated model changed very little from that of Gross's original model. One of the main reasons for updating the gas-phase mechanism was to remove the need for the arbitrarily-tuned NO-elimination reaction. Without the artificially tuned NO-elimination reaction, the updates to the gas-phase mechanism resulted in the amount of over-predicted NO being reduced by a factor of two. The NO needed to be reduced by more than two orders of magnitude, however, to match equilibrium conditions. Thus the artificially-tuned NO-elimination reaction has been left in the updated gas-phase mechanism, along with the updates from Lin *et al.*, and will persist until the gas-phase kinetics can be better described by future work.

The calculated final flame temperature of the updated model for a pressure of 20 atm dropped by 3 K, to 1388 K. The predicted equilibrium flame temperature at this pressure for AP is 1394 K, a difference of 6 K, or less than 1%, which is well within reason. Of the final mole fractions, all of the species predictions were within 2% of predicted equilibrium values except for Cl_2, which was 15% too high (predicted gas-phase mole fraction = 0.014) for the updated model. This over-prediction wasn't present in the original gas-phase mechanism and represents a shift in the kinetic pathway of chlorine due to the new Lin *et al.* reactions.

When the updated model results were compared to the low-pressure data of Ermolin *et al.*[33] for surface species and temperature profile, it was decided that a new condensed-phase mechanism might need to be formulated to more accurately predict the data. After significant effort, a new condensed-phase decomposition reaction was developed that more accurately described the Ermolin data, while still using the updated gas-phase mechanism for AP. The new condensed-phase reaction based on this optimization effort is presented in Table 11 along with those used in the original and updated models. The heat of reaction was calculated at 815 K,

which was the assumed melting temperature of the original Gross AP model. A condensed-phase activation energy of 28 kcal/mol has been used for each of the condensed-phase reactions. The difference between the pre-exponential of the updated model, $1.5 \cdot 10^9$, and that of the optimized model, $6.5 \cdot 10^9$, comes from a combination of the stoichiometric coefficient of AP having been increased from 10 to 46 and the heat release of the optimized reaction having affected the predicted burning rate.

Table 11 – Condensed-phase decomposition reactions for variations of Gross[17] AP model

Reaction	**ΔH_{rxn}, [cal/gm]**	**Model**
$10AP_c \rightarrow 7O_2+13H_2O+3N_2+4NH_3+HCl+HClO_4+Cl_2+3ClO_3+3Cl$	-61.5	Original
$10AP_c \rightarrow 7O_2+13H_2O+3N_2+4NH_3+HCl+HClO_4+Cl_2+3ClO_3+3Cl$	-61.5	Updated
$46AP_c \rightarrow 6O_2+36H_2O+3N_2+22NH_3+16HCl+30HClO_4+14NO+N_2O$	-1.7	Optimized

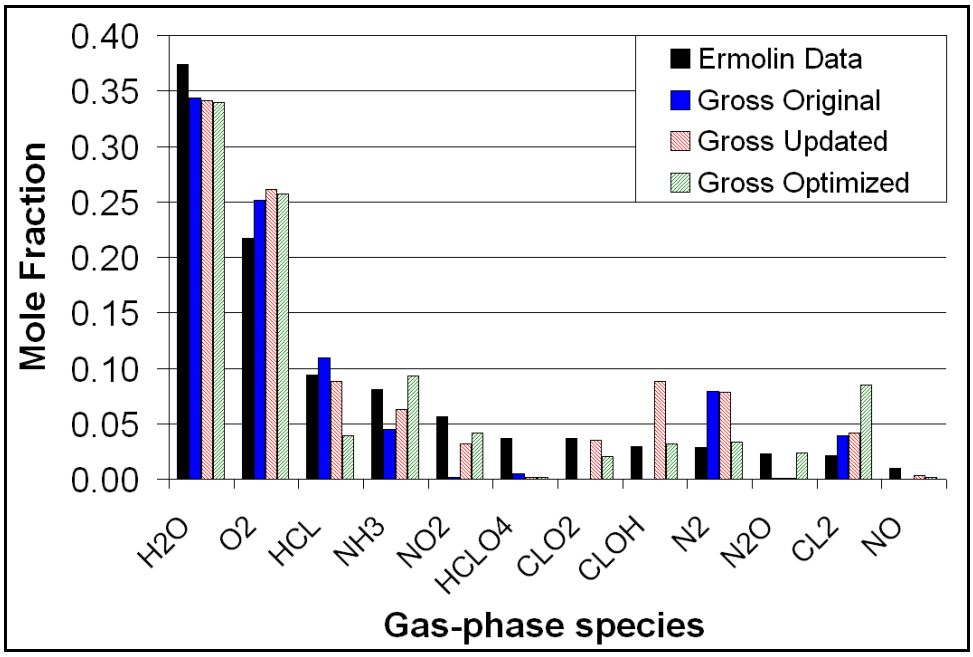

Figure 20 – Predicted surface species for variations of Gross AP model and data[33], 0.592 atm, T_{init} 533K

For the most part, the predicted surface species presented in Figure 20 varied little between the various models; some species are higher, some are lower, but all are reasonable. At least there are no missing surface species in the optimized model as there were in the previous two versions of the AP model. The predicted temperature profile of the optimized model, which is important for predicting burning rate, showed significantly better results. A comparison of the three variants of the AP model and the measured temperature data of Tereshchenko and Korobeinichev[130] is shown in Figure 21 (note: the x-axis has the same units in both plots).

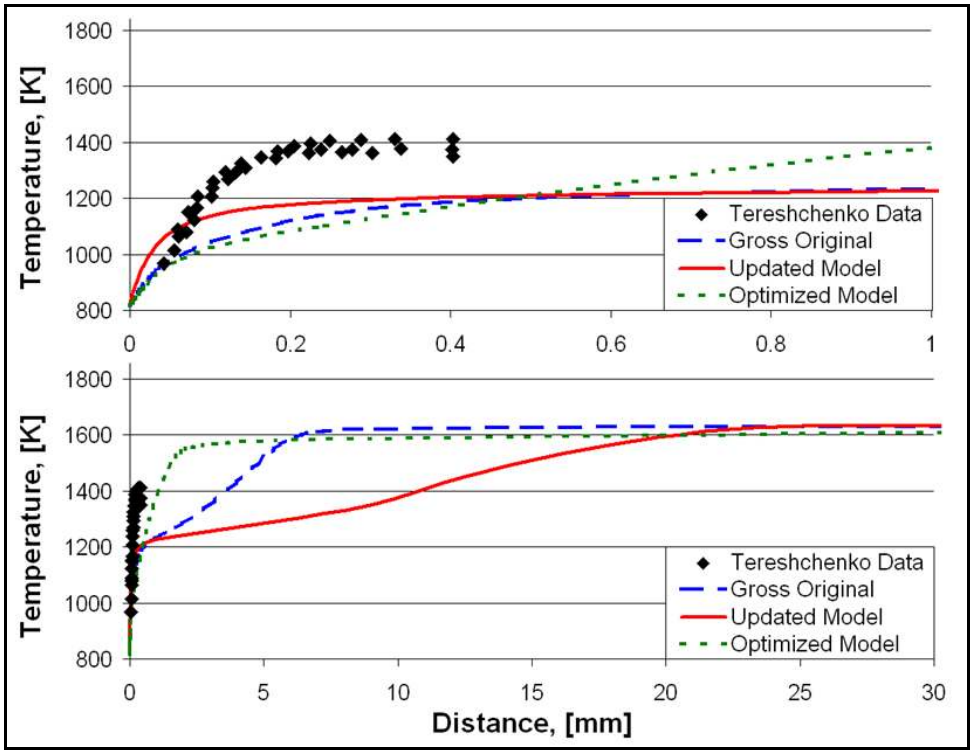

Figure 21 – Predicted temperature profile for variations of Gross AP model, 0.592 atm, T_{init} 533K, and data[130]

In this comparison, all three variations of the AP model seem to fall short of accurately describing the measured temperature profile in the region near the surface of the propellant ($x < 0.5$ mm). In the far field, each of the variations of the Gross model predict a final flame

temperature just above 1600 K, which is consistent with equilibrium calculations for conditions equal to the experiment but different than the data, which level out at around 1400 K. This discrepancy may be due to radiative heat losses but has not been invesitgated.

The above comparison suggested that additional work would be needed to describe the AP combustion at these conditions. It was uncertain how the under-prediction of the temperature profile at these low pressures would affect the predictions at higher pressure, where the accuracy of the solution was most desired. The optimized version of the model showed very little change in the temperature sensitivity, steady-state burning rate, or laser-augmented burning rate predictions when compared to that of the updated model. As such, it was necessary to look deeper into the underlying mechanics of the model and search for how the condensed-phase kinetics and heat release of the AP model might be more accurately described such that it could predict a larger set of data that included both temperature sensitivity (again) and laser-augmented burning rate.

4.3.2 Part 2: Rethinking the AP Model

There were a number of goals accomplished in this part of the current work. It had been seen in part one of the AP model work that steady-state combustion descriptors (burning rate, surface temperature, melt-layer thickness, final flame temperature/species, and temperature sensitivity) could be predicted satisfactorily, but that:

1) the laser-augmented burning rate for all the variations of Gross's AP model were significantly higher than what the data suggested, and
2) the calculated temperature sensitivity increased significantly when updates were made to the model, while other steady-state predictions stayed relatively constant.

These concerns needed to be addressed so that the AP model could later be applied to the ignition code with confidence.

One question that has been raised about AP is whether the condensed-phase decomposition is endothermic or exothermic. Both experimental and modeling efforts have been completed in the past that have presented the "correct" description as being one way or the other, though considerably more of them have suggested that it should be exothermic. In like manner to those publications of the past, the reasoning behind the choices made in determining the heat release for the AP model developed in Part 2 of the current work are presented here.

A very wide-ranged investigation of experimental data collected through thermo-gravimetric analysis (TGA) and differential scanning calorimetry (DSC) in the literature was completed by Vyazovkin and Wight[131] in 1999, as discussed in Chapter 2. They found that DSC data typically show three thermal events for AP between pristine conditions and complete decomposition. The first is the endothermic phase transition from the orthorhombic phase to the cubic phase at 513 K. The second is an exothermic peak, which reaches a maximum at ~27% decomposition (according to DSC experiments they completed as part of their work). The third event was found to be either exothermic *or* endothermic and that the determination of such was *dependent upon the conditions of the experiment*. For experiments where the decomposed gases of the second thermal event were kept within close proximity of the decomposing solid, the third thermal event was reported to be exothermic. If, however, the decomposed gases from the second thermal event were allowed to escape, or were purposefully removed from the system (for example, through vacuum), the final event was endothermic. Furthermore, when the decomposed gases of AP were removed, the slow-down associated with AP decomposition after ~30% of the solid had decomposed was associated with a change from an exothermic to endothermic process. T-Jump/FTIR data[132] from Brill *et al.* for AP at 13 atm and ~715 K show

similar results for the two decomposition-driven thermal events: the first decomposition event, an exothermic spike, is quickly followed by a second, much longer, endothermic tail.

Determining the necessary heat release for the condensed and gas phases in the current AP model was a difficult and time-intensive project. In completing this, the theory of older, more basic propellant models was reviewed. As part of this review, the results of the BDP[14] model were duplicated in Mathcad with a desire to understand how these simpler models performed and what could be learned from them. These efforts led to the realization that a propellant model could be formulated such that the balance of heat released in the condensed and gas phases varied significantly, and yet could still match burning rate versus pressure data accurately—a concept that is consistent with what has been previously reported in the literature[14]. In essence, a model with a condensed phase that is very endothermic coupled to a gas phase that is very exothermic, works just as well for making burning rate predictions as does a model with a condensed phase that is exothermic coupled to a gas phase that is also exothermic. The important part of coupling the two phases to one another, as discussed in the BDP papers[14], is to always have the predicted final flame temperature equal to the equilibrium flame temperature and thus conserve energy within the model's calculations.

Thus there is a given amount of uncertainty inherent in every propellant/ingredient model that is only validated against steady-state burning rate data. One good way to validate propellant models further is to compare their predictions to collected data that determine how the propellant responds to a given application of heat. Two such data sets are temperature sensitivity and laser-augmented burning rate. A third that has previously been used for this purpose, time to ignition, is probably not very helpful for AP since it has been observed[65] that there is essentially no decomposition of AP prior to the ignition point, and thus the heat release of the decomposition

should not directly influence these kinds of predictions. However, for ingredients such as HMX or AP/HTPB propellants, which have a significant amount of decomposition that occurs prior to the ignition point, this kind of analysis would be very pertinent.

After a considerable amount of effort, it was decided that in order for the AP model to predict these two sets of additional data, the condensed-phase heat release (originally proposed by Gross[17] to be +42 cal/gm, exothermic) needed to be endothermic instead. Two additional results strengthened consideration of this matter.

The first came from the work of Korobeinichev,[133] wherein he reported that to predict the measured concentration profiles of Ermolin *et al.*[134], the condensed-phase decomposition reaction of his model had to be structured such that 20-30% of the solid decomposed to give final products (an exothermic process), and the remaining 70-80% decomposed to give sublimation products and intermediates (an endothermic process). Korobeinichev suggested three possible decomposition reactions as part of this study, all of which were endothermic. Each suggested reaction, however, had inaccurate atomic balances and thus were not used by the current work.

The second result that strengthened the suggestion that the condensed-phase decomposition of AP should be endothermic came as a result of analyzing the condensed-phase portion of the model with a formal Design of Experiment (DoE) using a statistical software package, Jmp[135], to determine where the optimal solution of the described numerical space for the AP model was located. A Design of Experiment involves creating a system of linear equations and optimally selecting levels of each linear coefficient through a series of experimental runs to create a predictive model for the system. The system is then optimized by solving this set of linear equations. The parameters varied in this specific case were the condensed-phase pre-exponential, the condensed-phase heat release, and the gas-phase surface

heat flux. The predictions for each level of analysis were completed by using the AP model within the Phase3 code. The goal of this sub-study was to optimize both the steady-state burning rate and the temperature sensitivity of AP to those values observed in experimental data. The design space for this part of the work is shown in Appendix A, Table A1and Table A2.

The optimized DoE solution showed that the condensed-phase heat release at 1000 psi should be approximately -200 cal/gm (endothermic). At a temperature of 815 K (the defined melting temperature for the Gross model), the sublimation of AP (Equation 27)

$$AP \rightarrow NH_3 + HClO_4 \tag{27}$$

has a heat release of -365 cal/gm (endothermic). Thus it was determined that an optimal solution for the condensed-phase decomposition of AP could be one in which a majority of the decomposition products proceed through the sublimation pathway. Most investigators of the past, however, have suggested that the endothermic, dissociative sublimation reaction is the first decomposition step of AP and constitutes a minor portion of the overall exothermic decomposition. This suggestion, however, is in conflict with the collected observations of Vyazovkin and Wight[131] that the first decomposition step is exothermic in nature. All these various suggestions were taken into account and weighed against their effects upon the AP model, but it was ultimately decided that the AP model should have an endothermic description for the condensed phase as the results of the current work continually pointed in that direction.

Accordingly, the AP model in the current work was assembled using the following list of constraints and assumptions. It should:

1) include a two-step, serial-decomposition scheme to mirror low-temperature decomposition observations;
2) assume the first decomposition step (30%) to be exothermic;

3) assume the second decomposition step (70%) to be endothermic and contain mainly products from the dissociative sublimation of AP;

4) employ the gas-phase mechanism of Ermolin *et al.*[45,46] to describe the surface species, near-surface species profiles, and temperature profile of available data;

5) apply the condensed-phase work of Zhu and Lin[136], setting the activation energy of the initial exothermic step to 28 kcal/mol and the subsequent endothermic, sublimation step to 45 kcal/mol.

The main concept applied to the condensed-phase development of the AP model for the current work was to follow the low-temperature decomposition behavior of AP. This is most succinctly shown in the work of Behrens and Minier[24], where, for a given AP decomposition case that did not restrict the evolved species from escaping (chosen for presentation here as per the findings of the literature review by Vyazovkin and Wight[131]), there is first an evolution of near-final products that continues until ~30% of the mass has decomposed, and then an evolution of NH_3 and $HClO_4$ that is consistent with a shift to the sublimation pathway. They do not attempt to explain why this shift occurs, or under what conditions the shift may apply, but for the current work it is assumed that the condensed phase undergoes an identical shift in the decomposition regime to that observed during low-temperature decomposition. In the current work, the transition from the exothermic pathway (decomposition to near-final products) to the endothermic one (sublimation) within the model is assumed to occur after 30% of the mass of AP has decomposed. This is consistent with the phenomena observed by others where initial decomposition sites on AP crystals decompose to a local level of ~30% and then decomposition slows considerably[22,25,26,137]. The analogue to this phenomenon at higher-pressure steady-state burning conditions is that when the very active, bubbling froth of the AP melt layer contains more than 30% decomposed gases within a nucleus of a given (but unknown and thus undefined) size, then the decomposition pathway switches to an endothermic one. There is a possibility that

this same reasoning leads to the pressure deflagration limit (frothy layer collapses due to the balance between the rate of decomposing gases and the surface tension of liquid AP passing a critical point, thus leading to a large decrease in local nuclei with more than 30% decomposed gases) but was beyond the scope of this project.

The choice to split the condensed-phase decomposition into two parts also followed the first-principles study of Zhu and Lin[136] and their identification of two pathways through which the decomposition of AP could occur. The first was for the molecular complex H_3N—$HOClO_3$ (AP) to be released from the surface into the gas phase. This process, according to their calculations, has an activation energy of 28.1 kcal/mol, which is very consistent with what has been reported for AP decomposition, though previously this activation energy has been associated with the dissociative sublimation of NH_3 and $HClO_4$. The second pathway they found to be available for AP decomposition is through the dissociative sublimation of NH_3 and $HOClO_3$ from the surface. According to their calculations, the process of releasing the NH_3 molecule from the surface has an activation energy of 45.3 kcal/mol, and that for $HOClO_3$ is 43.5 kcal/mol. A single value for the sublimation of AP to NH_3 and $HClO_4$ of 45 kcal/mol was used in the current AP model.

A two-step condensed-phase mechanism was developed as part of the current work to describe AP combustion and predict the experimental observations of Ermolin *et al.*[33] and is presented in Table 12, with heat of reaction being calculated at the melt temperature of 735 K.

Table 12 – Proposed decomposition reactions for current AP model

Reaction	**ΔH_{rxn}, [cal/gm]**	**A, [s^{-1}]**	**E_a, [cal/mol]**
$12AP \rightarrow 4NO+2N_2O+4NH_2+9O_2+16H_2O+8ClOH+2Cl_2$	-53.6	$4 \cdot 10^8$	28,000
$AP \rightarrow NH_3+HClO_4$	387	$2 \cdot 10^{14}$	45,000

Calculations made as part of the current work showed that the pre-exponential of the exothermic, partial-decomposition reaction didn't affect any of the pertinent results. Thus, an intermediate value was used such that the completion of the exothermic reaction approximately coincided with the significant decomposition of the endothermic reaction to avoid plateaus in the predicted decomposition profile. Additionally, it was noted that a similar discrepancy in the final species fractions for NO, N_2, and O_2 was present in the predictions of the current model in a manner similar to the Gross model. Thus, the NO-elimination reaction of Gross was added to Ermolin's gas-phase mechanism and used to make predictions for the final model.

A comparison between the data of Ermolin *et al.*[33] and the predictions of both the current AP model and the prior three variations based on Gross's model is given in Figure 22.

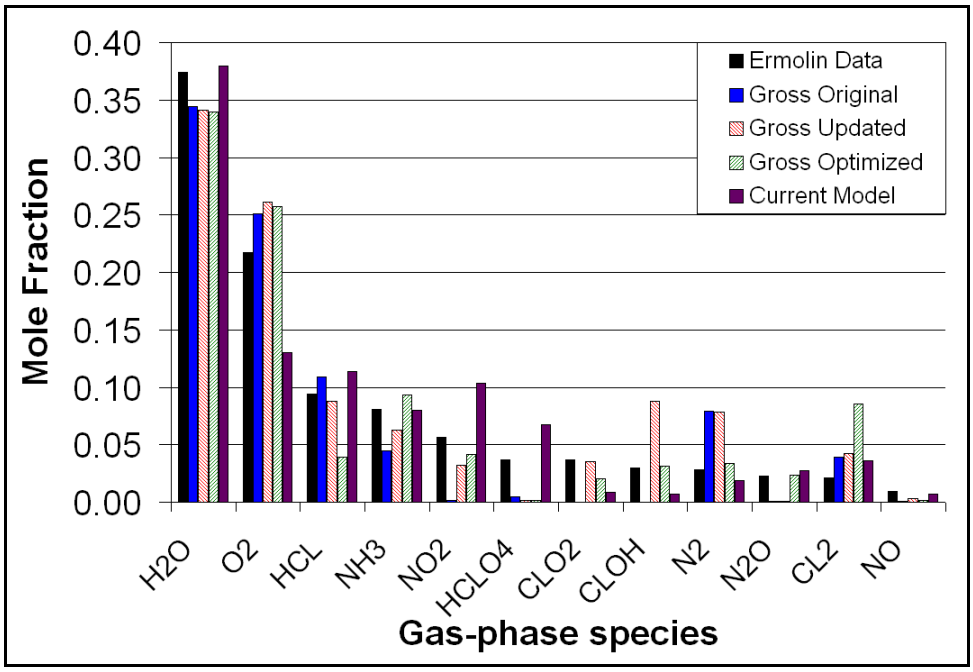

Figure 22 – Predicted surface species for variations of Gross AP model and data[33], 0.592 atm, T_{init} 533K

For the most part, the surface species predicted by the current AP model are very similar to those given by the optimized Gross model. $HClO_4$ is over-predicted now, whereas the previous versions have shown relatively little of this species at the surface. This prediction is attributed to the fact that the endothermic reaction (now 70% of the decomposition) includes only sublimation products (NH_3 and $HClO_4$) and does not include any radicals as Korobeinichev has suggested should be present within the sub-surface reaction zone.

One other major difference that arose as part of these changes to the AP model was the under-prediction of O_2 at the surface for the current model. One of the unexplained artifacts of the Ermolin and Korobeinichev work with AP was that their measured data showed a minimum in the O_2 mole fraction profile approximately 75 microns from the surface, which had not been seen previously in experimentation. This minimum was also still present when the mass fraction profiles were calculated from their data as part of the current work.

Their data, taken through mass spectrometric probing, discerned which species were present by determining the molecular weight of each measured species and then comparing those weights to species that could possibly be present. One difficulty inherent in such an analysis is that species with identical molecular weights will be impossible to differentiate from one another. There are three such overlaps within the list of possible measured species that would need to be differentiated from one another to have complete confidence in the data. These pairs are presented in Table 13.

Table 13 – Species pairs for the AP system

Compound	MW	Notes
NH3	17	Reported
OH	17	Probably small
H2O	18	Reported
NH4	18	Probably small
O2	32	Reported
NH2O	32	***Unknown***

Of these three pairs, the only one that probably can't be safely ignored is O_2-NH_2O. The reduction of NH_3 by oxygen and/or oxygen containing species, which has been investigated extensively in literature unrelated to propellant research, routinely includes NH_2O. The possibility of an overlap of NH_2O and O_2 is especially significant in light of two details. First, Korobeinichev[133] found that the inputs necessary for his model to predict the collected data of temperature and species profiles, when applying the Ermolin *et al.*[45,46] gas-phase mechanism, included 70-80% of the AP decomposition moving through the sublimation pathway. With such a large fraction of the AP decomposing to give NH_3, it seems probable that the concentration of NH_2O might possibly be higher than what has been presented by the data (<1%), since less than ~15% of the resulting decomposed NH_3 is still present by the time it reaches the surface.

The second detail that makes these data slightly suspect is the overall imbalance of atomic species reported at the surface. An atomic balance of the Ermolin *et al.*[33] surface species data is presented in Table 14 along with another option, which involves the inclusion of NH_2O.

Table 14 – Atomic balance of AP surface species data[33]

	CL	H	O	N
Data	96%	93%	113%	87%
Option	96%	101%	101%	104%

In this case, the data show that there is too much oxygen and too little nitrogen in equal but opposite amounts, with chlorine and hydrogen falling within ~5% of perfect balance. This imbalance of the atomic species of nitrogen and oxygen disappears within 150 microns of the surface, which coincidentally occurs downstream of the reported minimum in the O_2 profile. It was found by interpolation that replacing 30% of the reported O_2 at the surface with NH_2O (as both of these species have the same molecular weight) resulted in achieving a much more favorable atomic balance throughout the gas phase and is presented as the option in Table 14, showing all elements within 5% of atomic balance. This suggestion is approximately described by Figure 23, with the sum of the two profiles being an accurate representation of the data.

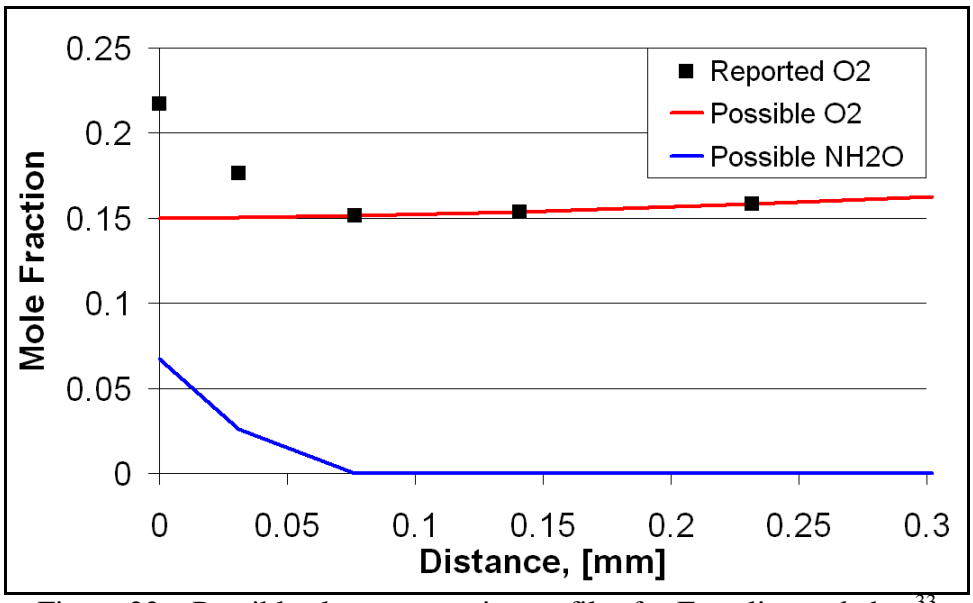

Figure 23 – Possible alternate species profiles for Ermolin *et al.* data[33]

Ermolin *et al.* have not included NH_2O in their final analysis of their AP gas phase mechanism in any of their published work that could be found, although the species has received initial investigation[138]. Although the above description is a possible simple answer to both the

atomic imbalance and the unexpected minimum in the O_2 profile, it is only a hypothesis posited by the results of the current work and has not been tested to any further degree. Thus for the purposes of the current work, the discrepancy of predicted O_2 at the surface has been set aside until the effects of including NH_2O in the overall gas-phase mechanism of AP can be determined. As an aside, making the above change to the data brings the O_2 mole fraction at the surface down to ~0.15, which is very close to the value predicted by the current AP model.

The current AP model was compared to the temperature profile near the surface of AP, as the previous model variations were in Figure 19. A comparison of all variations of the AP model explored by the current work is given in Figure 24 (note: the x-axis has the same units in both plots).

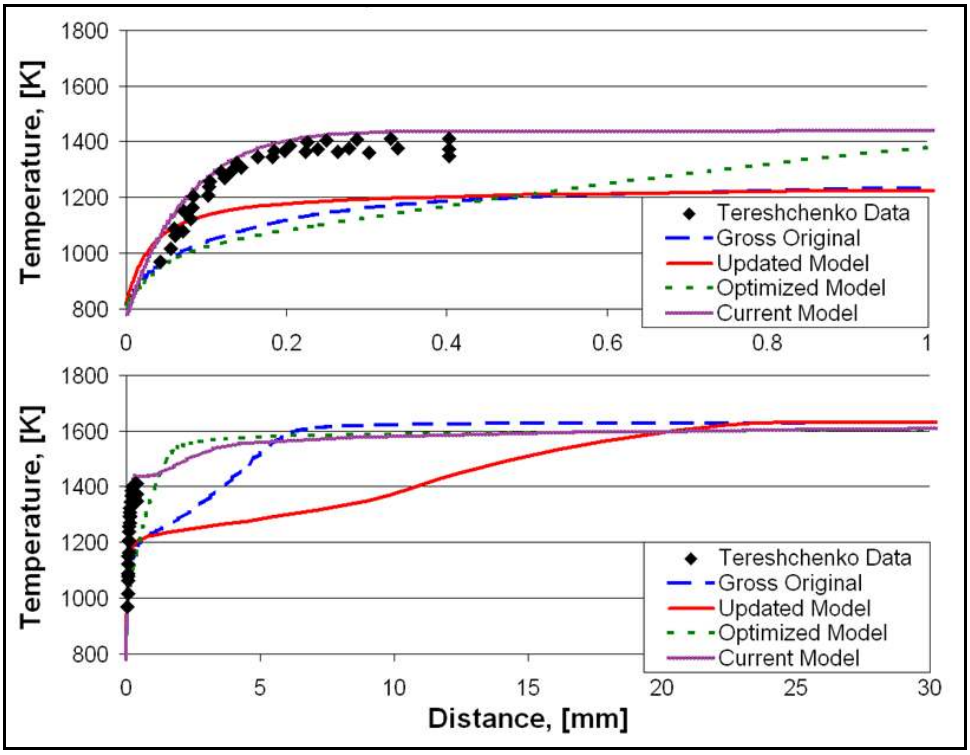

Figure 24 – Predicted temperature profiles for variations of Gross AP model and data[130], 0.592 atm, T_{init} 533K

The current model picks up the near-surface temperature rise within the first 0.25 mm much better than any of the previous models; although, the actual progression of the profile past 0.5 mm is oddly shaped. This shape is most likely due to the lack of some particular species in the condensed-phase decomposition reaction, and is similar to that seen in the Beckstead *et al.*[44] work for AP. In Korobeinichev's work, he stated that 70-80% of the condensed-phase decomposed to sublimation products and radicals. The possibility of including radicals as part of the sublimation reaction for the current AP model was given a small amount of attention but ultimately abandoned as the first several attempts made only minimal effect upon the predictions. Further work should be accomplished in this regard, since radicals more than likely play a significant role in this system and are not taken into account by the current AP model.

The burning rate prediction of the current AP model as it compares to experimental data[28,29] and Gross's original predictions is shown in Figure 25.

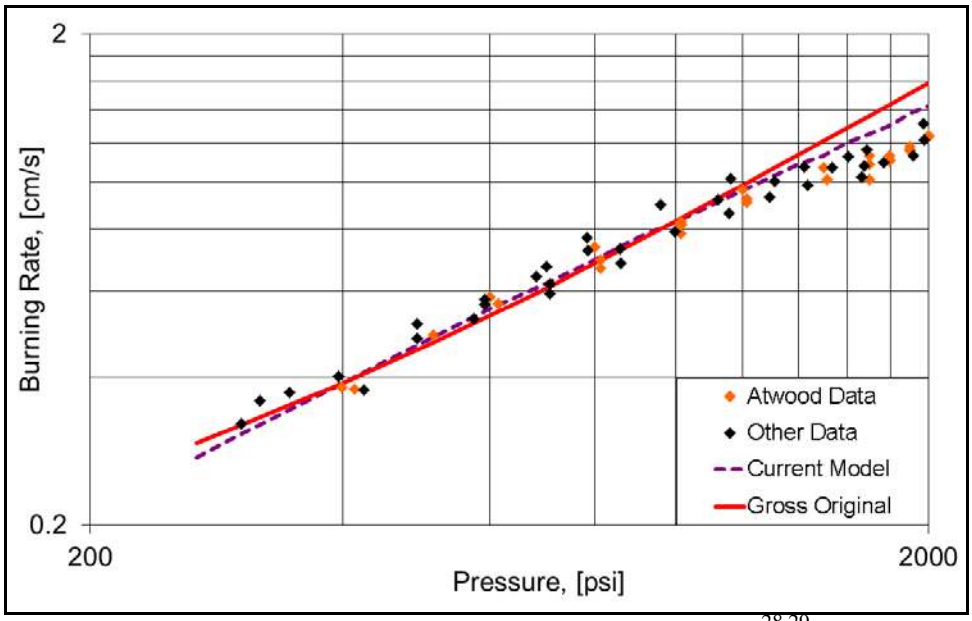

Figure 25 – Predicted burning rate of AP models and data[28,29], T_{init} 298K

The burning rate predictions aren't significantly different than those calculated by Gross's original model or the variations of his model that were reported in Figure 16. This was anticipated and even expected as per the discussion in Chapter 2 about propellant/ingredient models being able to accurately predict burning rate versus pressure. As opposed to any of the previous variations of the AP model however, the predicted melt-layer thickness of the current AP model varies between 2 and 3 microns across the first and second pressure regions and decreases with increasing pressure, which is consistent with experimental observation[28].

Predicted surface temperatures for the current model (Figure 26) fall between 890 and 970 K over a pressure range of 18 to 68 atm (300 to 1000 psi). Current predictions are now within the scatter of the data[139-143] and have a good trend. Model predictions are only reported here for pressures above a burning rate of ~0.3 cm/s, since that burning rate corresponds to a pressure approximately equal to the PDL of AP.

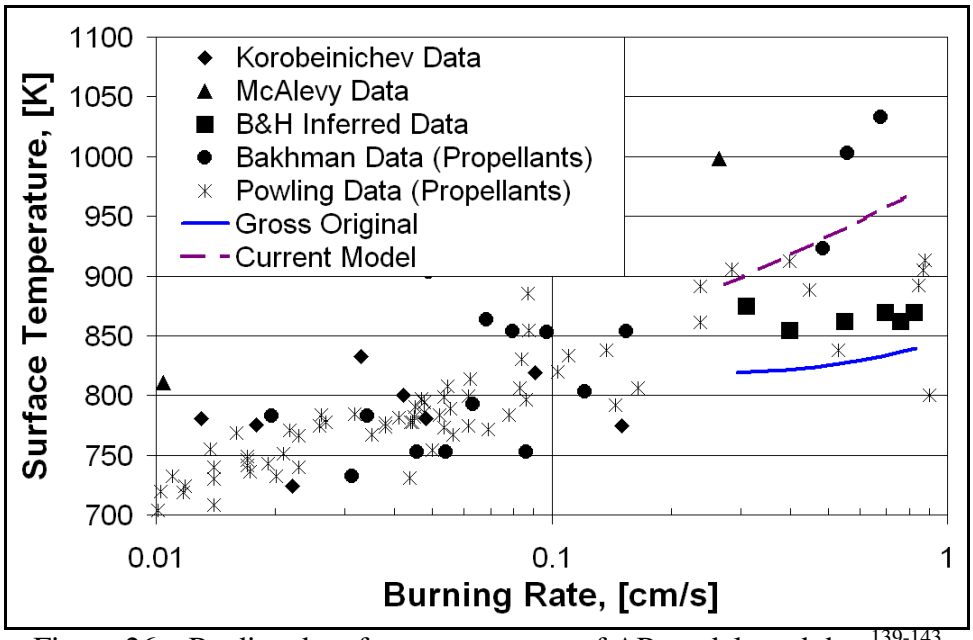

Figure 26 – Predicted surface temperature of AP models and data[139-143]

The surface temperature is defined in the model as the point at which 0.0001% of the condensed-phase propellant remains. Bulk measurements would most likely be lower than the predicted surface temperatures of an accurate model, and thus the current predictions are considered to be within a reasonable range.

The predicted temperature sensitivity (Figure 27) and laser-augmented burning rate (Figure 28) of the current AP model are more consistent with experimental data[29,37,126-129] than previous variants of the AP model. Comparison between the predictions of the new model and the data is quite good.

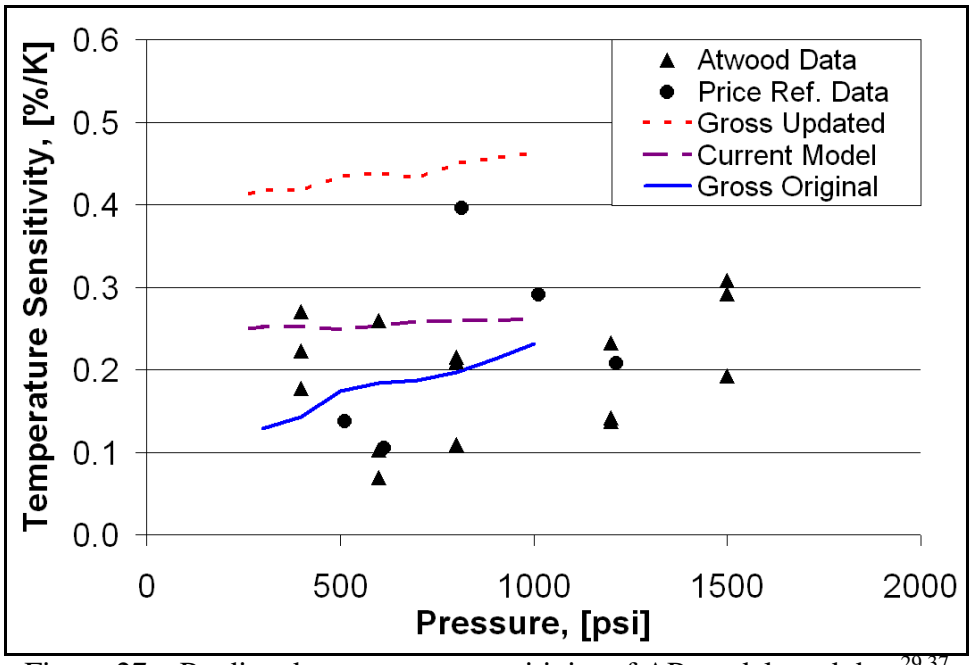

Figure 27 – Predicted temperature sensitivity of AP models and data[29,37]

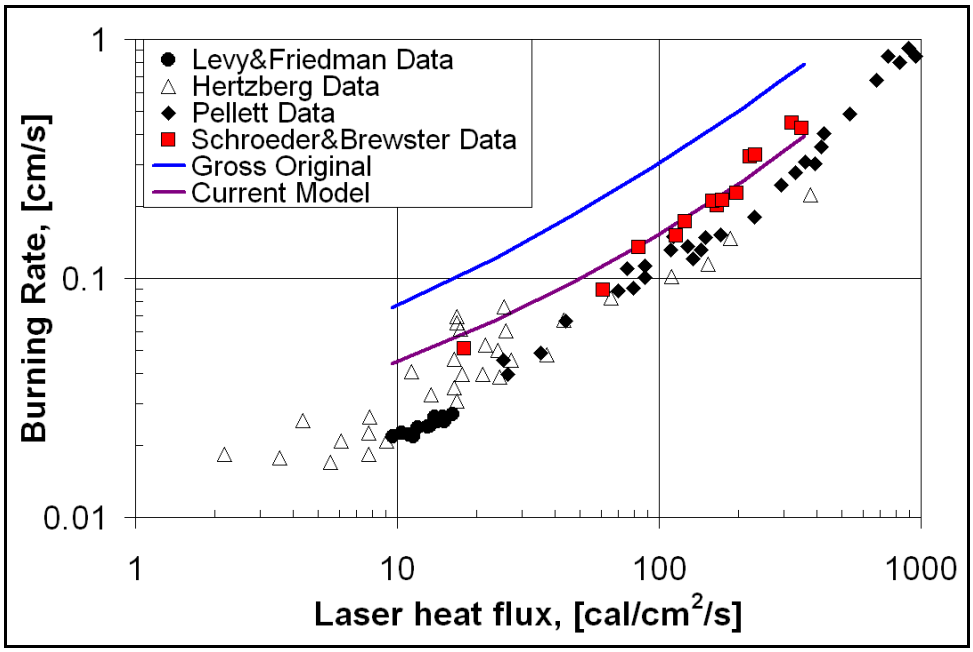

Figure 28 – Predicted laser-augmented burning rate of AP models and data[126-129]

The relationship between burning rate and applied heat flux from the laser-augmented combustion data begs that another comparison be made as well. A relationship between the applied heat flux of the laser augmented data[126-129] (above 0.25 cm/s) and steady-state burning rate data of AP[29] was determined by a least-squares regression. Linear and parabolic fits varied little from one another, and so the linear fit was used for comparative purposes. Using this relationship, a plot was constructed to show the correlation between the surface heat flux of AP for steady-state conditions and the pressure of the system. This relationship, which assumes that the heat flux applied by the laser is quantitatively equivalent to heat conduction from a flame (an assumption identical to that made by Phase3 for predicting laser-augmented burning), was then compared to the surface heat flux predictions for both the original Gross AP model and the new AP model. This comparison is given in Figure 29.

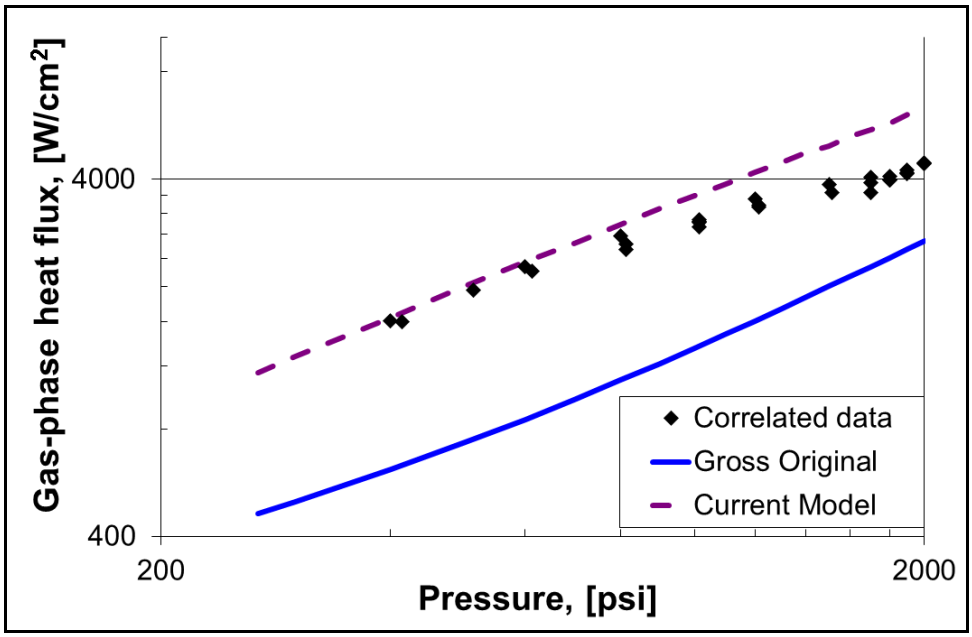

Figure 29 – Predicted gas-phase surface heat flux of AP models and correlated data[29,126-129]

The new model is considerably closer to the combined experimental data points than the Gross model. For the case of laser-augmented combustion, there are two factors influencing the amount of heat applied to the surface of AP. The first is the laser itself, and the second is the heat conducted back to the surface due to the flame. This analysis assumes perfect application of the laser heat flux to the surface of the monopropellant, whereas it has been observed[144] that AP reflects approximately 7.5% of applied laser light at a wavelength of 10.6 microns. This is consistent with the additional observation that the attenuation of a laser for HMX cases has been observed[145] to be less than 15% and AP has none of the effects seen to influence HMX laser-augmented conditions (liquid droplets above the propellant surface, absorbing gas-phase species, etc). The apparent decrease in the amount of heat actually absorbed by the propellant from the applied laser due to reflection and other considerations might also become more pronounced as the laser heat flux increases to very large values, although this has not been reported in literature

as having been observed and has therefore not been included in this analysis of the AP model. Additionally, any flame that might be present under laser-augmented burning conditions would probably be blown considerably far from the surface, as per the observations of Parr[146,147] and not make any significant impact upon the burning rate.

4.3.3 *SUMMARY*

Updates to the original Gross AP steady-state model were made to both keep the model up to date with various sources of literature and hopefully remove the need for the arbitrarily-tuned NO-elimination reaction within the gas-phase mechanism. The changes made reduced the mole fraction of NO in the final products by a factor of two, though it needed to be reduced by a factor of ~100% to predict equilibrium conditions. Updating the model resulted in temperature sensitivity predictions increasing by 2.5 times, which are significantly higher the data. Predictions of the melt layer thickness for the updated model grew by a factor of 12, but are still too thin as compared to the observed data.

Variants of Gross's AP model (original, updated, optimized), although able to predict many experimental data sets for combustion at steady state, were unable to accurately predict the laser-augmented burning rate of the crystal. As such, a new AP model was developed to include an overall endothermic condensed phase heat release and a previous gas-phase mechanism. The current AP model predicts all of the same experimental data sets that the variants of the Gross AP model did, and in addition can now predict the laser-augmented burning rate and low-pressure temperature profile data presented in the literature.

The work completed for the AP model that has been presented in Chapter 4.3 is shown in Figure 30 within the validation structure first presented in Chapter 3.

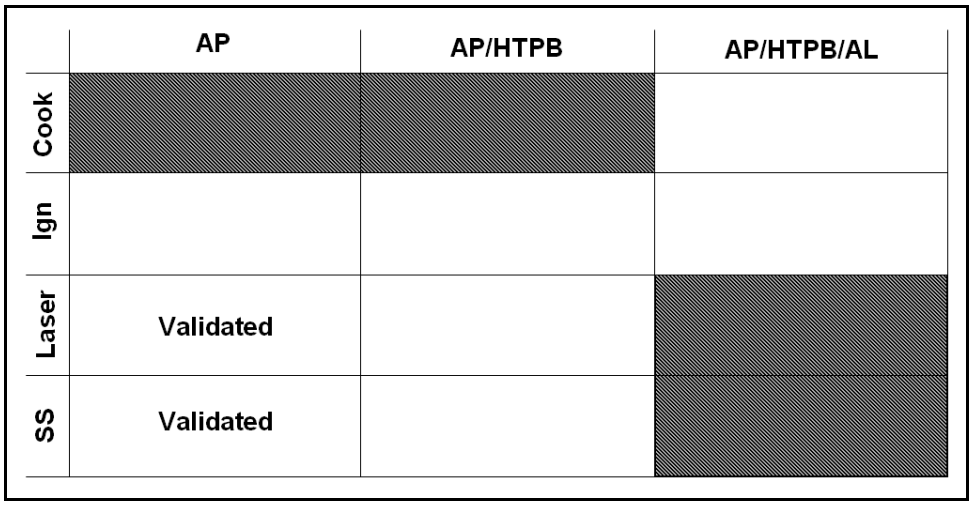

Figure 30 – Validation structure including work on the current AP model

4.4 IMPROVEMENT OF THE STEADY-STATE AP/HTPB MODEL

Two previous attempts have been made to model the steady-state combustion of AP/HTPB propellants at BYU[7,62]. The process of developing composite propellant models is much more complex than that for single propellants/ingredients (HMX, RDX, or AP) because they must be validated with respect to variations in propellant formulation as well. Additionally, interactions between condensed-phase species of each ingredient, resulting changes in decomposition products, gas-phase species, and diffusion flames under certain circumstances, all have the possibility of becoming significant.

The current work follows that of Tanner[62], which looked at AP/HTPB propellants with formulations from 60% to 80% fine AP. The formulations from his work that ended up being most pertinent to the current work were those for 75% and 80% fine AP. The physical properties used in the current AP/HTPB model for AP were the same as those used for the current AP model, and the properties used in the current AP/HTPB model for HTPB were the same as those used by Tanner.

Tanner's work included the improvement of a premixed AP/HTPB model originally developed by Jeppson[7]. Tanner's efforts were geared toward several main tasks:

1) simplify the condensed-phase description;
2) apply Gross's modified version of the universal gas-phase mechanism[17];
3) increase the formulation range over which the model could be applied;
4) provide a basis for propellant burning rate calculations in his aluminum-agglomeration model.

His research focused upon making these changes to the AP/HTPB model while still being able to accurately predict steady-state burning rate, final flame temperature, and final species concentrations. He also sought to keep the model's condensed-phase decomposition reactions consistent with the trends expected for variations in formulation due to the balance of fuel and oxidizer in the modeled propellant. No comparison was reported for temperature sensitivity, which is typically necessary to validate models of this type, or to laser-augmented burning rate, with which his research was not concerned.

After investigating Tanner's steady-state model, it was found that the predicted melt-layer was extremely thin, with 98% of the propellant mass decomposing within 1 picometer of the location of the defined melt temperature (location of the initiation of condensed-phase decomposition). It was also found that the remaining AP (2%, which was present due to a discrepancy between the initial formulation of the modeled propellant and the formulation-specific AP/HTPB condensed-phase decomposition reaction) accounted for all of the variation in predicted surface temperature.

Although the physical modeling of a propellant includes some fairly large assumptions, and despite the fact that very little is understood about what exactly is occurring beneath the defined surface of a propellant, it was decided that Tanner's full description of the AP/HTPB

condensed phase should be modified to something more physically realizable. It is also important to note that if Tanner's original model were to be applied to the current ignition code, it would have had no chance of converging to an answer due to the very fine kinetic time and length scales. To modify Tanner's AP/HTPB model into something easier to work with, the singular decomposition pathways for AP and HTPB were discarded and only the formulation-specific reactions for AP/HTPB from Table 7 (as originally proposed by Tanner) were used to describe the condensed-phase decomposition of the current AP/HTPB model. To use these singular AP/HTPB decomposition reactions within Phase3, the initial propellant formulations from Tanner's AP/HTPB model needed to be slightly modified so that no individual ingredient would react away before the surface condition of 0.0001% liquid volume fraction remaining was met. The changes necessary to accomplish this included altering all the initial propellant formulations by less than 1%.

A second difficulty that arose during the investigation of Tanner's AP/HTPB model concerned the gas-phase mechanism. During his work, Tanner noticed that the final flame temperature and final species were not being predicted correctly, similar in nature to what Gross experienced with his AP model, through for different chemical species. After doing a sub-study on the matter by including various species-elimination reactions within the gas-phase, he decided to add a new gas-phase reaction to the mechanism that would help rectify this discrepancy in final species and final flame temperature, which was presented in Equation 12. This additional gas-phase reaction was only included as a temporary fix for some deficiency in the ability of the gas-phase mechanism to drive the gas-phase predictions to equilibrium. Unfortunately, the impact of the HCN-elimination reaction was much larger than realized.

The most significant impact of the HCN-elimination reaction was that the predicted burning rate was increased by ~100%, due to an increase in near surface, exothermic reaction provided for by a local increase in H and CN radical concentrations. This effect in the near-surface reactions is most obviously realized when predictions of Tanner's AP/HTPB model are compared to AP/CTPB data from Ermolin and Korobeinichev[148], which was taken at a pressure of 0.592 atm and initial temperature of 298 K, as shown in Figure 31.

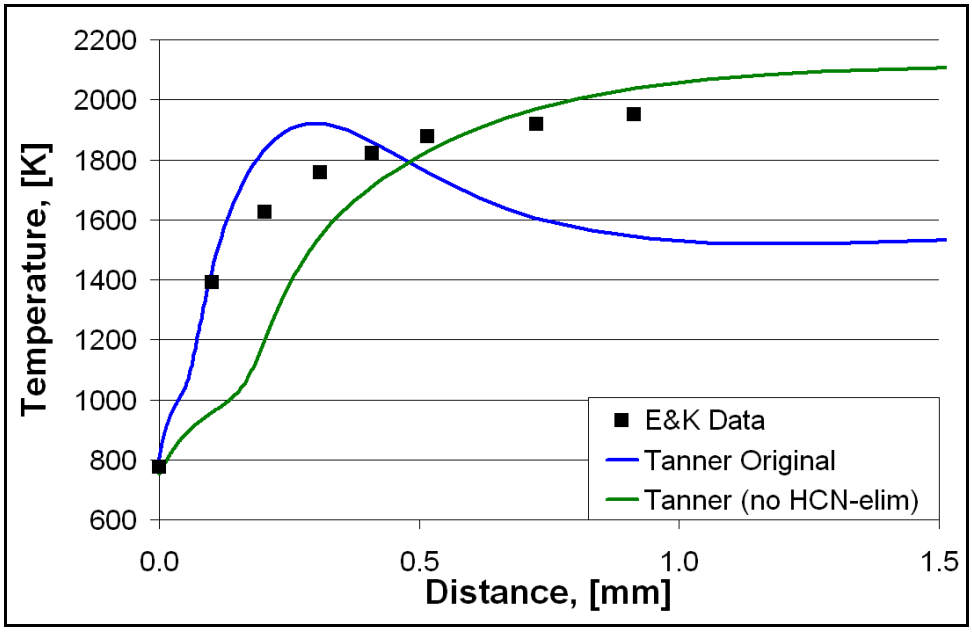

Figure 31 – Predicted temperature profile of Tanner AP/HTPB model, 77.5% AP, and data[148], 0.592 atm, T_{init} 298K

At higher pressures, this localized oscillation in the predicted temperature profile disappears with the contraction of the flame toward the surface. The largest concern in regard to this behavior, however, was that these non-realistic predictions might have a significant effect upon the laser-augmented burning rate and ignition predictions made with the AP/HTPB model, since these data have historically been taken at 1 atm.

The decomposition mechanism used in the current work included two of the condensed-phase reactions formulated by Tanner, those with 75% and 80% AP (AP75/HTPB25 and AP80/HTPB20, respectively), and a third that was developed as part of the current work for a formulation of 84% AP (AP84/HTPB16), which was constructed based on the trends of evolved species in Tanner's condensed-phase reactions for 75% and 80% AP. These three formulations were chosen to be used in the current work for three reasons.

First, there was significant data to be found in literature for steady-state burning of propellants with 75% and 80% AP. Second, these two formulations allowed for a consistent extrapolation of Tanner's condensed-phase reaction mechanism to 84% AP, for which little data could be found. Third, a decomposition reaction for a propellant formulation of 84% AP and 16% HTPB (AP to HTPB ratio of 5.67) was approximately equal to an AP/HTPB/Al propellant with a formulation of 68% AP, 12% HTPB, and 20% aluminum (AP to HTPB ratio of 5.25).

To mix an actual 84% AP propellant, a bi- or tri-modal size distribution of AP particles would need to be used to be physically realizable. Typical propellants containing more than about 80% AP have poor processing and mechanical properties[149,150], especially those with mono-modal distributions. Including multiple distributions of particles would most likely remove the propellant from a homogenous, pre-mixed regime under steady-state burning conditions at moderately high pressures, since diffusion flames come into play for propellants containing large-diameter AP particles. This formulation of the AP/HTPB model was developed expressly for the purposes of modeling ignition events. The results of the current ignition work have been represented as time to melt temperature with an insignificant amount of solid-phase decomposition. Thus the idea that interaction between the gas-phase and the solid is insignificant

prior to the point of ignition seems like a valid assumption. Consideration of post-ignition calculations would probably need to review this assumption in greater detail.

The activation energy of all the condensed-phase decomposition reactions for AP/HTPB were changed from 11 kcal/mol to 33 kcal/mol so that they would be more consistent with recent experimental observations[89,151]. The kinetic pre-exponential of the condensed-phase reaction was also changed to allow the model to duplicate the burning rate predictions of Tanner's original results. The final three AP/HTPB condensed-phase reactions that were used in this work are shown in Table 15.

Table 15 – Condensed-phase decomposition reactions for the current AP/HTPB model

AP/HTPB E_a: 33 kcal A: $7.0 \cdot 10^{10}$		HTPB	AP	C4H6	CO	H2O	HCN	N2	H2	CO2	ClOH	HCl	C2H2	NH3	HClO4
	75.03	1	31	13	4	34	6	4	8	4	12	2	10	17	17
% AP	79.90	1	41	11	2	44	10	4	6	6	16	2	12	23	23
	83.90	1	54	8	0	57	13	5	4	9	19	4	16	31	31

The condensed-phase reactions for propellants containing 75% and 80% AP used in the current work were identical to those of Tanner's work. Thus, the final flame temperature and final species predicted by the model used in the current work were both identical to Tanner's results and consistent with equilibrium conditions when including the HCN-elimination reaction. The same was found to be true for predictions from the new 84% AP reaction.

Comparisons of the thermal diffusivity and thermal conductivity for three different formulations of the AP/HTPB model, which are calculated by using Parr's thermal property fits and a volume-based linear-interpolation scheme, are shown in Figure 32 and Figure 33,

respectively. They are compared to data from Shoemaker[48] for the same three propellant formulations, and to data from Parr *et al.*[47] for a variety of propellant formulations ranging from 70% to 88% AP (MURI). Additionally, the calculated thermal conductivity of a propellant with 70% AP, 14% HTPB, and 16% aluminum, is compared to data from Parr *et al.*[47] for a set of aluminized propellants (MURI).

The model calculations seem to compare quite well to the Shoemaker data, though thermal conductivity is on the high end of the scatter. Shoemaker's thermal conductivity data for other propellant ingredients have been observed to be low when compared to more recent sources of data[47], and so the actual discrepancy between Parr's fits and Shoemaker's data may not be as large as it seems. Data for the non-aluminized MURI propellants is quite scattered with no specific propellant formulations having been presented. The calculated thermal conductivity of an AP/HTPB/Al propellant by the model is within the low range of the data, suggesting that the current approximation of the model may be underpredicting the contribution of aluminum to

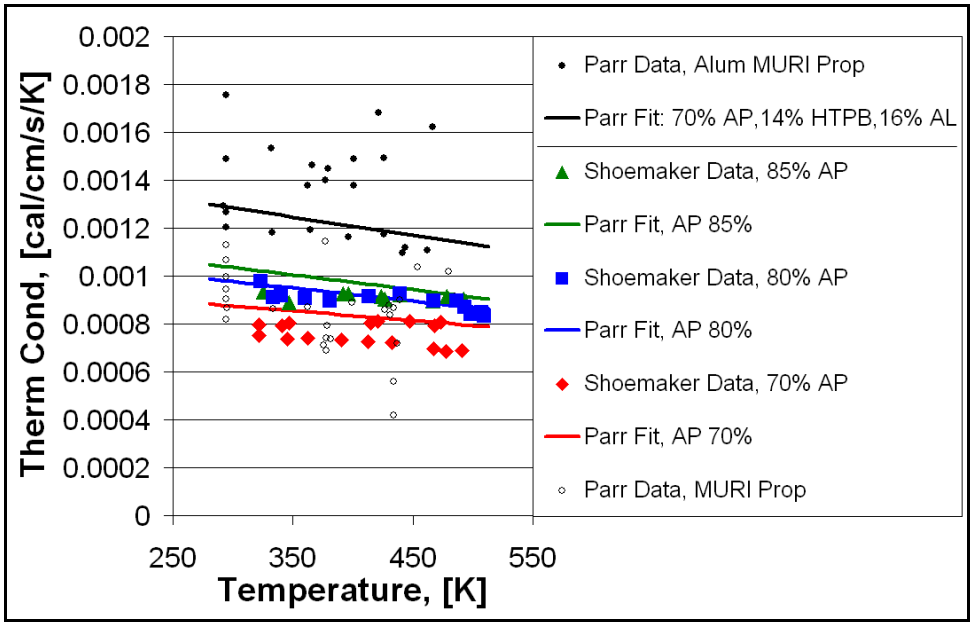

Figure 32 – Thermal conductivity fits used in current AP/HTPB model and data[47,48]

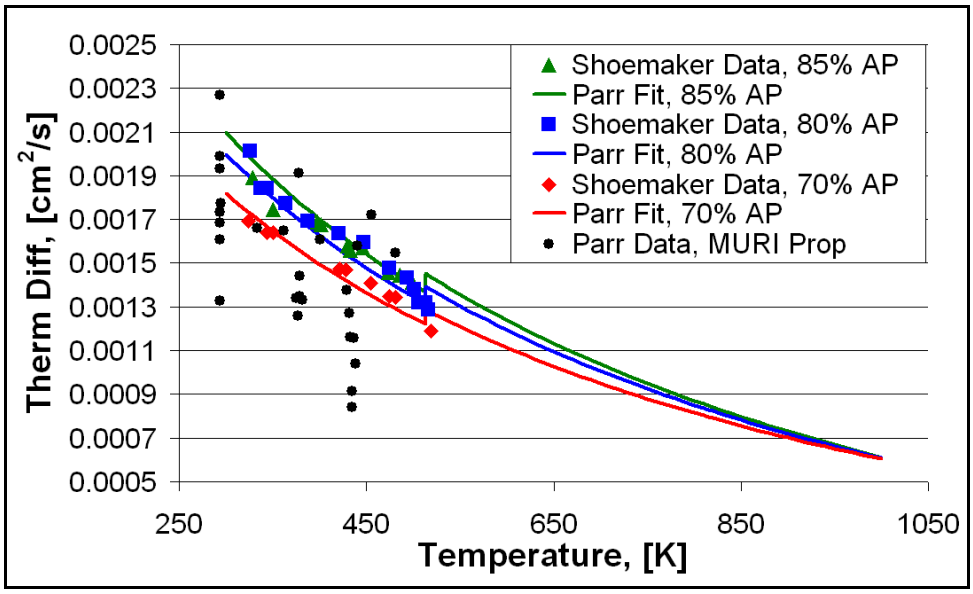

Figure 33 – Thermal diffusivity fits used in current AP/HTPB model and data[47,48]

the overall thermal conductivity of the propellant. The difference could even be larger than it seems, given the fact that the AP/HTPB thermal conductivity may be low. The relative accuracy of these calculations for the thermal properties of the propellants will allow for confidence when predicting ignition events.

The main rubric for comparison of the three AP/HTPB formulations of the current model in regard to one another is burning rate. An overall comparison of predictions for the AP/HTPB model against available experimental data[28,151,152] is given in Figure 34.

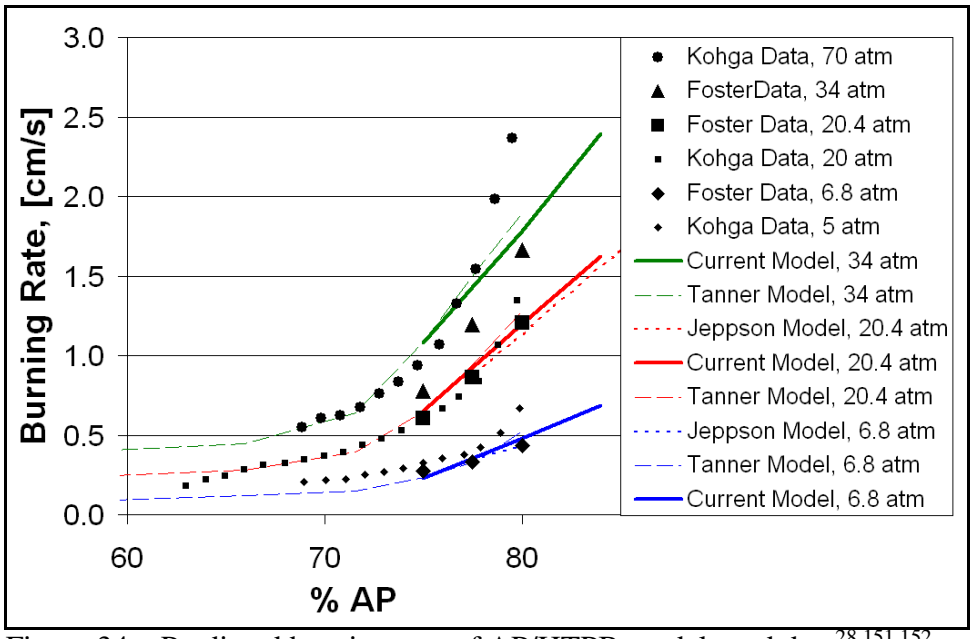

Figure 34 – Predicted burning rate of AP/HTPB models and data[28,151,152], T_{init} 298K

In this regard, the new predictions seem consistent with both the predictions of Tanner's previous models and also (for pressures of 6.8 and 20.4 atm) consistent with experimental data.

4.4.1 AP/HTPB Model: 75% AP, 25% HTPB

A comparison of predicted burning rate by the current model to experimental data[152-155] showed a trend that was too high with respect to pressure. This comparison for AP75/HTPB25 is given in Figure 35. Deviation of predictions from the data at 1 atm (14.7 psi) is significant (~40% too low). This trend is especially unfortunate in light of the fact that laser-augmented combustion and ignition data are typically taken at 1 atm and this was the ultimate purpose to which the AP/HTPB model was to be applied. Deviation is also significant at higher pressures, where it's possible that near-surface diffusion flames can change the combustion significantly, though these pressures were not of primary concern to either Tanner or the current work.

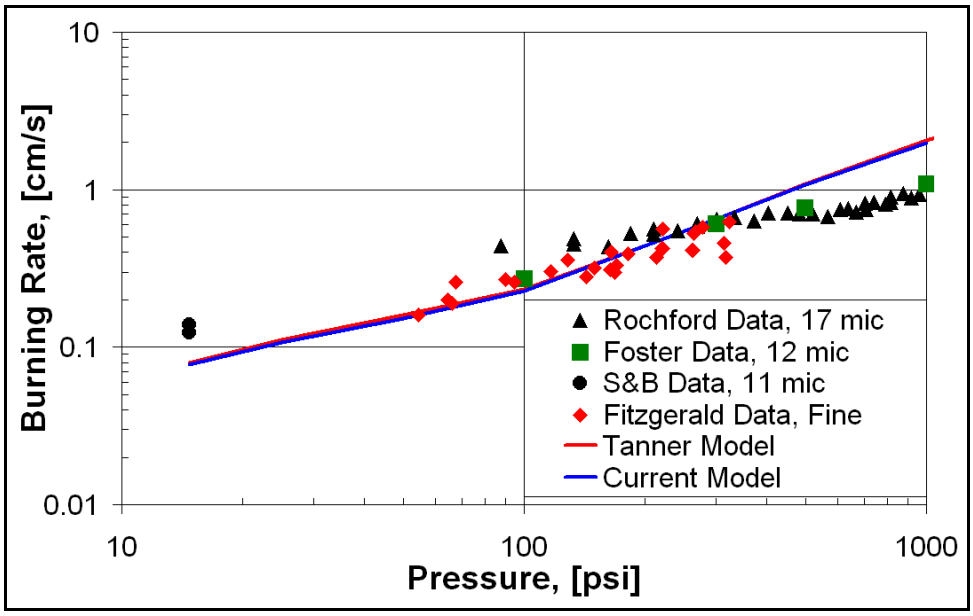

Figure 35 – Predicted burning rate of current and Tanner AP75/HTPB25 models and data[152-155] , T_{init} 298K

A comparison of the predicted temperature sensitivity of AP75/HTPB25 to data[151,153,155] is shown in Figure 36.

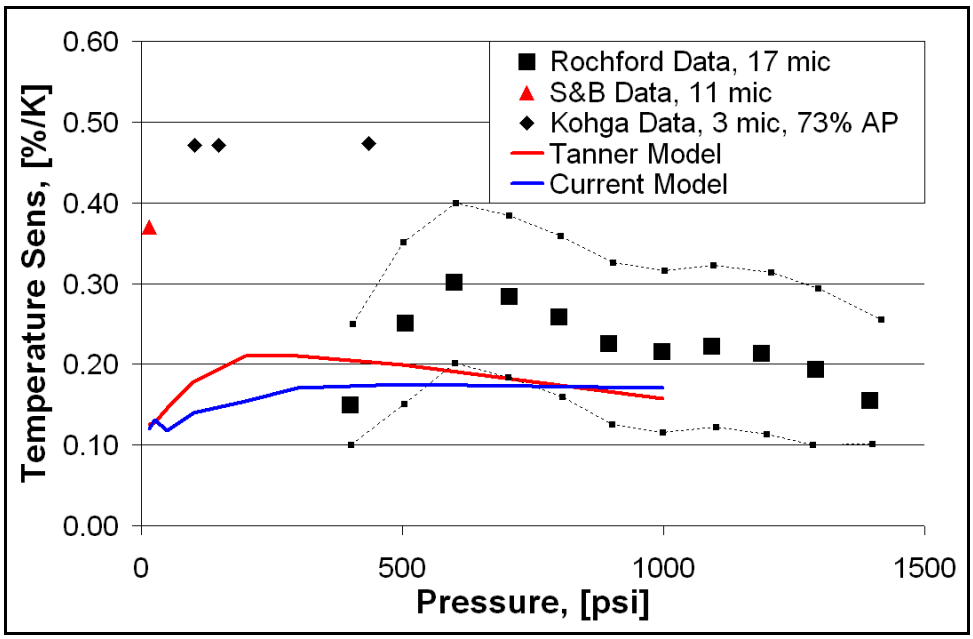

Figure 36 – Predicted temperature sensitivity of current and Tanner AP75/HTPB25 models and data[151,153,155]

The predictions are on the low end of the considerable data scatter. The predicted temperature sensitivity of the new model decreased slightly. In light of the trends observed during the development of the current AP model, the low predictions of temperature sensitivity here suggest that the condensed-phase heat release of the AP75/HTPB25 predictions is probably too endothermic.

A secondary source of evidence pointing toward the idea that the modeled heat release of the current AP/HTPB model is too endothermic can be seen in a comparison of the laser-augmented burning rate to data, as shown in Figure 37.

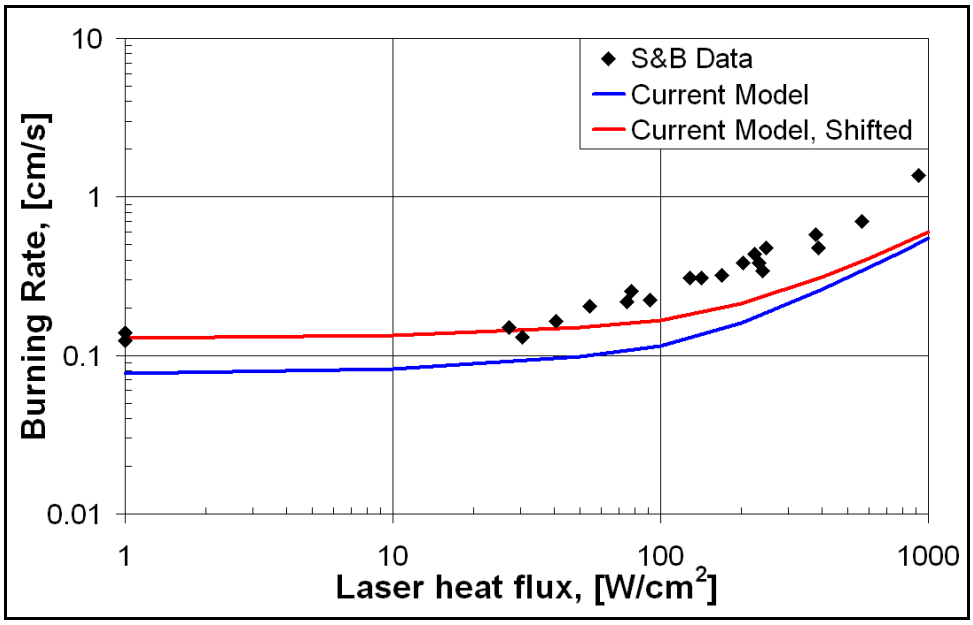

Figure 37 – Predicted laser-augmented burning rate of current AP75/HTPB25 model and data[153], 1 atm

The predictions are obviously low at low fluxes. This is due to the inaccuracy of the steady-state model's predictions at 1 atm. However, in this case the important factor is to predict the trend of burning rate with respect to the applied laser flux, since this specific relationship shows how the propellant responds to a given level of applied heat. To more accurately

determine the ability of the current AP/HTPB model in this regard, a second line that is labeled as "Shifted" is also shown in Figure 37, where a value of 0.052 cm/s (~40%) has been added to the burning rate at 1 atm to account for the inaccuracy of the base prediction. In this case, the slope of the graph is too shallow by a good margin, falling short on average by ~75% above a laser heat flux of 100 W/cm^2 and implying that the calculated condensed-phase heat release is too endothermic.

The melt layer predictions of AP75/HTPB25 (defined in the current AP/HTPB model as the distance between the location of the melt temperature, 735 K, and the surface) are reasonable, lying in the range of 1 to 1.5 microns between pressures of 10 and 1000 psi. No data were found for comparison. Predicted surface temperatures are low when compared to the propellant data of Powling[139] and Bakhman[141], as presented in Figure 38.

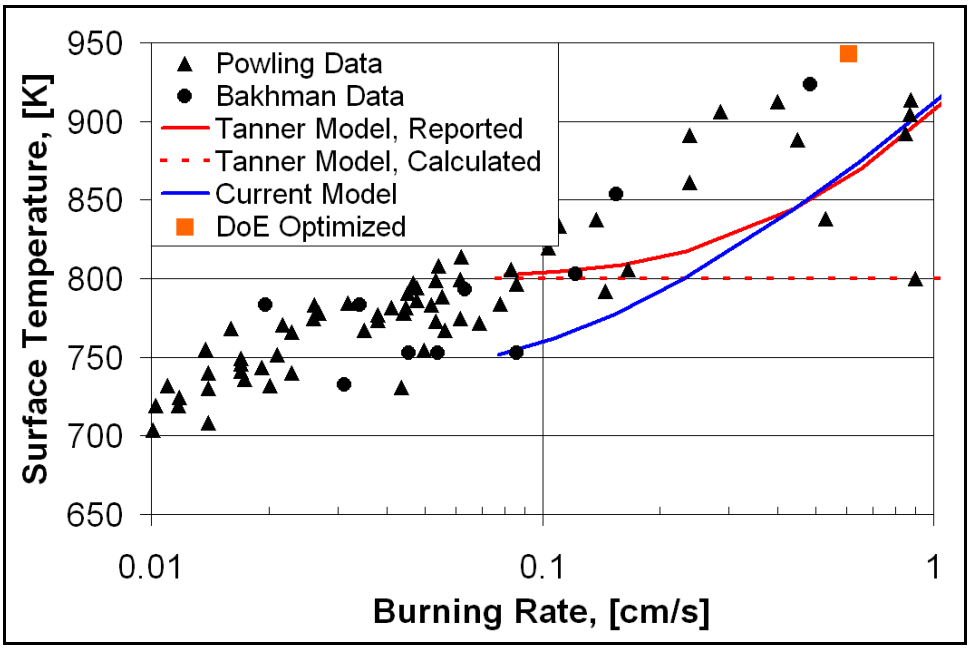

Figure 38 – Predicted surface temperature of current and Tanner AP75/HTPB25 models and data[139,141]

Predictions of all models in Figure 38 show a limitation in the predicted surface temperature due to the assumption that condensed-phase decomposition only occurs above the defined melt temperature (800 K for the Tanner models, and 735 K for the current work). In contrast, the data show surface temperatures as low as 700 K for very low burning rates. Since none of the models have included considerations for predicting such low surface temperatures, the leveling off in the predictions here is not concerning as it is obviously an artifact of the model's assumptions. Though beyond the scope of the current work, this assumption should be re-evaluated and its effects explored in the future.

Due to the inability of the current AP/HTPB model to accurately predict temperature sensitivity and laser-augmented burning rate, and the connection observed during the development of the new AP model between these two predictions and the description of the condensed-phase heat release, a Design of Experiment was conducted for this formulation of the AP/HTPB model in the same manner as that completed for the AP model. This was performed for a pressure of 300 psi, as this is a pressure for which the model most closely predicts the experimental burning rate of a 75% AP propellant. The design space for this part of the work is shown in Appendix A, Table A3 and Table A4. The optimal solution for the AP/HTPB DoE had a condensed-phase heat evolution of -150 cal/gm (exothermic) and surface heat flux of 370 W/cm^2. (This solution also corresponded to a surface temperature of 943 K, as shown in Figure 38.) Both of these values are significantly different from the current model—which has a condensed-phase heat evolution of 37 cal/gm (endothermic) and a surface heat flux of 1360 W/cm^2.

Another comparison can be made to give an approximate surface heat flux value for a 75% fine AP propellant by combining the laser-augmented heat flux data of Son and Brewster[153]

with steady-state burning rate data from Rochford (as referenced by Rasmussen and Frederick[155]), as was completed for AP and presented in Figure 29. This analysis for AP75/HTPB25 is shown in Figure 39.

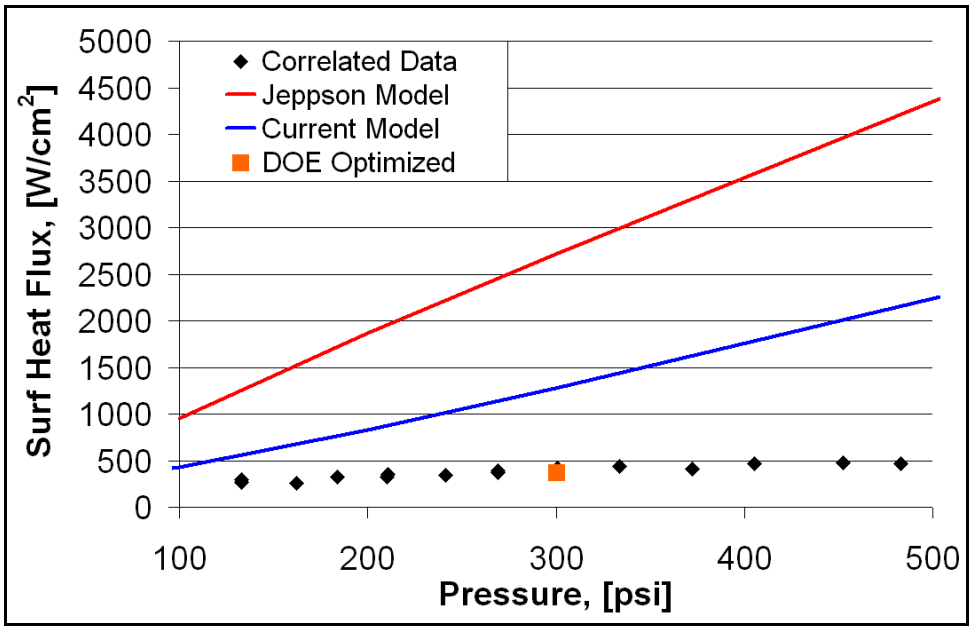

Figure 39 – Predicted gas-phase heat flux of AP75/HTPB25 models and correlated data[153,155] , 1 atm, T_{init} 298K

Although not precise (as this analysis assumes 100% absorption of the laser, while AP/HTPB propellants have been observed[93] to reflect approximately 10% of laser light at typical wavelengths) this comparison suggests that the current model deviates significantly from the experimental data, although the current model is quite a bit better than the previous Jeppson model. The fact that the optimal solution for the DoE lies in exactly the same region as this separate analysis of the experimental data gives additional credence to the idea that serious attention still needs to be given to the further modification of the AP/HTPB model in both the gas- and condensed-phase. This comparison suggests that the condensed phase for a modeled AP/HTPB propellant should be exothermic.

4.4.2 AP/HTPB Model: 80% AP, 20% HTPB

A comparison of the predicted burning rate for AP80/HTPB20 to both the Tanner predictions and experimental data[63,156,157] is given in Figure 40.

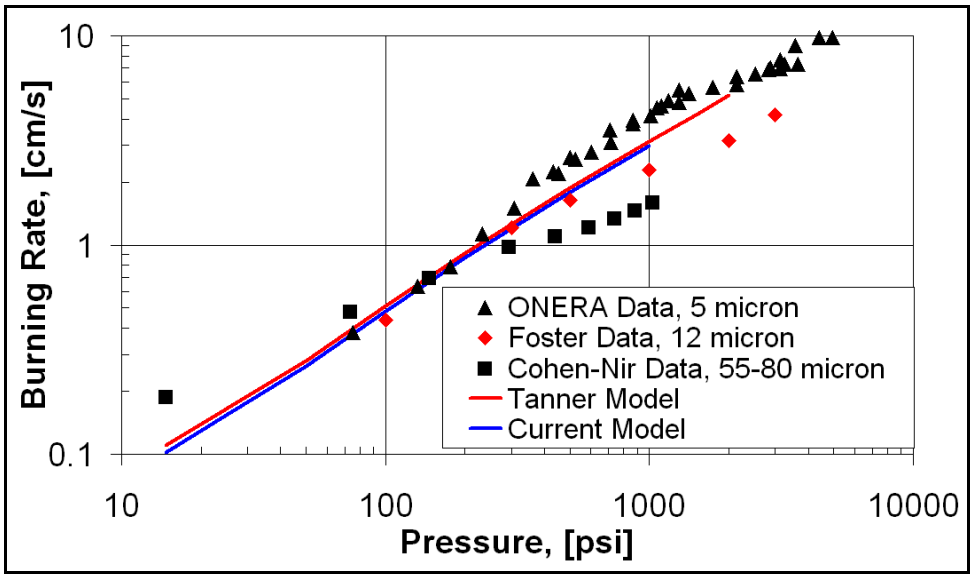

Figure 40 – Predicted burning rate of current and Tanner AP80/HTPB20 models and data[63,156,157], T_{init} 298K

The predictions are good at moderate pressures, falling within the scatter of the data. The trend at moderate pressures also looks much better than that for AP75/HTPB25. Although the Cohen-Nir data at high pressure (and large AP particle size) probably weren't burning under premixed conditions, the data were included here because of their extension to low pressure, where the premixed assumption of the current model more likely holds. As with AP75/HTPB25, the predictions at low pressure (15 psi) are still considerably different than the data suggest (~45% too low).

Calculated temperature sensitivity of AP80/HTPB20 is also much lower than the experimental data[157-159], as presented in Figure 41.

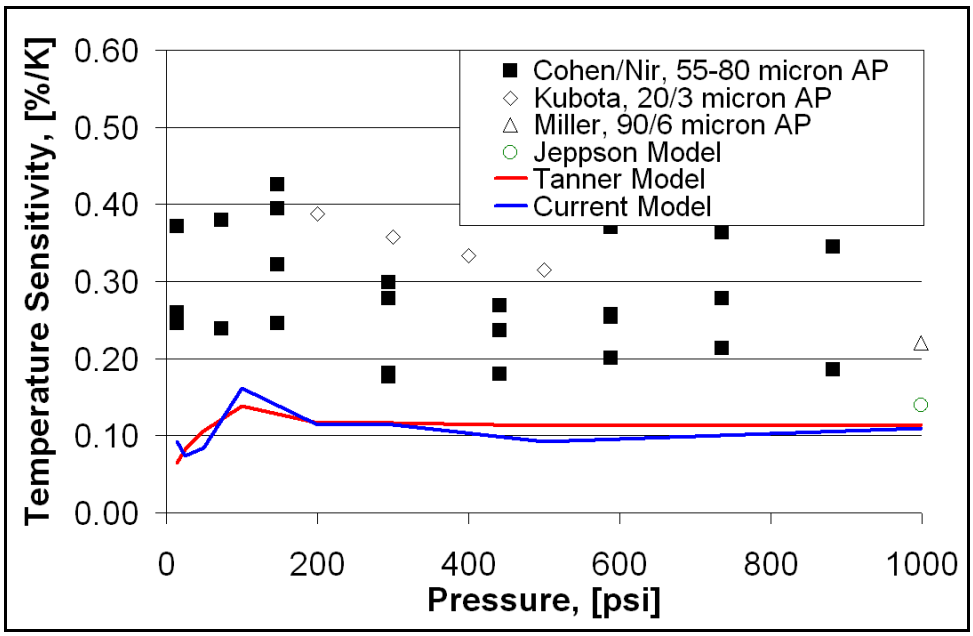

Figure 41 – Predicted temperature sensitivity of current and Tanner AP80/HTPB20 models and data[156,158,159]

The low temperature sensitivity predictions imply that the condensed-phase heat release for the AP80/HTPB20 formulation needs to be much more exothermic than it currently is (24 cal/gm, endothermic, at 300 psi). This is consistent with what was found for the AP75/HTPB25 formulation of the model.

Surface temperature data from Kubota[159] were compared to the AP80/HTPB20 model predictions. This is shown in Figure 42.

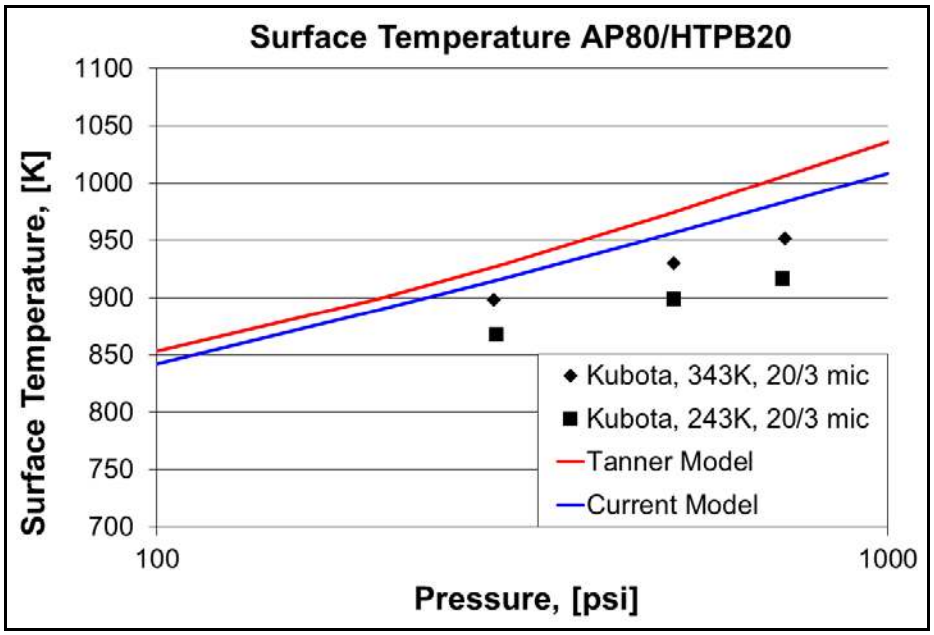

Figure 42 – Predicted surface temperature of current and Tanner AP80/HTPB20 models and data[159], T_{init} 298K

The model predicts these data fairly well (within 50 K) though high, but is still low as compared to the Powling[139] data presented in Figure 38. Predicted surface temperatures should probably be slightly higher than experimental data, which are collected as bulk measurements averaged over the entire propellant surface, while the defined surface temperature of the model is a point defined by a remaining liquid fraction of 0.0001%. Given the fact that the current propellant model already needs to be changed significantly to more accurately describe an AP/HTPB propellant, the level of accuracy of the model for this formulation was deemed acceptable.

4.4.3 AP/HTPB MODEL: 84% AP, 16% HTPB

There were relatively few sources of experimental validation found for this formulation of an AP/HTPB propellant. The first comparison was given in the extrapolations of Figure 34,

though this apparent validation relies completely on the observed trends of AP/HTPB propellants formulated with a smaller fraction of AP. The same trends are present for the AP84/HTPB16 formulation of the model that were observed in the predictions of the other two proposed formulations: a fair amount of accuracy at 6.8 and 20.4 atm, while over-predicting the system at high pressure, and under-predicting at low pressure.

Korobeinichev *et al.*[160] report data for an 84% AP CTPB-propellant at a pressure of 0.08 atm as shown in Figure 43.

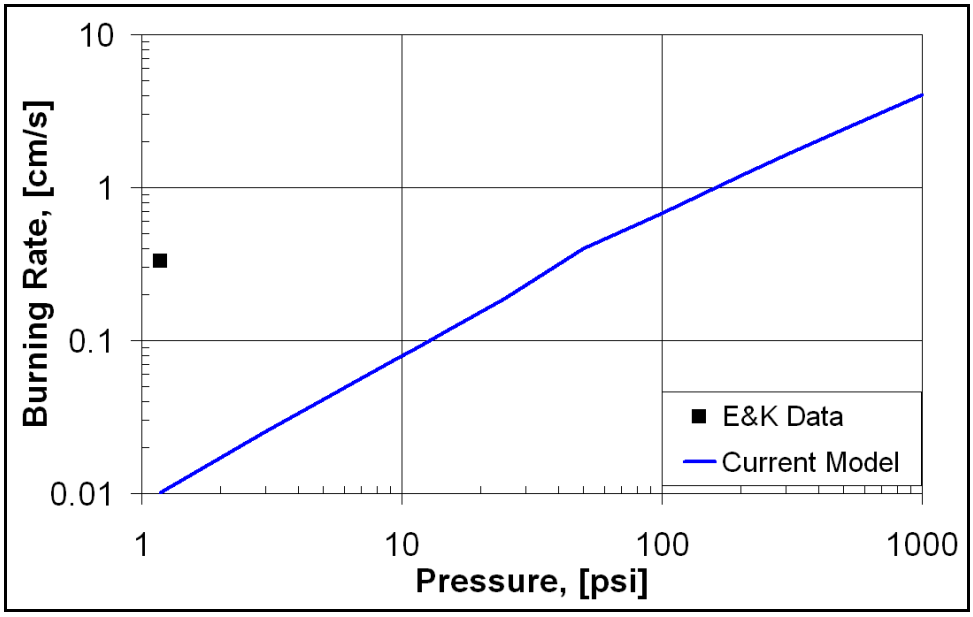

Figure 43 – Predicted burning rate of current AP84/HTPB16 model and data[160], T_{init} 298K

The single data point at 0.08 atm (1.17 psi) is more than an order of magnitude larger than that predicted by the model. There are effectively two ways to make the predicted burning rate higher in a propellant/ingredient model. Either the gas-phase heat flux at the surface (currently, ~15 W/cm^2) or the exothermicity of the condensed phase (currently, ~30 cal/gm, exothermic) needs to be increased. The predicted gas-phase heat flux near of the surface of the

propellant can be compared to the gas-phase data of Korobeinichev *et al.*[160]. A comparison of their data to both the Jeppson model and the current AP/HTPB model for this formulation is given in Figure 44.

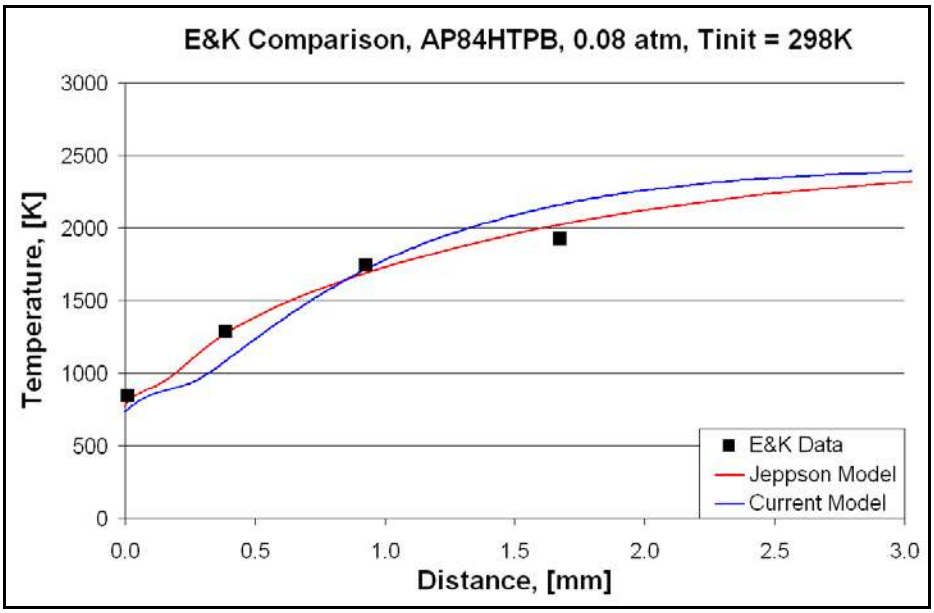

Figure 44 – Predicted temperature profile of current and Jeppson AP84/HTPB16 models and data[160], 0.08 atm, T_{init} 298K

The predicted temperature rise near the surface is in excellent agreement with the data. Thus, the possibility of affecting a change upon the surface heat flux through the gas-phase mechanism to increase the predicted burning rate of the propellant seems like the wrong choice. The second option is to increase the exothermicity of the condensed phase, an option that is consistent with what has been seen for the other two formulations of the AP/HTPB model.

4.4.4 *SUMMARY*

The current steady-state AP/HTPB model predicts a few experimental data sets, but falls short in describing several others, most noticeably those necessary for proper validation. Burning

rate, final species, and final flame temperatures are accurate. It is desired that the model should be able to predict laser-augmented burning rate, temperature sensitivity, and surface temperature as well. A minimal set of changes was made to Tanner's original model so that it could be applied toward ignition simulations, which resulted in the model predicting a more consistent melt layer thickness. Current results suggest that the condensed-phase decomposition of the AP/HTPB model needs to be exothermic instead of endothermic, with a much smaller amount of heat being released in the gas-phase flame. Such a change will require a very large effort, including both the condensed-phase decomposition scheme and gas-phase mechanism as well. The application of the current AP/HTPB model to the ignition code will include the steady-state modeling assumption that no condensed-phase decomposition occurs below a melting temperature of 735 K.

The work completed for the AP/HTPB model that has been presented in Chapter 4.4 is shown in Figure 45 within the validation structure first presented in Chapter 3.

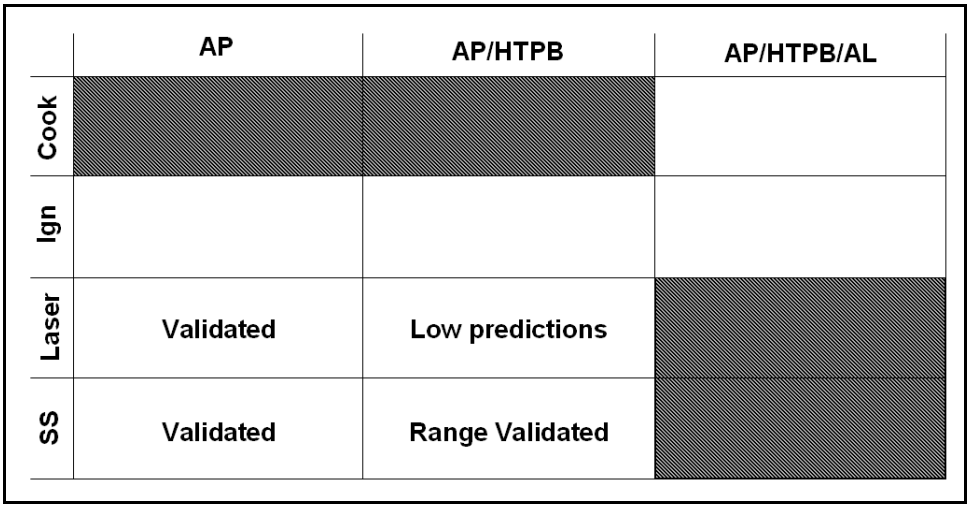

Figure 45 – Validation structure including work on the current AP/HTPB model

4.5 HMX IGNITION

After having made so many changes and improvements to the ignition code, it was important that the HMX model be re-validated against the ignition data of HMX, for which the ignition code was originally developed to predict. A localized comparison of the improved ignition code results, Meredith's original results, and HMX ignition data[95] is given in Figure 46.

It is encouraging to see that the changes made to the ignition code to allow for the modeling of other propellant ingredients, and to make its calculations more consistent with the assumptions in the Phase3 code, have only affected HMX ignition predictions slightly.

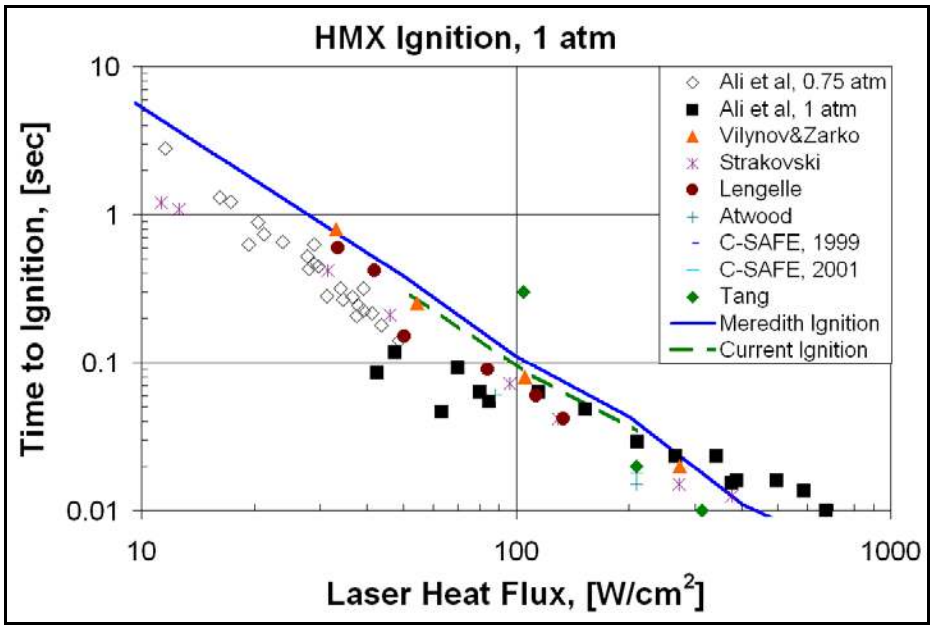

Figure 46 – Predicted time to ignition of current and Meredith HMX models and data[95], 1 atm, T_{init} 298K

4.6 SUMMARY OF FOUNDATIONAL WORK

It was important that each of the propellant/ingredient models that form the foundation of the final predictions (AP/HTPB/Al cookoff) be validated against as much pertinent data as possible. Additionally, it was important to make sure that the codes emplying those models were

verified to a point such that we could have confidence in their predictions. The two propellant/ingredient codes, Phase3 and the ignition code, were verified and then improved to be able to apply the propellant/ingredient models that formed the core of this work. HMX predictions from the new ignition code compared well to previous calculations made by the original ignition code and still compared well to the data. The updated AP and AP/HTPB steady-state models have been validated against the data and seem to be performing well.

The work presented in this chapter has formed a foundation for the next application of the steady-state models: the ignition code and making predictions for laser-driven ignition events.

Few things are harder to put up with than
the annoyance of a good example.
-- Mark Twain

CHAPTER 5: IGNITION

After validating the steady-state propellant/ingredient models using Phase3, they were next applied to the ignition code for the purpose of predicting the transient response of a propellant/ingredient to an external source of heat. It is an important concept that the previous validation of these steady-state models, which has been presented in Chapter 4 for AP monopropellant and several formulations of an AP/HTPB propellant, can only allow for the correct prediction of the final condition of a laser ignition prediction: laser-augmented steady state. In the development of a steady-state model, the heat evolution predictions of the condensed and gas phases can contain a wide range of variability. In like manner, it is possible that a wide range of validated steady-state models, each with variously defined chemical-kinetic reaction schemes in the condensed and gas phases, can accurately predict laser-augmented burning rates. Ultimately, it is up to the developer to decide when the accuracy of a model is "good enough" with respect to both steady-state and transient ignition predictions and when more work needs to be accomplished.

Ignition results for the current work will be presented in this chapter from the AP model, the AP/HTPB model, and the AP/HTPB/Al model via the application of heat by CO_2 laser. Predictions of time to a surface temperature of 513 K for the AP/HTPB and AP/HTPB/Al models are presented along with the ignition results, since condensed-phase decomposition has been seen to affect these propellants at sub-melt temperatures. Cookoff predictions for the

AP/HTPB/Al model are also presented, along with comparisons to available data. Additionally, an effort to further validate the steady-state models, or suggest direction for further research based upon the results of the current ignition work, will be made.

5.1 AP IGNITION

Predicted ignition results for AP in the current work are presented as time to melt temperature, which is assumed to be equal to the time to first decomposition or a surface temperature of 735 K. The connection between the melt temperature and first decomposition is consistent with the assumptions made in Phase3 as part of the current steady-state model. This connection between melt temperature and first decomposition is also consistent with the observations of Atwood[65] for the ignition of AP. It is assumed that reactions occurring within the gas and condensed phases subsequent to reaching the melting condition begin sufficiently fast after this point to allow the propellant ingredient to transition to self-sustaining combustion after removal of the laser flux over a period of time on the order of several milliseconds. As such, ignition predictions for AP are functions only of the thermal conductivity, melting temperature, and as will be shown, the absorptive properties of the crystal with regard to laser light.

Two initial ignition simulations were completed using the original Gross AP model to ascertain the effects of using a penetrating/absorbing laser versus applying the laser heat only as a boundary condition. (Prior to this work, HMX ignition predictions only included application of the laser heat as a boundary condition at the solid/gas surface interface.) The results of this sub-study for the current AP model compared to data[65] in Table 16. The value of "Log-Slope" presented in Table 16 is the slope of a straight line passing through the data/predictions on a log-log plot. This value is used to determine how well the predictions fit the trend of the data in this

region. For all ignition predictions presented here and later, the laser heat flux is approximated as a near-square wave with a rise time of 0.2 ms[161] and is assumed to be composed of monochromatic light.

Table 16 – Initial ignition predictions using the Gross[17] AP model

Ignition, 34 atm	Laser Flux [cal/cm^2/s]	Time to Ign [ms]	Log-Slope [--]
Atwood Data (2007)	50	61.95	-1.41
	100	23.28	
Abs/Pen Laser (239 cm^{-1})	50	89.16	-1.46
	100	32.32	
B.C. Laser	50	41.36	-1.97
	100	10.58	

Since the Gross model was never used for ignition calculations, the large difference between the data and predictions is unsurprising. The reason for making this comparison was only to determine the best way to apply the heat of the laser for ignition simulations. (Predictions made by the current model showed similar results in regard to the desired trend since all thermal parameters between the two models are similar and no condensed-phase decomposition is accounted for during these simulations.) As presented, the Log-Slope of the predictions when applying the laser heat as a boundary condition is too steep by 35%, whereas that for the absorbing/penetrating laser is within 4%. This result is consistent with the observation[144] that AP crystals are fairly transparent to the wavelength of laser light typically used, as previously mentioned in Chapter 4. The absorption parameter of AP, as measured by Isbell and Brewster[144], is on the order of 10^2 cm^{-1}, rather than 10^3 cm^{-1} like most other propellants/ingredients. As such, it was decided to include the penetrating/absorbing laser sub-model for all AP, AP/HTPB, and AP/HTPB/Al ignition predictions made in the current work.

5.1.1 *RESULTS AND DISCUSSION*

Intial results for AP ignition using the current model are compared to experimental data[65,87] in Figure 47.

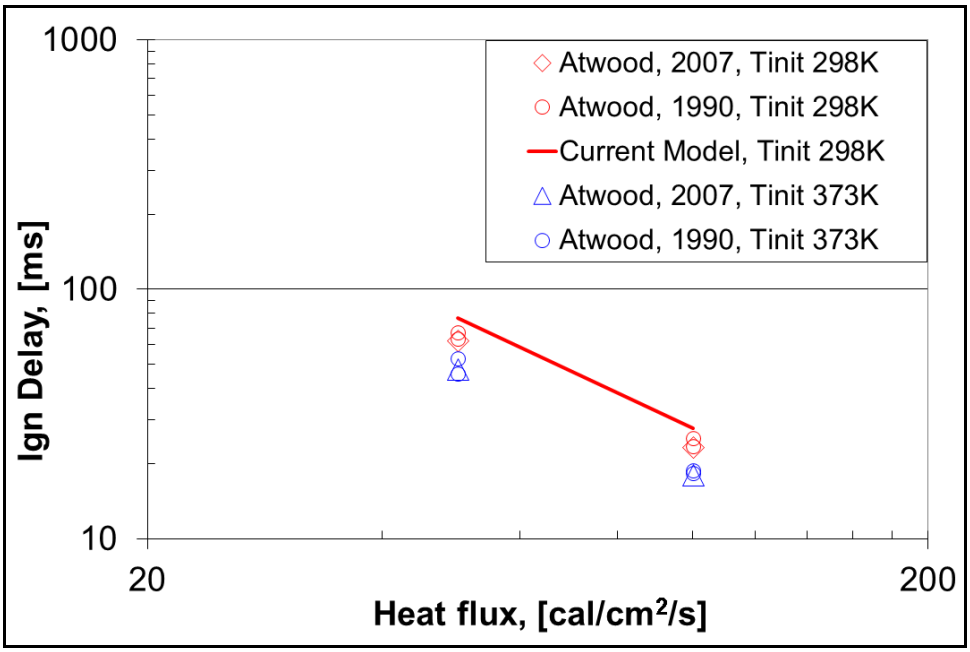

Figure 47 – Initial AP ignition predictions using current model and data[65,87], 34 atm

Although the ignition predictions for AP at an initial temperature of 298 K are high (simulations taking too long to heat up), the slope of the predictions is very similar to the data. Two primary factors in predicting time to ignition are the thermal conductivity and melt temperature (or initial decomposition). AP is fairly unique in that neither an accurate melt temperature nor thermal conductivity (for temperatures above 513 K) has been well-defined by experimental observation. In an effort to find possible reasons for the long prediction times of the model, a parametric sub-study was conducted using the current model in Phase3 to define a relationship between melting temperature and the thermal conductivity of solid AP that could be

used to explore the possible prediction space of the ignition calculations. This was accomplished by comparing the cubic-phase-thickness predictions of the current AP steady-state model to the data of Beckstead and Hightower[140]. The following assumptions were made to accomplish this:

1) sub-melt decomposition (below 735 K) is insignificant;
2) the thermal conductivity of orthorhombic AP is equal to that measured by Parr[123];
3) the thermal conductivity of cubic and melted AP are equal at the melt temperature and have the same trend with temperature, a trend observed by Osman[162] for perchlorate salts—although the thermal conductivity may change to a reasonable degree at the cubic transition temperature of 513 K;
4) the trend of thermal conductivity with respect to temperature for AP is equal to that measured by Parr[123] for all temperatures within the model.

Using the current steady-state AP model and the above assumptions, a relationship between the A-parameter of Parr's thermal conductivity fit for temperatures of interest (A+B·T) and the melt temperature of the solid was constructed by matching the steady-state burning rate of the propellant through the following iterative procedure:

1) define the melt temperature of AP in the model (ranged from 620 K to 870 K);
2) define the thermal conductivity of cubic-phase and melted AP (A-parameter);
3) vary the condensed-phase pre-exp to predict burning rate[163] accurately;
4) compare the predicted cubic-layer thickness to the B&H[140] data;
5) if the predicted cubic-layer thickness was different than the data, return to step 2;
6) if the predicted cubic-layer thickness was accurate, record both values (melt temperature and A-parameter);
7) return to Step 1 until the entire range of melt temperatures is populated.

Through this method, Equation 28 was derived, which is a fit of the necessary A-parameter of Parr's thermal conductivity fit for a proposed melt temperature, T_m, that will fit the AP cubic-phase thickness of Beckstead and Hightower[140].

$$A_{Parr}(T_m) = 4.08 \cdot 10^{-2} - 1.4 \cdot 10^{-4} \cdot T_m + 1.7 \cdot 10^{-7} \cdot T_m^{\ 2} - 6.89 \cdot 10^{-11} \cdot T_m^{\ 3} \quad (28)$$

This correlation was then used to make a variety of ignition predictions toward determining the combination of melt temperature and thermal conductivity that would result in accurate ignition predictions for AP, while using the temperature-insensitive laser-absorption parameter suggested by Isbell and Brewster[144] of 239 cm^{-1}. This process resulted in an optimized melt temperature of 657 K and an A-parameter for the cubic- and melt-phase thermal conductivity of $1.906 \cdot 10^{-3}$ to predict the available time to ignition data.

There are a couple of troubling things about these results.

1) a melt temperature of 657 K for AP is considerably lower than what has been historically suggested by other research;
2) the optimized A-parameter suggests that the thermal conductivity of the cubic-phase is 25% higher than that of the orthorhombic phase, which seems like a large difference;

If the above assumptions are valid, the final results are still dependent upon the accuracy of the laser-absorption parameter and its insensitivity to temperature. Isbell and Brewster's[144] laser-absorption data for AP has a significant amount of variation around the laser wavelength of 10.6 microns, as shown in Figure 48. It has been reported[164] that this local variance is due to the breathing frequency of the perchlorate ion being close to this wavelength of radiation. This concept is similar to that of the breathing frequency of water being close to the wavelength of radiation used within a microwave oven.

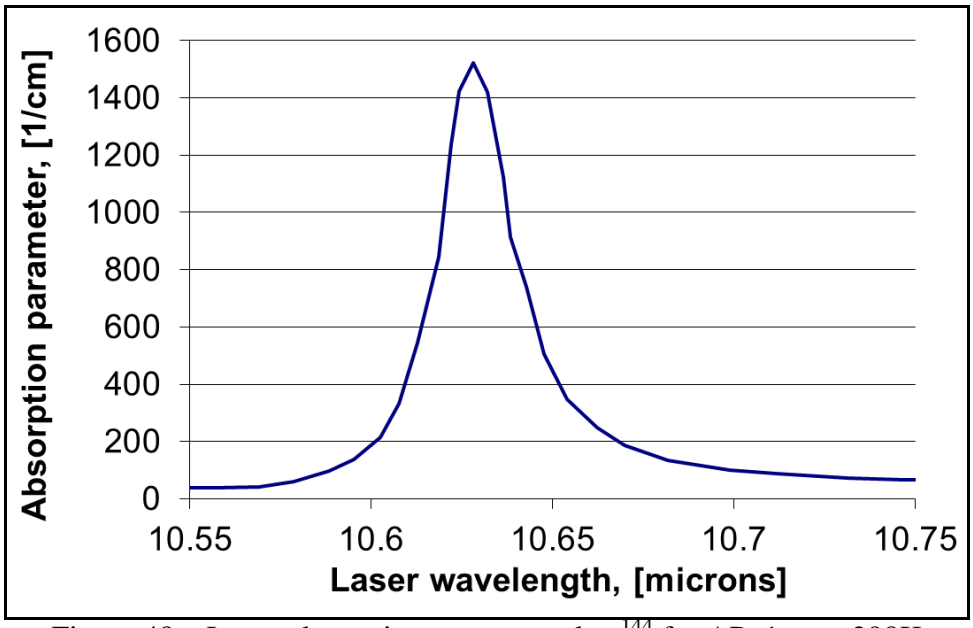

Figure 48 – Laser-absorption parameter data[144] for AP, 1 atm, 298K

An additional calculation was completed to find the value of absorption parameter for temperatures above 513K needed to correctly predict the data using the thermal conductivity and melting temperature of the current AP model. This optimized value was 405 cm^{-1}, a value not too different than the datapresented by Isbell and Brewster[144]. Ignition predictions using these revised parameters for AP and pertinent experimental data[65,87] are shown in Figure 49. These predictions were made using the absorption parameter value suggested by Isbell and Brewster for orthorhombic AP (239 cm^{-1}), and the optimized value (405 cm^{-1}) for all temperatures above the cubic-phase transition temperature of 513 K.

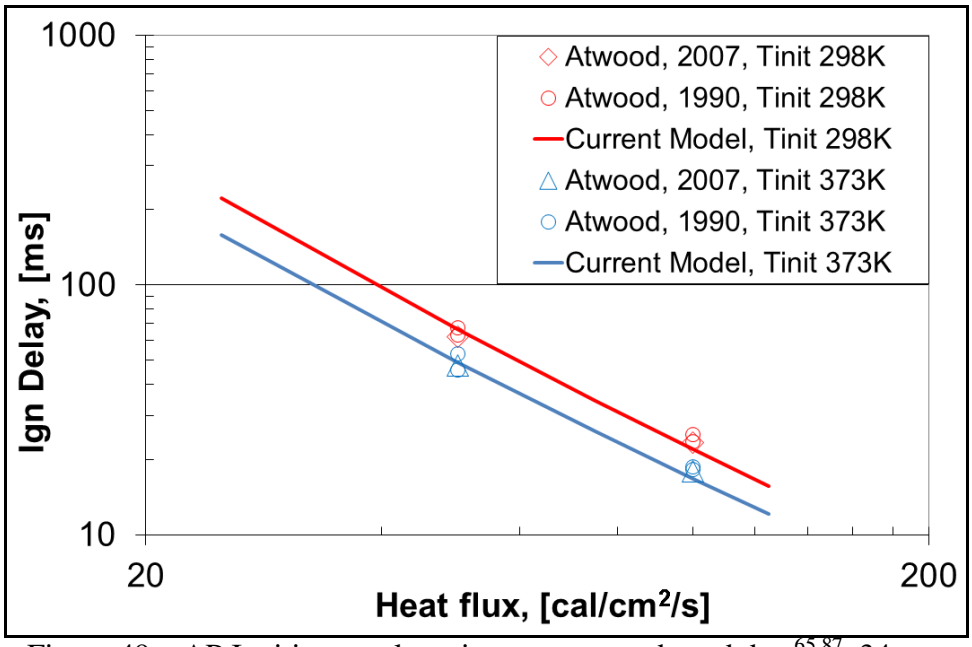

Figure 49 – AP Ignition results using current mode and data[65,87], 34 atm

The validity of these optimized calculations rides on the idea that the effective absorption parameter of the AP crystal varies with respect to temperature. One concept that suggests the absorption of the laser by AP should be a function of temperature is that the electrical conductivity of the solid, which directly impacts the absorptivity of other materials to radiation, varies with respect to temperature. It is well-documented that AP is electrically conductive[165-167] in the range of 300 to 600 K (increasing conductivity with increasing temperature) and also at the burning surface[168] during steady-state deflagration. It is unknown how this property of AP, or its variance with temperature, might affect the effective absorption parameter, which has only been measured[99] at 298 K.

It is also interesting to look at how ignition predictions evolve as a function of time. A time track of the predicted burning rate, surface temperature, and maximum gas-phase temperature versus simulation time for AP ignition is shown in Figure 50.

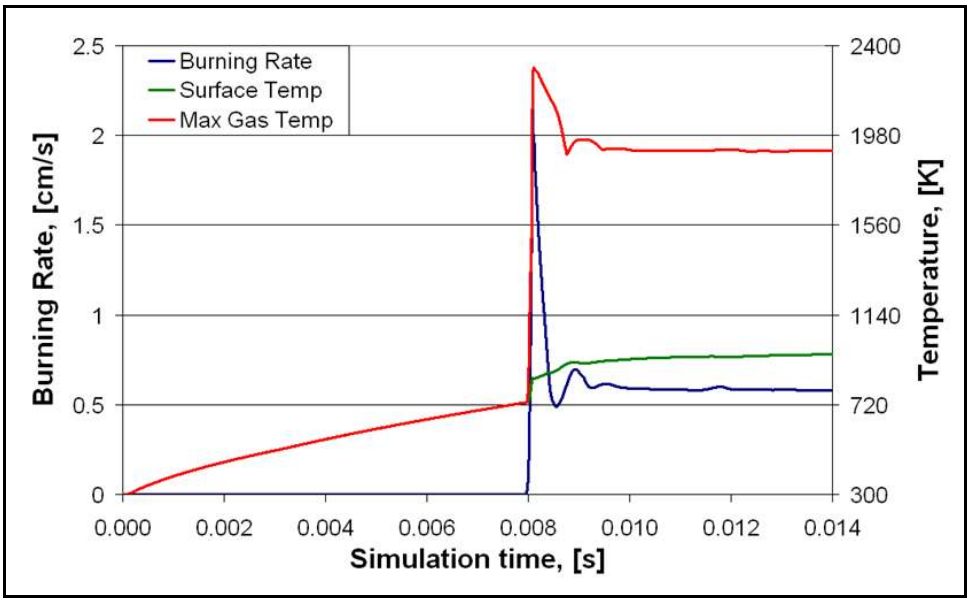

Figure 50 – AP ignition predictions for current model, transients of burning rate surface temperature and flame temperature

Oscillations such as these that occur just after the point of ignition within a model, occur because of the difference between the state of the condensed-phase solution at steady state and that at the point of ignition. At the point of ignition, the modeled surface of the propellant/ingredient will have a void fraction that is very small (only a small portion of the material will have decomposed); at steady-state the void fraction at the surface will be very low (identically zero, but assumed to be 0.0001%) . As the rate of condensed-phase decomposition is dependent only upon temperature, the large amount of material present near the surface results in an initially large rate of decomposition to be predicted.

The first feature in Figure 50 that is immediately apparent—while keeping in mind the similar plot for HMX in Figure 10—is the sharpness of the burning rate curve at the point of ignition. At a surface temperature of 735 K, the condensed-phase decomposition reactions begin and spike rapidly. This effect is due to the assumptions of the AP model concerning the initiation of sub-melt decomposition and ignition time being equal to time to melt temperature. The

ignition code's improved ability to transition from inert heating to decomposing solid over a very small time scale is evident here. After the initial spike, the model transitions to augmented, steady-state burning quickly. For the current AP model, this oscillatory transition time varied from 2 to 20 ms for heat fluxes in the same range as the collected data.

The second interesting feature of Figure 50 is the overshoot of the predictions for burning rate and maximum gas-phase temperature. This phenomenon is consistent with the behavior of other ignition models that include an exothermic condensed phase. Upon initial inspection, the overall endothermic decomposition of the current AP model probably shouldn't produce such an effect. However, the first 30% of all decomposition that occurs in the current AP model is assumed to be exothermic. The decomposition rate during this time is calculated as if 100% of the AP present will eventually decompose along the exothermic path, and so the calculations only see the exothermic portion of decomposition during this time. The overshoot observed here is consistent with both the model's assumptions and the presented calculations of previous predictions made by the ignition code (Figure 10).

In fact, this initial exothermic decomposition is probably too exothermic, as evidenced by the very large overshoot in the initial burning rate. This could possibly be remedied by proposing an initial condensed-phase decomposition step that is more consistent with species seen during partial decomposition. If such a step were taken, the model would then have to be altered to contain a bubble-phase reaction to occur sub-surface between the decomposition products of the new initial exothermic reaction and the sublimation products of the currently proposed endothermic decomposition step, to predict surface species that are consistent with observed data[33]. This type of setup is consistent with that used by the Beckstead *et al.*[44] AP model. The current work, however, has only taken into account the accurate prediction of the surface species

data and has not made any changes to the steady-state model to more accurately predict conditions specific to ignition.

The third interesting feature in Figure 50 that should be noted is the relaxation to, and final values of, laser-augmented steady-state burning rate. Unfortunately, the ignition simulation results have final gas-phase predictions that were quite different from what was expected, with predicted final flame temperatures being too high and predicted burning rates too low when compared to predicted results from Phase3. A grid-refinement study was completed for ignition cases involving a 100 cal/cm^2/s heat flux to see what effect, if any, refining the grid would have upon these predictions. The spacing of grid points in the gas phase of the ignition code was uniform in all cases presented for the current work, unless otherwise specified. Figure 51 presents the final flame temperature and laser-augmented burning rate predictions of the AP model in the ignition code as it depends on the gas-phase grid.

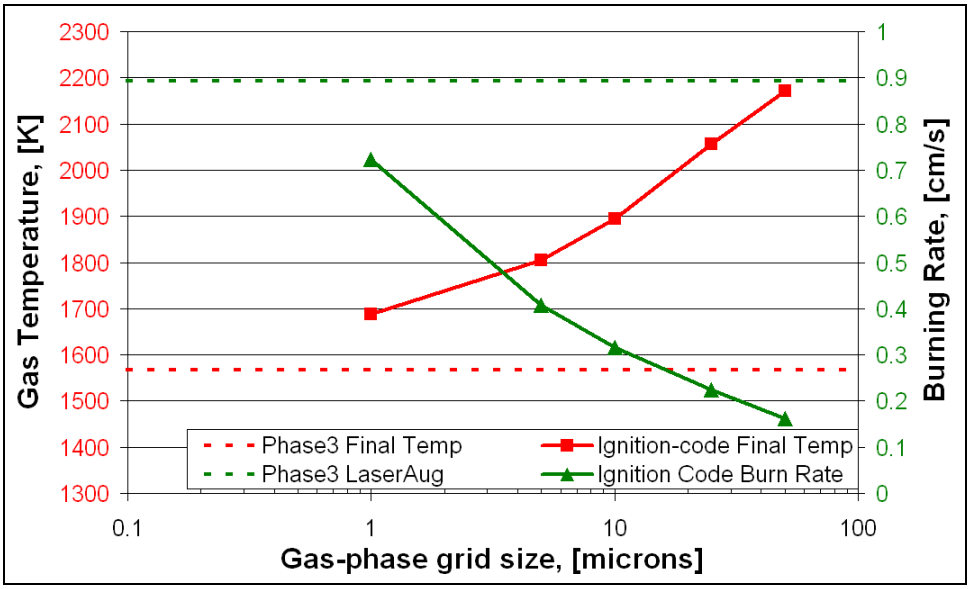

Figure 51 – AP ignition code verification, gas-phase grid-refinement study, 34 atm, 100 cal/cm^2/s

Values used for comparison in Figure 51 (final flame temperature and laser-augmented burning rate) were calculated using the Phase3 code. These predictions should be identical to the final values calculated by the ignition code after all of the transients have died out. Predicted values from the ignition code were close to those calculated by Phase3. Using a gas-phase grid that is sufficiently refined (less than 1 micron grid resolution according to the trends of Figure 51) resulted in the ignition code correctly predicting both laser-augmented burning rate and final flame temperature accurately.

Arguably, the most important section of the grid to have the proper refinement is near the solid surface, as this is where the steepest gradients are present for the physical processes of the model. Refining the grid sufficiently at the surface, however, was seen to not be the sole problem as an additional grid refinement study, which used a grid that was fine near the solid surface and progressively larger out into the far-field, failed to show any significant degree of improvement. This result may be due to the fact that the discretization of the gas-phase equations is currently implemented in the ignition code only for uniform grids, and that as a given discretization becomes more non-uniform more error will be present in the solution.

In general, using a grid with a high level of refinement was prohibitive due to the very small time step that had to be employed to keep the convective-CFL number ($u \cdot \Delta t / \Delta x$) below 1, for numerical stability. Simulations completed that used a uniform gas-phase grid with a spacing of 5 microns (the grid size used for all simulations in the current work, unless otherwise specified) already necessarily dropped down to timesteps on the order of five nanoseconds during the ignition transient for an AP simulation. Making further reductions became increasingly expensive with regard to overall wall-clock time. It is good that the code is exhibiting trends that are consistent with making correct final predictions.

Although no data could be found in the literature for time to ignition for AP with respect to pressure, calculations were made to determine if the model's results were consistent with what would be expected. Predicted times to ignition (surface temperature of 735 K) varied by less than 5% for pressures of 1 to 34 atm. This very minimal amount of variation for time to ignition versus pressure is consistent with the fact that no sub-melt decomposition is present in the current model and thus there is no thermal effect of decompostion prior to ignition. Therefore, the only mode of variation in predicted time to ignition is the effect of thermal diffusivity on the surrounding atmosphere as it conductively cools the surface. The trend with respect to pressure is correct in this regard, with simulations at higher pressure taking slightly longer to reach the ignition (melting) temperature for a given level of laser heat flux, since the effect of gas density at higher pressures will lead to more heat being conducted away from the surface of the propellant/ingredient.

As currently presented, the calculated predictions of the current AP model do not include the time corresponding to the most interesting part of the ignition process: the transition to steady state. This transition encompasses the region of time in which an ignited propellant ingredient will or will not be able to transition to steady-state burning. The ability of a heated propellant/ingredient to transition to steady-state burning has historically been viewed as being dependent upon the amount and location of energy stored within the condensed and solid phases. This is determined by the temperature profiles within the condensed and solid phases at the time the heat flux is removed. High heat fluxes applied to the propellant/ingredient result in a steeper temperature gradient. Steeper temperature gradients result in a smaller portion of the propellant being at a raised temperature and thus reactive state. When the laser heat is removed, if there isn't enough propellant/ingredient that is sufficiently reactive due to raised temperatures, then the

reactive portion of the propellant/ingredient will burn away and the gas-phase flame will blow out.

A comparison of the predicted temperature profiles for the current AP model at steady state and those at the predicted ignition times for several levels of laser heat flux is given in Figure 52. Times at which the ignition results were taken are significantly different from one another, but correspond to each simulation reaching a surface temperature of 735 K.

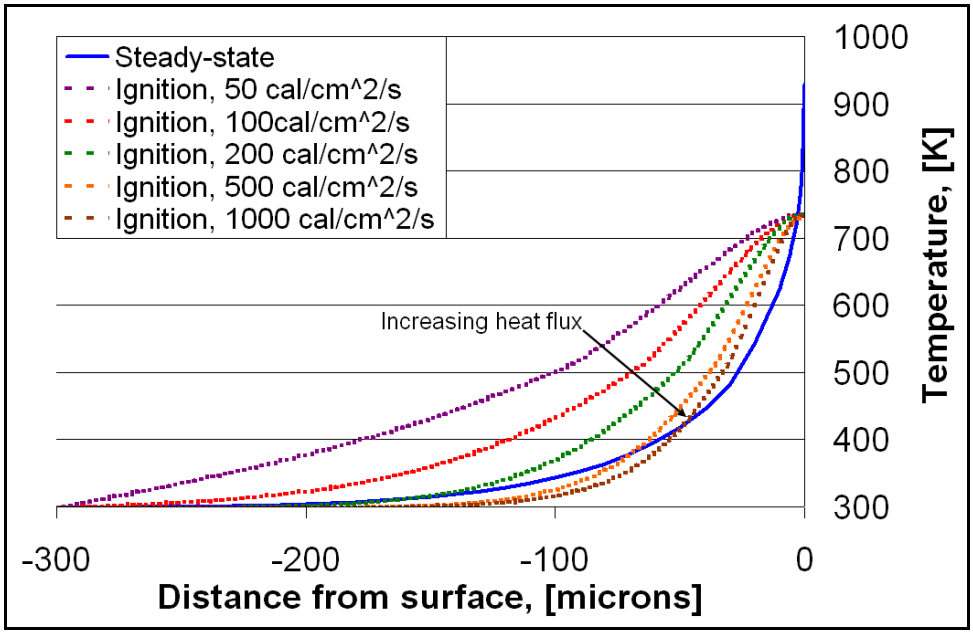

Figure 52 – Predicted temperature profiles of current AP model, 34 atm

It is interesting to note that experimental data confirm that each of the three lower heat flux cases presented in Figure 52 should transition to steady-state burning, and that each of the predicted condensed-phase temperature profiles at ignition is significantly shallower than the profile prediction at steady state. This suggests that there should be enough predicted energy within the propellant ingredient for a transition to steady-state burning to occur once the laser heat source is removed. These results corroborate the concept typically used to describe this

condition in reality that AP samples will tend to transition to steady-state burning for conditions included these levels of heat flux. Based on the trend of the results in Figure 52, a significantly higher laser heat flux would be necessary for AP to have an experimental go/no-go time that diverges from the time of inert heating (as previously described in Figure 8). Indeed, it wasn't until the modeled laser heat flux was higher than 1000 cal/cm^2/s that the ignition code predicted a condensed-phase temperature profile for AP that even approached the steepness of that predicted by the steady-state model.

There are three main factors that can also be considered as important when determining the go/no-go point of actual propellants/ingredients from the perspective of the gas phase:

1) the ability of the kinetics to respond quickly enough to the loss of thermal input and avoid blowing out the near-surface flame;

2) the time over which the laser flux is removed;

3) the relative amount of laser heat being applied to the propellant/ingredient under augmented conditions versus those at unaugmented conditions.

Upon initial inspection, the first factor is possibly beyond experimental control. If, however, such a determination were able to be made, it would very likely come about by investigating the effect of pressure on go/no-go times. At higher pressures, the kinetic rate of gas-phase reactions would be higher, and thus they would be able to respond to a given change in applied heat more quickly and thus be more resistant to being blown out. This factor would evidence itself as shorter go/no-go times for identical levels of heat flux at higher pressures, which is consistent with what has been observed[66] for composite propellants in the past. Although, this concept probably has some cross-over effects with the second factor: the gas-phase heat flux near the surface of the propellant/ingredient.

The second parameter of primary importance to the ability of a propellant/ingredient to transition to steady-state burning after a laser-driven ignition event is the difference between the

heat flux at the surface of the propellant/ingredient under laser-augmented conditions (including the laser flux) versus those at un-augmented steady state. For instance, it would be easier for a propellant/ingredient with a steady-state heat flux of 800 cal/cm^2/s (at a given pressure) to transition to steady-state burning after the removal of a 200 cal/cm^2/s heat flux (laser heat is ~20% of the total), than it would be for a propellant/ingredient with a steady-state heat flux of 100 cal/cm^2/s to transition to steady-state burning after the removal of the same laser heat flux (laser heat is ~67% of the total) if the heat is ramped off over the same period of time. Knyazeva and Zarko[79,80] reported that if a propellant/ingredient is exposed to a heat flux of greater than 37% of its steady-state surface heat flux at a given pressure, then the propellant/ingredient combustion would become unstable and would extinguish. This result, however pertinent, is dependent upon both the accuracy of the combustion model that they used and the rate at which the heat flux was removed. A longer removal time for the laser would allow for a greater heat flux to be applied to the propellant/ingredient model while still allowing for the predictions to transition to steady state burning regardless of how large the flux level was.

The third factor affecting the ability of a propellant/ingredient to transition to steady-state burning after a laser-driven ignition event is a straight-forward concept: any propellant/ ingredient exposed to any level of laser heat flux should be able to transition to steady-state burning if the laser heat flux is removed at a slow-enough rate and the propellant/ingredient will deflagrate at the pressure of the experiment. It is unclear how varying the ramp-off time of the laser might affect go/no-go data that has previously been collected. Vilyunov and Zarko[67] have reported that typical HMX propellants at 10 atm with a laser heat flux of 20 cal/cm^2/s will transition to steady state if the laser is ramped off over more than 3 milliseconds, but extinguishes if the ramp-off time is less than 1 ms. No application of this study, however, could

be found for AP/HTPB propellants. It would be very interesting to see new research accomplished to explore the effects on ignition data of varying the laser ramp-off time and what we might be able to infer from those relationships when comparing them to applicable propellant/ingredient models.

It has already been shown how times to ignition can be affected by treating the laser heat flux as a boundary condition applied at the surface of the propellant/ingredient versus applying the penetration/absorption parameters from literature[99] in a Beer's law sub-model, which is how it is handled in the current code. The predicted results when using these two methods are different at laser-augmented steady-state conditions. The ignition code was used to determine this for an AP case with a laser heat flux of 100 cal/cm^2/s. The burning rates for the two cases were nearly identical (less than 2% difference in final values), but the predicted surface temperature for the penetrating/absorbing laser was 40 K higher than that for the boundary-condition laser case. These results are consistent with what is expected. Burning rate is determined by the amount of heat supplied to the surface of the propellant/ingredient. The amount of heat is identical in both cases. A laser applied at the boundary condition implies a higher heat flux at the surface of the propellant/ingredient, which for an approximately constant value of thermal conductivity, necessitates a steeper temperature profile and thus higher predicted surface temperature.

5.1.2 *FURTHER ATTEMPTS TO VALIDATE THE STEADY-STATE MODEL*

In an effort to explore the AP steady-state model to its fullest extent, the ignition results were examined to see if they might elucidate something more that might be applied to its further development. Six sub-studies were completed to determine an optimal melt temperature for AP

at six separate levels of solid-phase absorption parameter by using Equation 28 and the process earlier described for determining the optimal melting temperature or laser absorption parameter. These results, optimized to accurately predict the time to ignition of AP at a laser flux level of 100 cal/cm^2/s, showed that varying the absorption parameter continuously between 190 and 750 cm^{-1} corresponded to optimized melt temperatures ranging from 635 to 898 K. This range of melt temperatures encompassed the entire range of values that have, to our knowledge, been previously proposed for AP. A list of these three correlated input parameters for the current AP model at six separate levels of the continuous range is presented in Table 17.

Table 17 – Possible inputs for current AP model

LaserAbsParam [cm^{-1}]	MeltTemp [K]	A-param, λ [cal/cm/s/K]
190	635	$2.076 \cdot 10^{-3}$
340	705	$1.645 \cdot 10^{-3}$
425	745	$1.515 \cdot 10^{-3}$
590	822	$1.388 \cdot 10^{-3}$
750	898	$1.266 \cdot 10^{-3}$

This range of absorption parameter corresponds to a variance in the laser-light wavelength according to Isbell and Brewster[144] from 10.6000 microns to 10.6167 microns; a window of less than 0.16%. The predictions of the current models assume monochromatic light, which is possibly not the case in reality. If the CO_2 laser-light wavelength is assumed to be exactly 10.6 microns, then the above analysis implies an AP melt temperature of 635 K, which again seems low when compared to historically suggested values, and a thermal conductivity increase at the 513 K interface of 37%, which also seems quite high. Additionally, these predictions were made for a simulation where 100% of the laser is absorbed by the solid. The solution for a system where a portion of the laser is reflected away, however, which is probably

more consistent with reality, would result in a yet lower necessary melt temperature and correspondingly higher thermal conductivity shift at the cubic-phase transition temperature.

Predicted times to ignition for AP at 34 atm using two separate levels of absorption parameter (one with a modeled melt temperature of 657 K and the other for the current model) are shown in Figure 53 along with data from Atwood *et al.*[65,87] Predictions and data are both reported as time to first-decomposition, which is equivalent to time to melt temperature for model predictions. It is important to note that the results presented in Figure 53 constitute separate models with significantly different inputs and do not only represent the simple variation of the laser absorption parameter for AP.

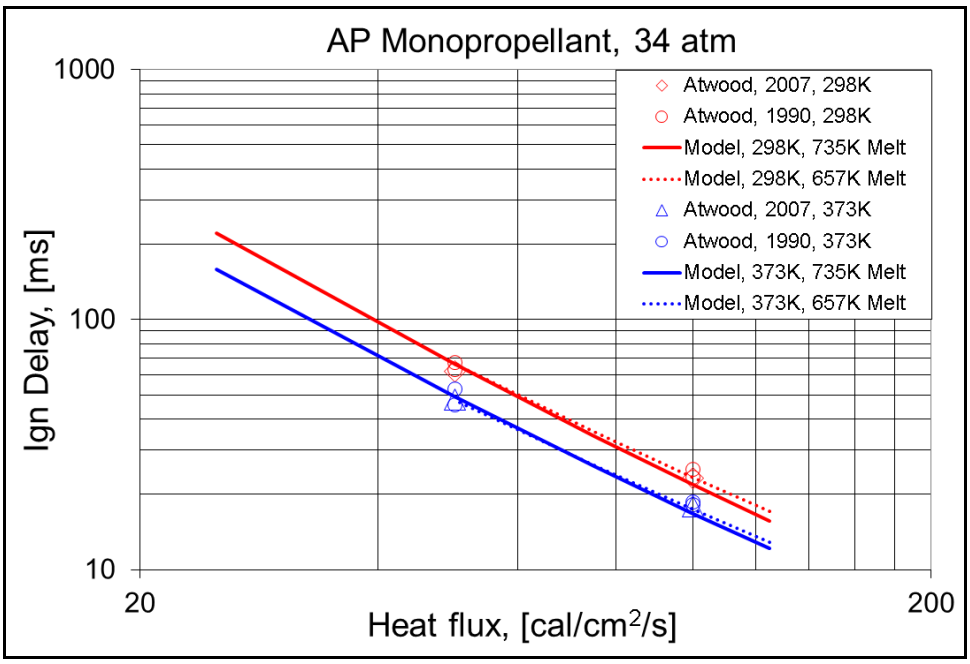

Figure 53 – Predicted times to ignition for two variations of the current AP model and data[65,87], 34 atm

Predictions compare favorably to the data. Three things in particular are noted about the predictions of the two trial models presented:

1) the predicted difference between the two trial models is very small;
2) the predicted difference decreases as initial temperature increases;
3) the predictions begin to diverge noticeably from one another at higher heat fluxes.

This result suggests that the melt temperature, thermal conductivity of the cubic and melt phases, and laser absorption parameter might be inferred by extending predictions and data to a higher heat flux. Extending the predictions to 3000 cal/cm^2/s, however, (the maximum heat flux level applied to a sample of AP[128] that could be found by a literature search) only resulted in a 20% difference between predicted results, with actual times to ignition being sub-millisecond. It seems likely that such an extension to the experimental data, if completed, would probably fall within the scatter of the data and also make the rise time of the laser[161] a significant portion of the prediction time, thus negating the ability to infer anything of value.

There is also a suggestion in Figure 53 that AP ignition data taken for samples at initial temperatures lower than 298 K might be able to tell us something more since the predictions between the two presented models (with defined melt temperatures of 657 K and 735 K) are further apart for those with an intial temperature of 298 K than 373 K. This suggestion is somewhat counterintuitive, in that heat has historically been *added* to AP when collecting experimental data, but given the results of the current model another sub-study was completed in this vein. The results, however, showed relatively little difference (less than 15% between models with defined melt temperatures of 657 and 898 K) for calculations made using an in initial temperature of 225 K. This sub-study did show, however, that the predicted LogSlopes of the various trial models with an initial temperature of 298 K had a range of values from -1.63 for the 898 K melt temperature model to -1.48 for the 657 K melt temperature model. This result again suggested that, if the model's assumptions are correct, then the actual melting temperature of AP might be in the lower portion of the range included in Table 17, as Atwood *et al*.[65]

reported the LogSlope of their collected data with an initial temperature of 298 K to be -1.41. It would be most elucidating, however, to have additional ignition data for AP over a wider range of heat fluxes, as that currently available does not seem to be able to provide more specific conclusions by comparison to the current AP model.

5.1.3 *SUMMARY*

Time to ignition data for the current AP model have been presented and compare quite well to experimental data (± 10%). Since no experimental data report accurate melting temperature or thermal conductivity (above 513 K) for AP, a range of possible model inputs (thermal conductivity, melting temperature, and laser absorption parameter) has been presented that allow for the accurate prediction of time to ignition. The current model uses a set of inputs that includes a melting temperature of 735 K. Transient results of the ignition model are consistent in behavior with previous calculations made for HMX using the ignition code. Ignition data used for comparative validation of the model span a very small range. More ignition data for AP with respect to levels of heat flux would be helpful for future development.

The work completed for the AP ignition model that has been presented in Chapter 5.1 is shown in Figure 54 within the validation structure first presented in Chapter 3.

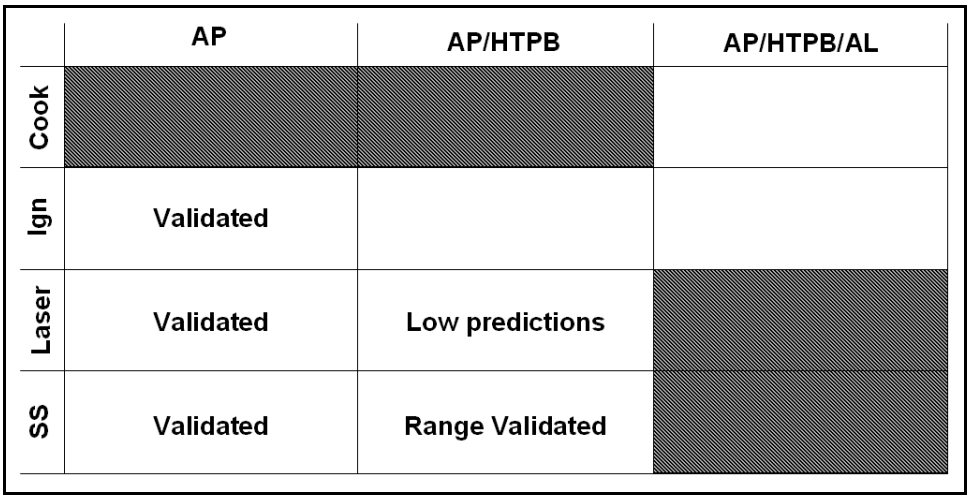

Figure 54 – Validation structure including work on the current AP ignition model

5.2 AP/HTPB IGNITION

While improving the AP/HTPB ignition model, a large focus was placed upon the validation of the individual components that formed the complete model. Input parameters for the AP/HTPB model include those for AP that have been used in the current AP steady-state model, which have been validated against available experimental data in Chapter 4. They also include those for HTPB that have been used in previous AP/HTPB models[7,62] at BYU and/or taken from recent experimental measurement. Additionally, it was important that the same assumptions be used in the steady-state and ignition codes so that predicted results from the the AP/HTPB model could be compared to one another directly.

One concept of the ignition model that must be addressed before any results are presented includes the current assumptions regarding condensed-phase decomposition within the model. The Phase3 steady-state propellant code employs the assumption that condensed-phase decomposition begins at the melt temperature of the modeled ingredient/propellant. This value is typically measured for a single propellant ingredient (like monopropellant nitramines, for which

the code was originally developed) but becomes somewhat arbitrary when considering a model for propellants that contain multiple ingredients with various melt temperatures. When modeling propellants such as AP/HTPB that have evidenced significant decomposition[89,90,139,169] at temperatures lower than the temperature defined in the current AP/HTPB model (735 K) and that have also been seen to begin decomposing very early-on in relation to the go/no-go point in ignition work[65], using the assumption that no sub-melt decomposition is present at sub-melt tempearatures may negatively affect the modeled results.

Despite experimental observations to the contrary, the results for the current AP/HTPB ignition model have been treated in like manner to the AP ignition model, wherein time to ignition is reported as time to heat the surface of the propellant to the assumed melt temperature of 735 K. This choice is consistent with the assumption made in the current steady-state AP/HTPB model. This defined surface temperature condition is also in the same region as ignition temperatures that have been reported as being used in industry[170] (700-750 K) and by Eager *et al.*[171] (833 K) for propellants of similar formulation.

The primary reason for making the decision neglect sub-melt decomposition within the current AP/HTPB ignition model was due to convergence issues within the ignition code when using the AP/HTPB gas-phase mechanism with Tanner's HCN-elimination reaction. Inclusion of this reaction in the gas-phase mechanism led to near-immediate divergence of all calculations attempted (for ignition and cookoff) within the ignition code, while not including it allowed for simulations to be completed without issue. Thus, the HCN-elimination reaction was removed from the gas-phase mechanism for all simulations made by the current model. Removing the HCN-elimination reaction from the AP/HTPB steady-state model resulted in a drop of the predicted burning rate by 50%. All calculations that have been made using the current AP/HTPB

model for times that predicted significant condensed-phase decomposition had low burning rates due to this issue. Thus, any possibility of making valid predictions using a model that used sub-melt decomposition were lost, as well as any confidence in the simulated region of time after the point of ignition. Thus no transient predictions or transitions to steady-state augmented burning seem credible or will be discussed in the results of the AP/HTPB ignition model. These predictions should be considered by future efforts, after the short-comings of the current AP/HTPB model have been rectified. Predictions presented from the current work only include simulation times when the predicted burning rate of the propellant/ingredient is assumed to be near zero.

5.2.1 Results and Discussion

There are three metrics available in reported experimental data for validating any ignition model: time to first decomposition, time to ignition (first light, somewhat arbitrary), and go/no-go time. Time to first decomposition has been assumed to be at a surface temperature of 513 K, time to ignition at a surface temperature of 735 K, and go/no-go times are not predicted.

Time to first decomposition was reported by Atwood *et al.*[65] and determined by an observable, physical change in the surface of the propellant. Model predictions for a time to surface temperature of 513 K have also been made, since the cubic phase transition has been suggested[172] as the approximate temperature at which significant reaction in the AP/HTPB condensed phase begins to occur. Predictions of time to ignition (735 K, solid lines) and time to assumed first decomposition (513 K, dashed lines) for AP80/HTPB20 and AP84/HTPB16, along with corresponding data from Atwood *et al.*[65,88], are presented in Figure 55.

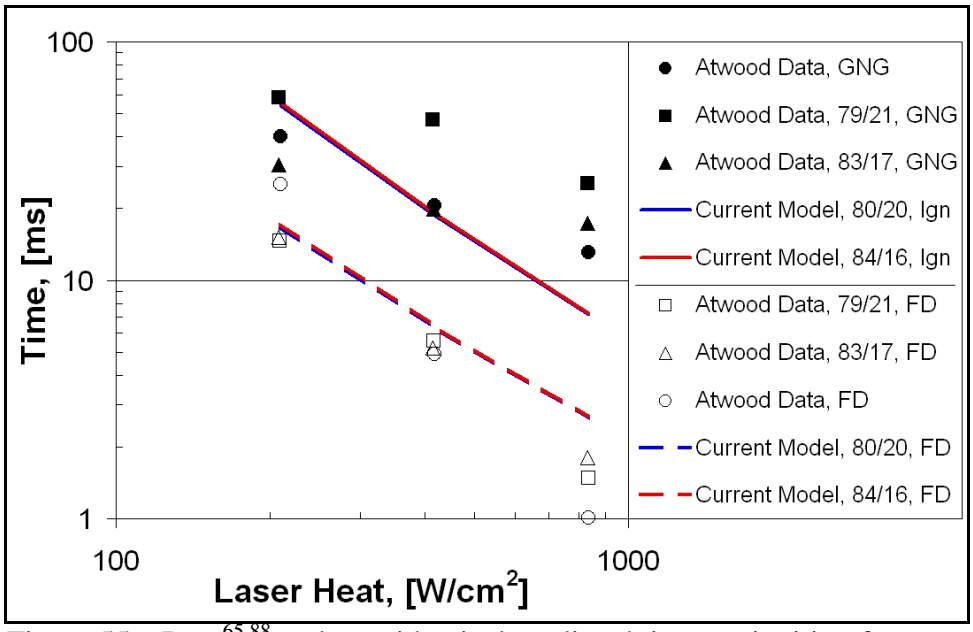

Figure 55 – Data[65,88] and near identical predicted times to ignition for two formulations of the current AP/HTPB model, 1 atm

The difference between the predictions for these two formulations of the AP/HTPB model is very small and may be occurring because no sub-melt decomposition has been accounted for in the current ignition model. The only affected difference between the two is a very small change in the effective thermal conductivity of the modeled propellants due to formulation. It is immediately obvious that the model predictions have slopes that are steeper than the go/no-go data and more shallow than the first-decomposition data. There are several possible reasons for these differences in regard to the model.

Parameters of greatest impact on AP/HTPB time to first decomposition predictions are the thermal conductivity and laser-absorption parameter of the solids. The temperature range in which these calculations are made (298 to 513 K) contain the most accurate and repeatable measurements of thermodynamic properties for AP (data varies by ±11% around the thermal conductivity fit) and HTPB (data varies by ±40% around the thermal conductivity fit). The current codes use a volume-averaged, linear-interpolation method to calculate the overall

propellant thermal conductivity for the AP/HTPB model. The analysis presented previously in Section 4.3.3 on steady-state modeling of AP/HTPB propellants suggests that the thermal diffusivity of the AP/HTPB model was being described accurately, but that the application of Parr's fits in the model were possibly over-estimating the thermal conductivity to some small degree.

The amount of variability present for AP absorption of the laser was presented in Figure 48, and includes a possible range of values that could feasibly work within the construct of the AP model (Table 17) and thus be applied to the AP/HTPB model. There is significantly less variability in the absorption parameter of HTPB, which has been observed[144] to have a value of 361 cm^{-1}, varying by less than 3% over the range of laser-light wavelength to which AP has been applied in the current model.

Any variance in the amount of applied laser energy that is absorbed by the solid propellant has not been considered by the model. It has been reported[145] that 15% of the laser applied to HMX during laser-augmented combustion is lost due to reflectivity and/or attenuation due to absorbing gas-phase species and liquid droplets above the surface. The reduction of the apparent laser energy absorbed by the surface of a propellant/ingredient has been reported[173] for AP (7.5%) and AP-based propellants (10%).

There is also one factor concerning the experimental data that should be addressed. Atwood *et al.*[88] brushed ZrC powder onto the surface of the propellant to "enhance the absorption" of the applied laser energy for ignition data. They stated that this coating made the absorptivity of the heat source (CO_2 laser or arc-image) more uniform. It is unknown how the application of this powder, and/or its uniformity on the surface, might have affected the way the laser was absorbed, the way/amount in which the laser might have been reflected, or the level to

which it might have affected the heating rate of the propellant surface due to direct heating of the powder by the laser. Additionally, the chemical kinetics at the propellant surface might have also been affected since ZrC has been reported[174] elsewhere to be a catalyst for AP-based propellants. None of these possibilities has been taken into account in the current model.

Ignition predictions for the current AP/HTPB model are compared against a wider range of AP/HTPB ignition data[65,87,91-94,116,175,176] in Figure 56. Note that some of the data have been designated as first-light (FL), which signifies the initiation of significant gas-phase reaction and is assumed to be approximately equal to (but just longer than) the time of first decomposition.

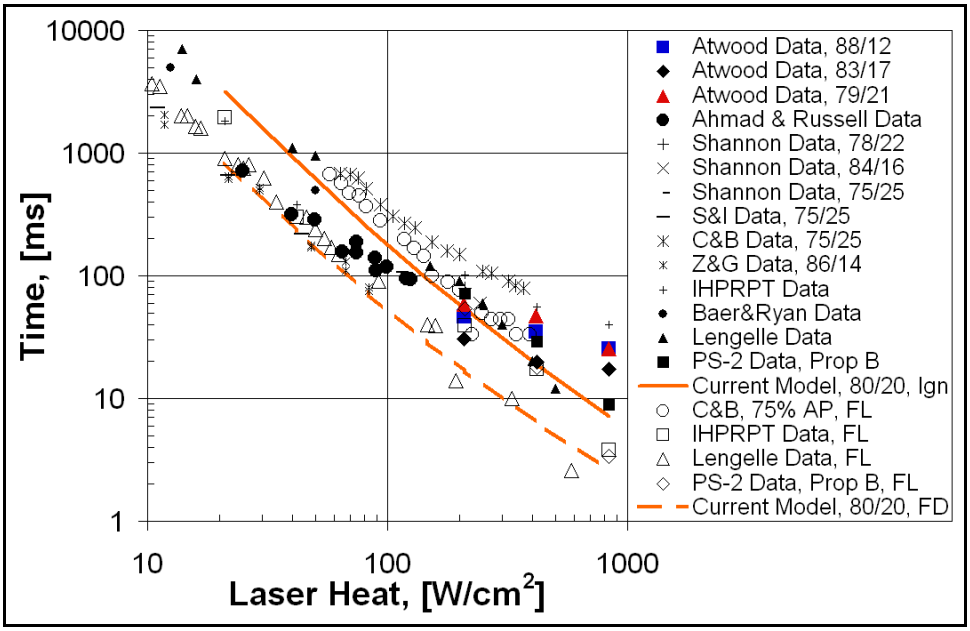

Figure 56 – Predicted time to ignition and time to first light for current AP/HTPB model and data[65,87,91-94,116,175,176], 1 atm

The AP/HTPB ignition data are bounded by the predictions of a time to surface temperature of 513 K and 735 K. Predictions are quite good at lower fluxes but begin to under-predict time to ignition at high heat fluxes. The predictions based on a time to surface temperature of 735 K are very close to the recent first-light data of Cain and Brewster, which

data are similar to the assumptions made in the model (CO_2 laser, first light reported, and fine AP particles—2 micron—used in the propellant), though these data are fairly different than the other sets in the graph. Some of the data sets presented contain propellants with small fractions of carbon, iron oxide, or nitramines, and include vaious sources of heat supply (conduction by hot gases, ARC-image lamps).

Predictions reported in Figure 56 will shift slightly upward if laser reflection is taken into account (predicted time to temperature will become longer) An AP/HTPB model with a condensed-phase heat release that is exothermic, as has been suggested by the current work, would lead to predicted ignition times that were shorter, if sub-melt decomposition were included. An approximate effect of applying an quasi-exothermic, sub-melt decomposition and data[65,87,91-94,116,175,176] is shown in Figure 57.

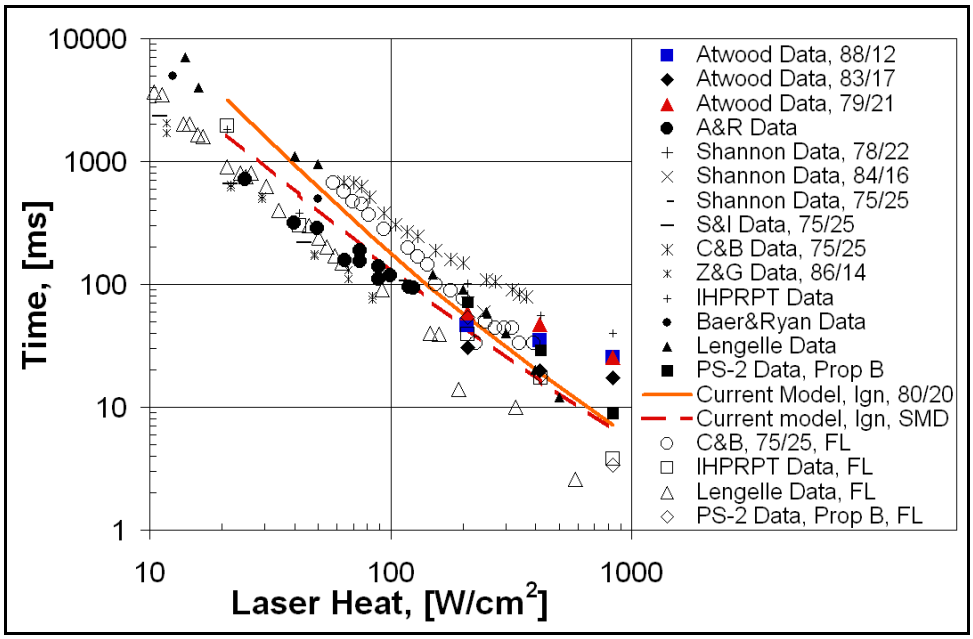

Figure 57 – Effect of sub-melt decomposition on current AP/HTPB model and data[65,87,91-94,116,175,176], 1 atm

The exothermic approximation made for these results was accomplished by changing the heats of formation for AP and HTPB to result in a condensed-phase heat relase of ~150 cal/gm, exothermic. Two levels of condensed-phase decomposition (pre-exponential values of 10^7 and 10^9) were investigated within the temperature range over which AP is assumed to be in the cubic phase by the current model (513 to 735 K). These two values represent a case where decomoposition over this temperature range is three orders of magnitude less than that of the melt layer (more consistent with observations[119] for RDX, upon which the Phase3 code was based) and another where the decomposition is only a single order of maginitude less than that in the melt layer (more consistent with an assumption of continuous condensed-phase kinetics). The case with a pre-exponential of AP/HTPB decomposition of 10^9 was the only one at which a significant difference between the predictions was noticable within the range of applicable heat fluxes, and thus only predictions made for this level of decomposition have been reported in Figure 57. Although the overall effect is not large, this graph does show that the effect of sub-melt decomposition becomes more pronounced at lower heat flux levels and would become even more prominent for the lower heat fluxes associated with cookoff.

A majority of the ignition data presented for AP/HTPB are at the go/no-go point of the propellant sample, which is very ill-defined for making such determination within the model. Experimental go/no-go data are reported as the time at which 50% of the samples attempted will transition to steady-state burning once the heat source is removed. Such a comparison, were it to be made by prediction, would call for an extremely precise description of the reactions and kinetics within the propellant model, which the current AP/HTPB steady-state model does not have.

In reality, the ability of an AP/HTPB propellant to be able to transition to steady-state burning after the removal of the heat flux is likely dependent upon the amount of heat held by the propellant as compared to that under steady-state burning conditions. This comparison can be made by looking at the predicted temperature profile within the solid propellant at the time of ignition and that for the predicted propellant at steady state. Ignition temperature profiles that are steeper than those at steady state will more than likely extinguish, while those that are more shallow should be able to transition to steady-state burning. This comparison for AP80/HTPB20 is given in Figure 58.

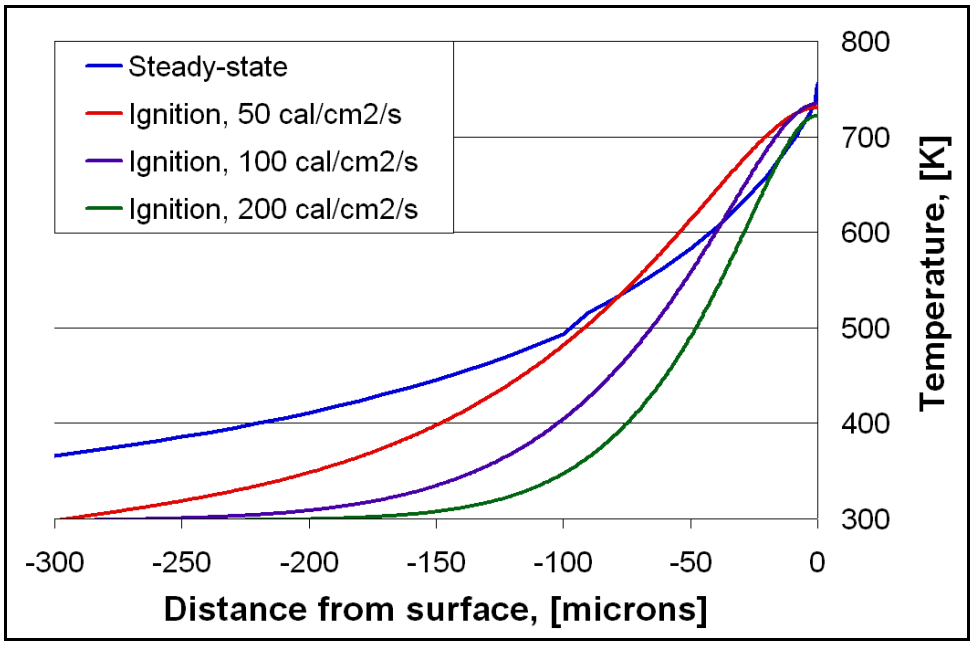

Figure 58 – Predicted temperature profiles of current AP80/HTPB20 model, 1 atm

In the above figure, the case for 50 cal/cm^2/sec looks to be reasonably close to the temperature profile prediced at steady state, though it is difficult to say as the temperature profile of the steady-state model is extremely steep near the surface. The profiles will of course be

altered for a condensed-phase model that includes exothermic decomposition occurring earlier than the melt temperature. An exothermic decomposition would not only shorten the time to ignition but will also have the propensity to widen the thermal layer of the propellant that is at a raised temperature due to the fact that heat is being generated at points within the sub-surface by decomposition.

The largest and possibly most important factor relating to the accuracy of go/no-go predictions is an accurate portrayal of evolved/absorbed heat associated with condensed-phase decomposition. Reactions in the condensed phase lead to the evolution of gas-phase species, which in turn react in a gas-phase flame. Propellant ingredients such as AP, which appear to have an endothermic condensed-phase decomposition, should then be dependent upon the heating and subsequent ignition of the evolved gas-phase species before being able to reach a go/no-go condition. In contrast, AP/HTPB propellants appear to have an exothermic condensed-phase decomposition and might be able to reach a condition whereupon the reactions in the condensed phase could thermally run away and lead to the go/no-go condition before an actual gas-phase ignition event occurs.

5.2.2 SUMMARY

The current AP/HTPB model describes ignition data across a wide range of fluxes, bounding the data for time to surface temperature of 513 K (assumed first decomposition) and 735 K (assumed ignition), but were unable to predict the trends of go/no-go times. Go/no-go predictions are much more difficult to predict as they require a very accurate representataion of the kinetics and heat release associated with the deflagration of the propellant/ingredient. Predictions from the current AP/HTPB and model are based upon the current Phase3 assumption

that no sub-melt decomposition occurs prior to ignition. This assumption should be relaxed in the future, allowing the kinetic decomposition of the condensed phase to determine ignition times, instead of simply the predicted temperature of the propellant surface.

The work completed for the AP/HTPB ignition model that has been presented in Chapter 5.2 is shown in Figure 59 within the validation structure first presented in Chapter 3.

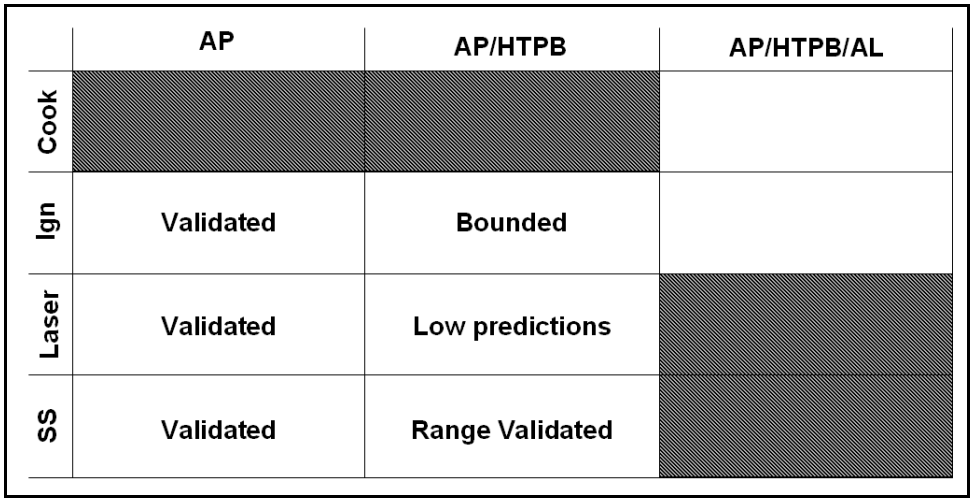

Figure 59 – Validation structure including work on the current AP/HTPB ignition model

5.3 AP/HTPB/AL IGNITION AND COOKOFF

After the AP/HTPB model was validated against experimental data for steady-state and ignition conditions, it was applied toward defining the AP/HTPB/Al model. The kinetic decomposition scheme for the AP84/HTPB16 formulation of the AP/HTPB model was used to describe the condensed-phase kinetics of the AP/HTPB/Al model, since the ratio of AP to HTPB in that formulation is very similar to a typical aluminized propellant. As with the AP84/HTPB16 formulation of the AP/HTPB model, there has been no consideration of multi-modal distributions of AP that would be necessary to make realistic propellants with this formulation.

Although non-realistic, this is consistent with the idea that there is no affect of multi-modal distributions upon the physical properties of the propellant built into either model, and that the current predictions of the model are for times prior to those when multi-model distributions of AP might make an effect upon ignition predictions. Looking into the necessary multi-modal distributions of AP and their further effect upon simulations was beyond the scope of the current work.

The only difference in the calculations of the AP/HTPB and AP/HTPB/Al models is the inclusion of inert aluminum in the AP/HTPB/Al model. There is no current consideration of aluminum in the gas phase or for kinetic reactions involving aluminum in either phase of the current model. Additionally, the aluminum reflection model detailed in section 4.2 was employed for the AP/HTPB/Al model simulations in all presented ignition calculations. Laser heat lost due to reflection according to the sub-model varies linearly from 0 to 37% for aluminum backscatter values ranging from 0 to 100% within the reflection sub-model. This range is dictated by the absorption of laser light as it passes through the modeled components of an AP/HTPB propellant. Assumptions used for that sub-model are that 0% of the incident laser light is absorbed by the aluminum particles, 14% is back-scattered, and the remaining 86% is forward-scattered. These parameters within the reflection sub-model led to 6% of the incident laser heat being lost due to reflection. The current assumption for the AP/HTPB/Al ignition model is that time to ignition is equal to the time the surface takes to reach a temperature of 735 K, which is consistent with the assumptions made for the AP/HTPB steady-state model.

5.3.1 Ignition Results and Discussion

Predicted times to ignition for the AP/HTPB/Al model are compared to experimental data[115,175] in Figure 60.

There are two groups of data presented in Figure 60, nearly all of which are bound by the first-decomposition and ignition predictions of the model. The first group is from a number of different sources (designated by **: Atwood Ign, Baer, Lengelle, and China Lake) that were all referenced by Wilson *et al.* for their work with an AP/PBAN/Al propellant.

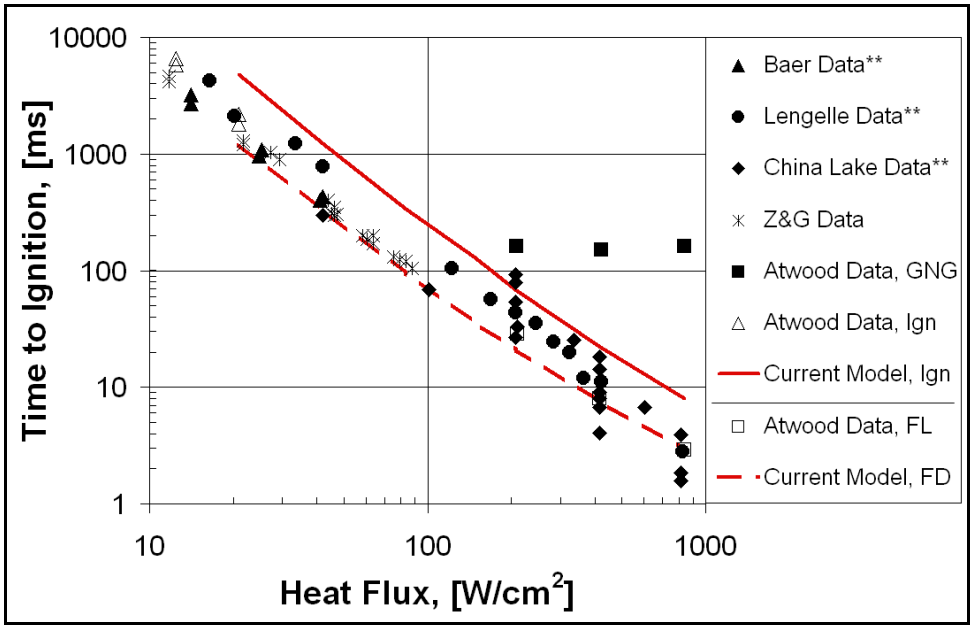

Figure 60 – Predicted time to ignition and time to first light for current AP/HTPB/Al model and data[65,115,175], 1 atm

None of these external data sets were reported with references, formulations, or experimental conditions; however, this group of data was compared to the experimental cookoff data collected by them. The formulation of their propellant was reported as being an 80% solids loading of AP and aluminum in a PBAN binder, without specificity for either component; however, all of their figures referred to "NASA production samples", which for the space shuttle

propellant are typically closer in formulation to 86% solids loading (AP and aluminum) in a PBAN binder. In this case, the most important parameter is the loading of aluminum, since it will contribute the greatest effect upon the overall thermal conductivity of the propellant.

When comparing this first group of referenced data and the Zanotti and Galfetti[175] data to the most recent Atwood *et al.*[65] data, it looks as if all the experimental data points excluding the Atwood set are more consistent with first-light times rather than go/no-go times. The current formulation of the AP/HTPB/Al model is most consistent with the propellant used for the go/no-go data set from Atwood *et al.*[65] for an AP/HTPB/Al propellant with 68% AP and 20% aluminum (overall 88% solids loading), although the predictions of the model are furthest from it.

The trend of the ignition predictions in Figure 60 looks fairly good when compared to all of the data, but the go/no-go data from Atwood *et al.*[65] obviously occur at significantly longer times than those predicted by the model at these levels of heat flux (by 2 to 20 times). In this heat flux range, the large difference between data and model predictions is similar to that from the AP/HTPB model, upon which the AP/HTPB/Al model is based, and is determined by the amount of time necessary for the chemistry within the condensed-phase decomposition to develop to a point such that it can transition to steady-state burning when the heat is removed. This larger difference for the AP/HTPB/Al model is also due to the extra time needed for the propellant to absorb the necessary amount of near-surface heat to reach the point of ignition. Heat collects less efficiently at the surface for aluminized propellants because more heat is reflected away from the propellant due to the aluminum particles, and heat is also conducted more quickly into the bulk of the propellant, due to the higher thermal conductivity.

A comparison of the predicted temperature profiles for the AP/HTPB and AP/HTPB/Al models is presented in Figure 61, although there is currently no steady-state AP/HTPB/Al model to which these profiles may be compared.

The temperature penetrates farther into the propellant for the AP/HTPB/Al model, since the heat absorbed near the surface of the propellant is conducted away more quickly by the higher thermal conductivity of the propellant. The predicted temperature profiles are compared at the approximate time of ignition, which is different for each level of modeled heat flux, but occurs at conditions where the surface temperature is approximately equal to the ignition temperature of 735 K in every case.

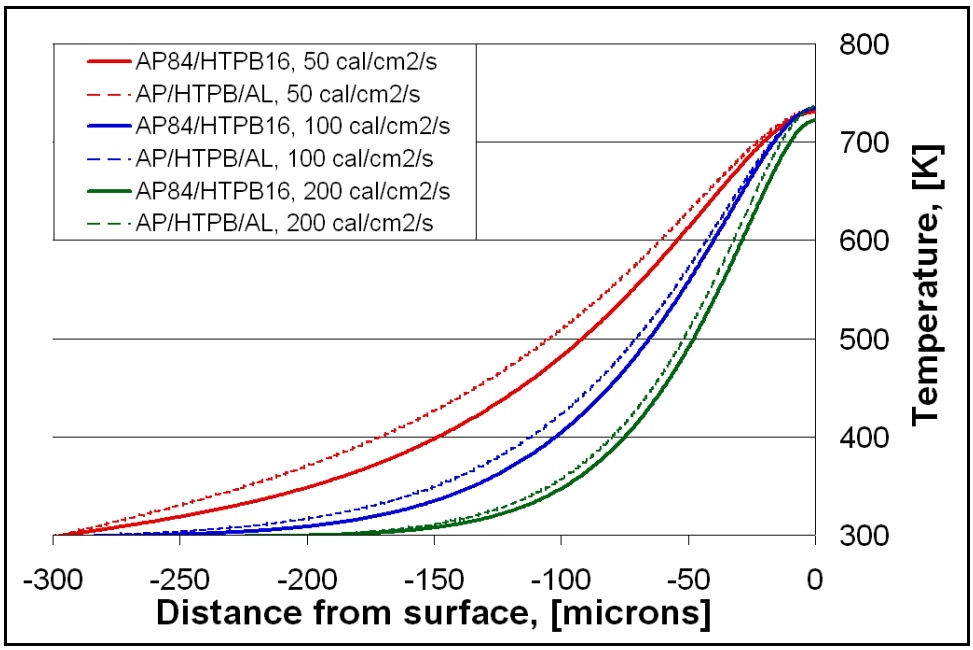

Figure 61 – Predicted temperature profiles at ignition for current AP/HTPB and AP/HTPB/Al models, 1 atm

A comparison of predicted times to 513 K for both models and first decomposition data is given in Figure 62.

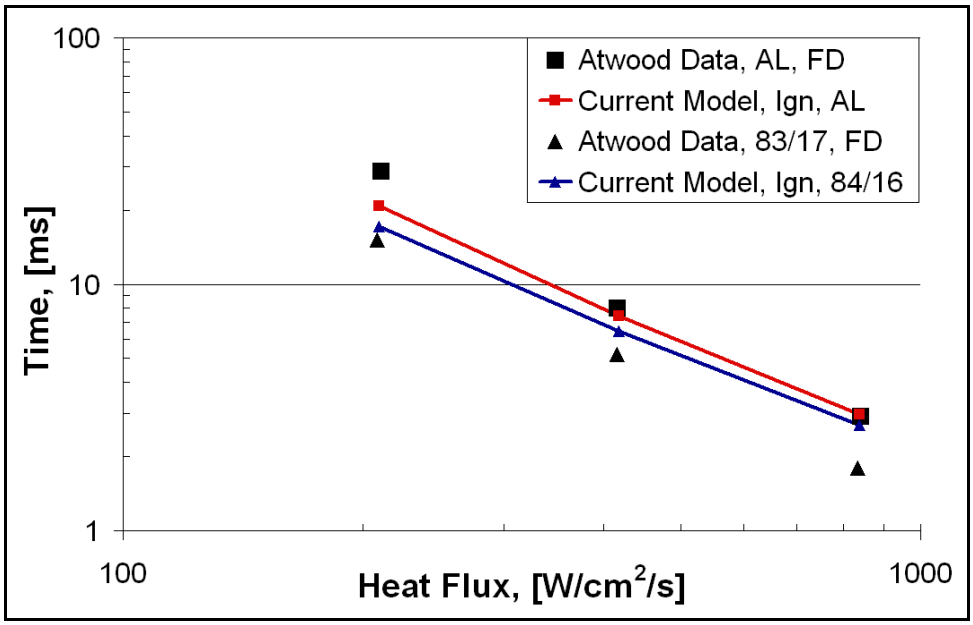

Figure 62 – Aluminum effects on current model of predicted time to first decomposition and data[65], 1 atm

The predictions are quite similar to the data. If the assumptions of the current model are valid, then it seems as if the AP/HTPB contribution to the thermal conductivity of the modeled propellant might be too high due to the too-shallow slope of both predictions. This is consistent with what was seen in the AP/HTPB model. The contribution of aluminum to the thermal conductivity may also be too low, since the difference between the two predictions is smaller than the spread in the data. Although, this possibility is difficult to determine because the difference between the preidictions of the two models is probably due to both the increased thermal conductivity and increased laser light reflection of the aluminized propellant. These two trends in the predictions (slope too steep and difference between predictions for aluminized and non-aluminized propellants) are consistent with what was presented in Figure 32, which compared the thermal conductivity data from similarly formulated propellants to the approximations used within the current models.

A comparison of predicted times to ignition for the AP/HTPB model and experimental go/no-go points[65] is quite different, as shown in Figure 63.

It is unclear exactly why there is such a large difference between this specific data set (Atwood[65], go/no-go) and the various others that were presented in Figure 60. The difference between the AP/HTPB and AP/HTPB/Al predictions and the corresponding data is quite large, not only in value but also in slope. Arguably, the majority of the difference between the AP/HTPB/Al predictions and data can be attributed to the same cause of the difference between the AP/HTPB model and data: the additional time required by the propellant's decomposition chemistry to reach a point at which the transition to steady-state combustion may be attained.

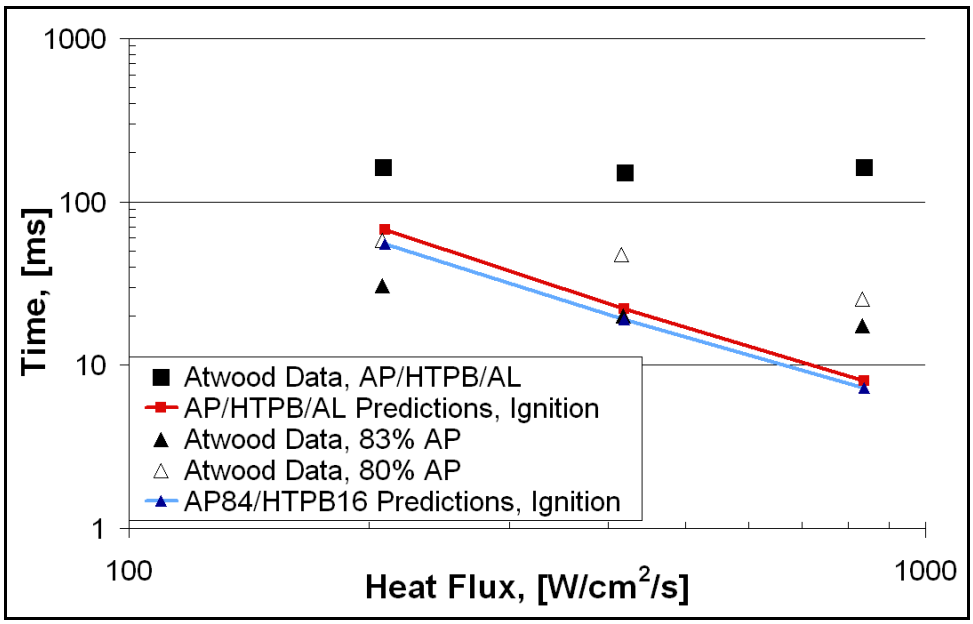

Figure 63 – Aluminum effects on current model of predicted time to ignition and data[65], 1 atm

Another portion of this larger difference between the AP/HTPB/Al predictions and data might come from the amount of time it takes the propellant to come to an augmented burning rate, which is affected by the higher thermal conductivity of the aluminized propellant. Also,

prior to entering the gas-phase, aluminum acts primarily as a heat sink, and thus the need for additional energy within the condensed-phase, and thus additional time is required for the modeled propellant to be heated by the laser. The amount of aluminum that is uncovered as the solid AP/HTPB propellant begins to decompose is also possibly playing a significant role. Aluminum particles present near the surface during this span of time (between the first decomposition of the propellant and the go/no-go time) may have the chance to agglomerate, ignite, lift into the gas-phase domain, and increasingly scatter the laser light before it ever reaches the surface of the propellant, if time scales are sufficient. All of these possible effects will tend to increase the amount of time it takes for a modeled propellant to reach a go/no-go condition as it inhibits the amount of heat that is applied to the surface of the propellant.

The variation of predicted time to ignition for given levels of defined backscatter within the aluminum reflection sub-model is shown in Figure 64 with go/no-go data[65].

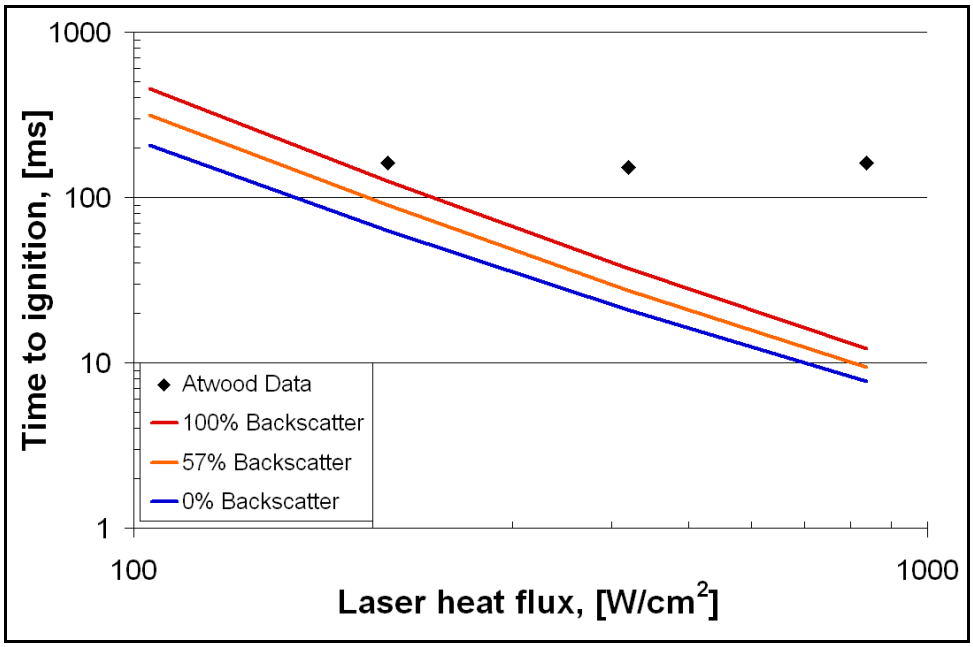

Figure 64 – Aluminum reflection parameter variance within AP/HTPB/Al model and go/no-go data[65]

The predictions for the current model assume that 14% of the laser light incident upon the aluminum particles will be back-scattered, while the remaining 86% will be forward-scattered. The resultant spread of the predictions ranges between 60% and 120% across this range of heat flux. The results at low heat fluxes for the maximum amount of back-scatter from the aluminum particles nearly makes up the entire difference between the predictions and the data; however, it is unlikely that the laser light back-scatters so perfectly (100%) from the aluminum particles, since the dominant scattering angle at these particles sizes is near forward.

Mie scattering calculations show a cross-sectional increase of the aluminum particles (over their geometric cross section) by approximately a factor of 2, varying slightly with the size of the particle. When including these effects, the predicted times to ignition become an additional 10% longer. Although this is an important effect to consider for the reflection sub-model, the laser-driven ignition predictions and experimental go/no-go times are still fairly far from one another at these relatively high levels of heat flux. The difficulty in using comparisons such as these for validation is that the aluminum reflection model becomes a very important parameter for making ignition predictions of an AP/HTPB/Al propellant (resulting in predictions varying by a total of 70 to 130%), but doesn't affect cookoff predictions at all. In essence, without some sort of separate validation, the reflection sub-model becomes a tuning parameter for ignition predictions and doesn't add anything of value to understanding or predicting cookoff. Earlier validation of the AP/HTPB/Al model to ignition data in Figure 60 is thus the primary source of validation for this level of the model.

The work completed for the AP/HTPB/Al ignition model that has been presented in Chapter 5.3.1 is shown in Figure 65 within the validation structure first presented in Chapter 3.

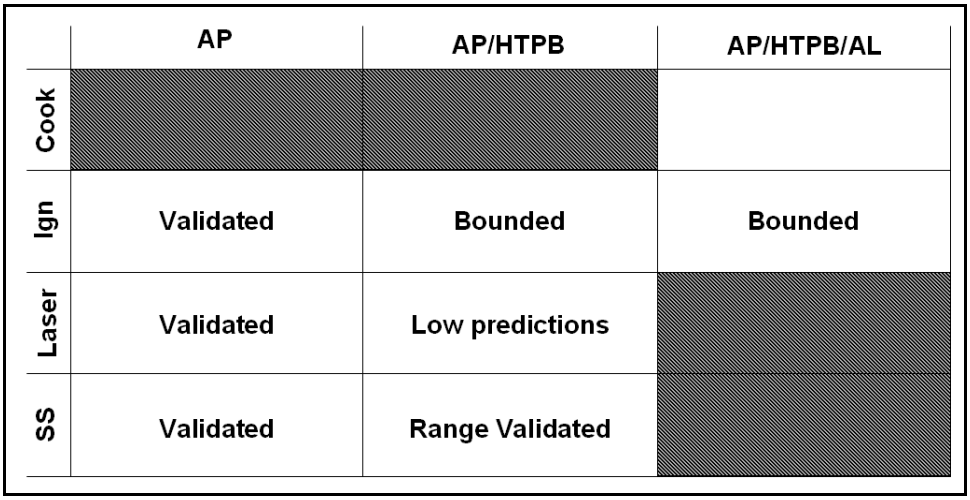

Figure 65 – Validation structure including work on the current AP/HTPB/Al ignition model

5.3.2 COOKOFF RESULTS AND DISCUSSION

Cookoff systems typically include a sample of propellant or high explosive material that has been confined within a given container. This container, and the enclosed propellant, are heated by an external source (fire, oven, electric blanket) until an ignition event occurs. These events can range from being relatively small (fast cookoff, high heat flux) where only a small portion of the propellant is heated before the point of ignition, to explosively large (slow cookoff, low heat flux) where a majority of the propellant is heated to a reactive temperature before ignition.

The results from AP/HTPB/Al cookoff model were surprising on the whole and yet very consistent with what had been seen during the prior validation of the propellant/ingredient models. A comparison of the experimental data and model predictions for three different cookoff scenarios is given in Figure 66 along with data[114-116].

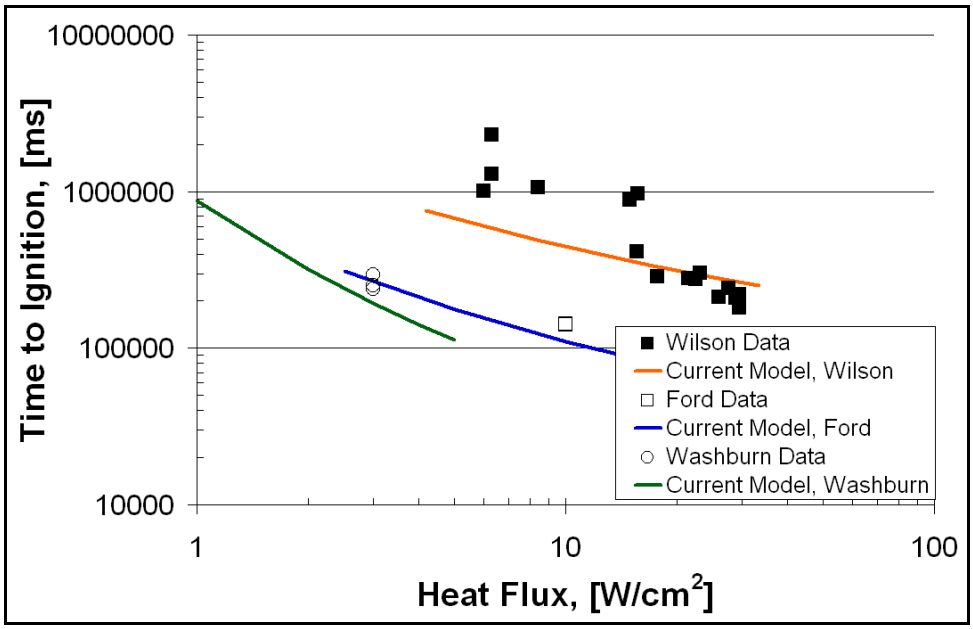

Figure 66 – AP/HTPB/Al cookoff predictions for the current model and data[114-116]

The predictions are for time to a surface temperature of either 435 K or 550 K (reported surface temperatures at ignition for the data sets), values which are much lower than the previous criteria (735 K). Predictions show ±25% variation compared to data when using an ignition temperature within the model that is consistent with the data. On the whole, predicted times to ignition are shorter than indicated by data, especially for the data of Wilson *et al.* at lower heat fluxes, although these data had a higher reported ignition temperature (reported ignition temperatures varied significantly across their data). Predictions of these three data sets are specific for each set as the physical geometry and physical components of each set were different. Propellant surface temperatures for the Ford *et al.* data set were reported as being ~435 K at the time of ignition. The Wilson *et al*. data set surface temperatures vary from 400 K to 525 K with an average at ~460 K, and the average for the Washburn *et al.*[116] data is ~550 K. All of the reported times to ignition vary significantly from one another, and thus predicted times to an average of the reported surface temperatures in the data are presented in Figure 66 for each data set. All simulated liners/insulators were modeled using the assumption of HTPB thermal

properties, assuming no decomposition, due to a lack of pertinent data on the various materials used in the experimental works.

The current AP/HTPB/Al model is based on the kinetic decomposition scheme of the AP84/HTPB16 formulation of the AP/HTPB model, which is assumed to reach "ignition" when the surface of the propellant has reached 735 K. The simulated propellant has no condensed-phase decomposition prior to this temperature. This assumption was made both to keep the propellant ignition models consistent with the steady-state models and to allow for convergence of the ignition code. Two of the experimental data sets for cookoff reported the ignition event to occur once the propellant surface had reached a temperature of ~435 K. This observation is consistent with what has been observed in the past by others[114,177] for cookoff systems that included insulators and liners. The more recent findings of Washburn *et al.*[116] have shown ignition temperatures in the realm of ~550 K for a cookoff system that only included the propellant and steel casing, which is more consistent with surface temperatures associated with the bare ignition data of AP/HTPB propellants[47,178].

Temperatures at the inner steel surface of the cookoff system reported by Wilson *et al.*[115] and a comparison of the predicted propellant surface temperatures of the current model to data are given in Figure 67.

It is likely that the reported low surface temperatures at ignition of Wilson *et al.*[115] are due to the thermal expansion of the steel container/article and opening of an air gap (added resistance to heat flow) between the propellant/liner/insulator and the steel case. The size of the air gap has been reported by Meredith and Beckstead[3] as being a significant variable for predicting time to ignition for cookoff systems. The size of any air gaps in the referenced

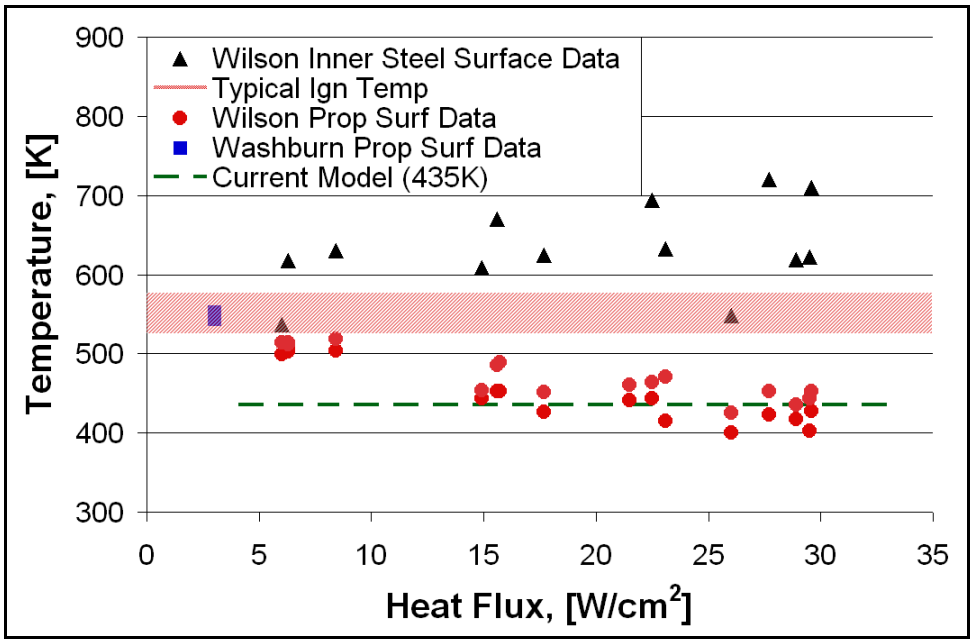

Figure 67 – AP/HTPB/Al precictions of surface temperature at ignition for the current model and data[115,116]

systems are unknown. This phenomenon could lead to decomposed products from the propellant being ignited by the hot inner surface of the steel. This possibility is consistent both with what is reported by Washburn *et al.*[116] and also with the reported result that the "surface temperature at ignition" for the Wilson *et al.* data approaches a more typical value of ~550 K at lower heat fluxes where the temperature difference between the propellant and the stell shell will not be as large.

A comparison of the predicted surface temperature rise as a function of time was also compared to the Ford *et al.* data[114] as an additional source of possible model validation, and is presented in Figure 68.

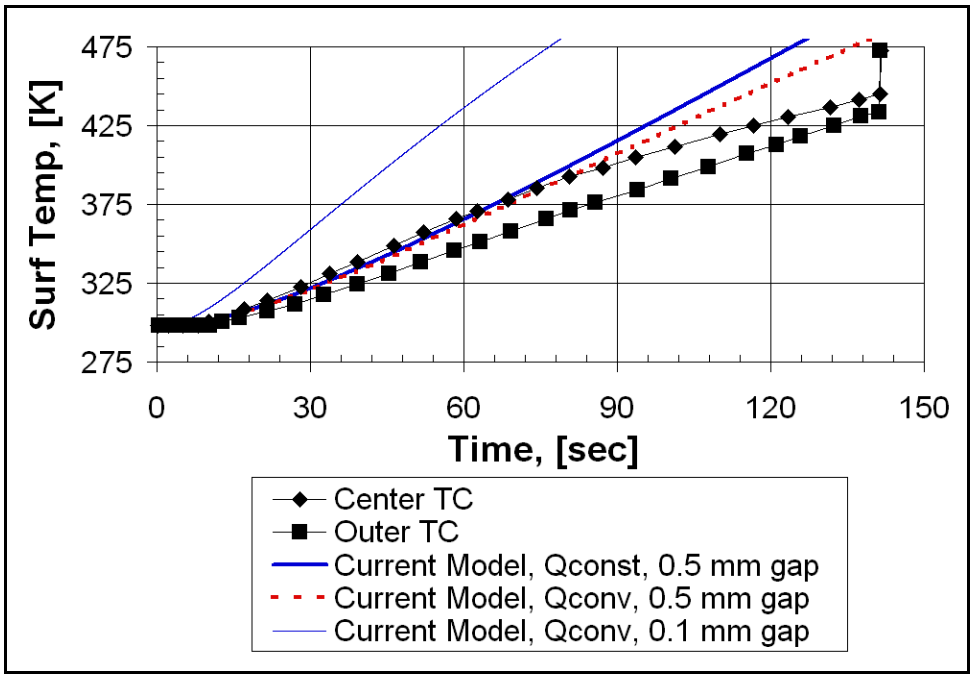

Figure 68 – Predicted surface temperature of an AP/HTPB/Al cookoff simulation for two boundary-condition types and data[114], 10 W/cm^2

Properties for the liner, insulator, and steel shell used in this calculation were those presented by Ford *et al.*, except for those of the actual propellant, which were calculated by the current model. Propellant property differences between those reported (measured) by Ford *et al.* and those used in the current model were within ±30% of each other across the temperature range of interest (298 to 435 K). Three different simulations are presented in Figure 68 for comparison: one base case and two variants. The first variant included a new application of the external heat flux (convective versus constant heat flux) and the second variant included a change in the size of the air gap between the propellant and liner. The thermal expansion of a cylindrical steel shell was calculated to grow to ~0.3 mm prior to the ignition point by completing a simple thermal analysis of the steel using a thermal expansion coefficient of $1.1 \cdot 10^5$/K. The predicted temperature profile of the base case at ignition using the current model was nearly identical to the modeling efforts reported by Ford *et al.*

The base case was run with a constant external heat flux of 10 W/cm^2 with an air gap of 0.5 mm. Comparison to the data is quite good early on, but the predictions rise significantly higher than the data at longer times. This indicated that something had probably changed within the experimental system that has not been accounted for in the model. A convective boundary condition was also applied to the model that included a convective gas temperature of 1570 K and heat transfer coefficient of 80 W/m^2/K, as reported by Ford *et al.* Using this boundary condition curtailed the divergence of the predictions from the data somewhat but not nearly enough. Reducing the length of the air gap to 0.1 mm changed the results significantly, and although varying the size of the air gap in this direction probably makes the simulation more consistent with the experimental setup, it moves the predictions even further from the data.

A compliation of the ignition data, cookoff data, and predictions of the current model for AP/HTPB/Al propellants is given in Figure 69.

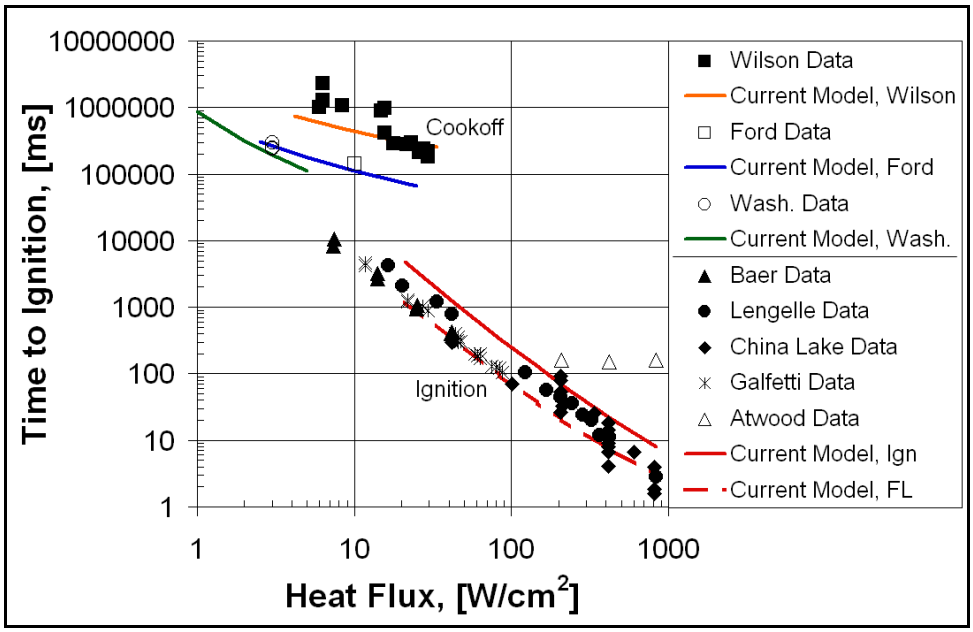

Figure 69 – AP/HTPB/Al ignition and cookoff predictions with data[65,114-116,175], 1 atm

At first glance, such a discrepancy between the location/trends of the cookoff and ignition data/predictions seems odd. The difference, however, is one that has been addressed before by Meredith and Beckstead[3]. They reported that it is the heat flux that reaches the surface of the propellant, and not the heat flux applied to the outer casing, that is the important parameter when considering cookoff data. This interfacial heat flux can be altered significantly in cookoff systems by a number of factors, including: the properties of the liner(s), the metal casing, the external conditions, the properties of the propellant, the length of the air gap, and others. It is difficult to compare ignition events for these two configurations (ignition and cookoff) because ignition data typically use precise heat flux control (quick ramp, followed by an overwhelming majority of the time being spent at a constant applied heat flux), whereas cookoff systems typically deliver a heat flux to the surface of the propellant that varies significantly.

One way of comparing these two disparate kinds of predictions is to determine the total energy absorbed by the propellant by the time of ignition. This is made by integrating the heat flux at the surface of the propellant with respect to time. Calculations for the AP/HTPB/Al ignition data and current model predictions for the cookoff cases are presented in Figure 70. As the necessary data (heat flux at the propellant surface) were not reported with the cookoff data, the current model has been used to predict the total energy flux applied to the surface of the propellant for these data sets using as assumed air gap of 0.5 mm.

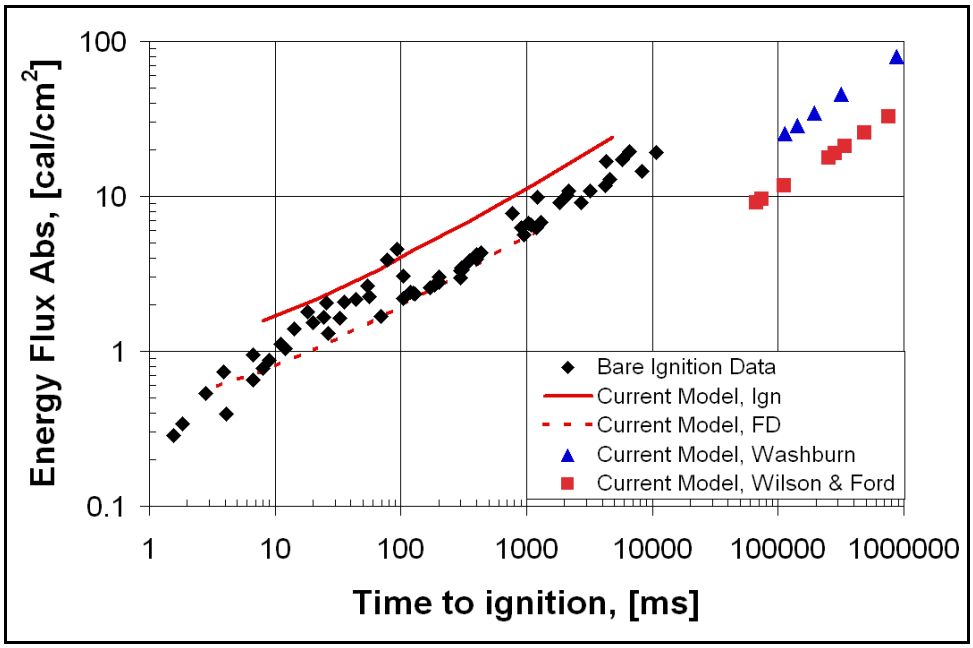

Figure 70 – Total energy applied to ignited propellants at time of ignition, calculated from data[65,114-116,175] using current model

Figure 70 is a representation of the total energy flux received by the propellant at the time of ignition. The data points above should all lie along a similar line if the relationship between time to ignition and energy flux received by the propellant is similar; a difference in a given data set suggests that something is affecting the time to ignition. Predictions calculated from the simulation of the Washburn *et al.* data presented in Figure 70 are much closer to extrapolations of the bare propellant ignition data than that of either Wilson *et al.* or Ford *et al.* These sets of predictions seem to imply that the cookoff propellants are probably igniting early when compared to the bare-surface ignition data. Assumptions concerning the liners/insulators within the cookoff model for representing each set of data are also probably affecting the results. Additionally, the size of the air gap between the propellant and the steel case, the location of the air gap, the transient growth of the air gap, and the increasing pressure of the system, are also probably important factors, but have not been included in the current analysis. The temperature

of the steel shell at the time of ignition should probably also be taken into account, since the decomposed products of the propellant will be in close proximity to it and could be leading to the apparently early ignition of these systems.

5.3.3 SUMMARY

AP/HTPB/Al ignition predicitions bound nearly all of the pertinent data between predicted time to first decomposition/light (at 513 K) and predicted melt temperature (735 K). The remaining differences between predictions and go/no-go times probably arise from the description of the condensed-phase propellant decomposition kinetics not accurately predicting the pre-ignition regime, and the increased time associated with the effect of adding aluminum to the simulated propellant.

AP/HTPB/Al cookoff predictions are within ±25% of the data, typically being low (early). Remaining sources of variability may include: liner/insulator properties, accuracy of propellant properties, transient thermal expansion of the steel shell, and possible early ignition due to the proximity of decomposed gases to the heated steel shell of cookoff test articles.

The work completed for the AP/HTPB/Al ignition model that has been presented in Chapter 5.3.1 is shown in within the validation structure first presented in Chapter 3. The completion of this structure, starting with the steady-state predictions for AP combustion and moving upward to this final configuration with the full propellant, has allowed for the final predictions to be made with confidence regardless of the very small amount of data available for validation purposes.

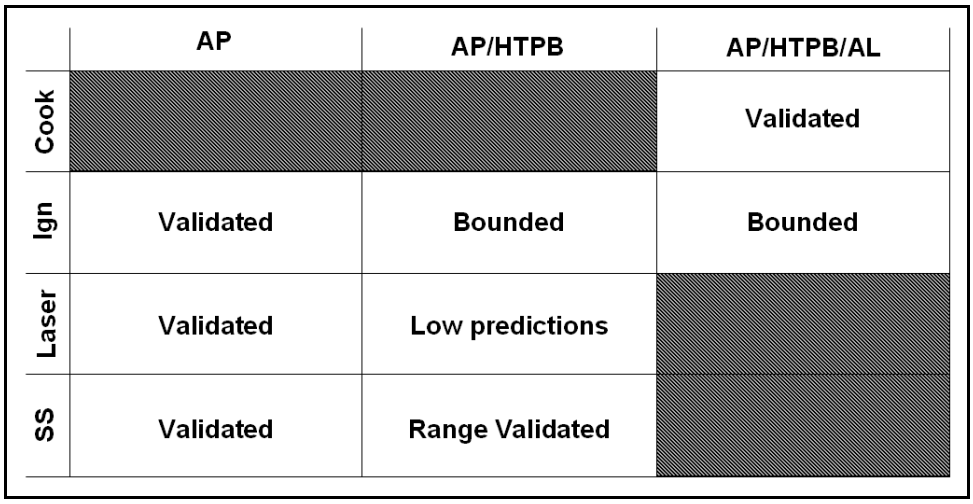

Figure 71 – Validation structure including work on the current AP/HTPB/Al cookoff model

There are those who would misteach us that to stick in a rut is consistency and a virtue, and that to climb out of the rut is inconsistency and a vice.
-- Mark Twain

CHAPTER 6: SUMMARY AND CONCLUSIONS

A significant amount of work has been accomplished toward improving two propellant simulation codes and then seeking to understand at a foundational level solid propellant/ ingredient models and their application toward steady-state and transient ignition predictions. The current work has made it a considerable point of focus to verify and validate the propellant codes and models, build upon the knowledge gained during that process, and then apply that knowledge toward making predictions in which confidence could be justified. A summary of each effort previously presented will be given here, along with a brief opinion of the current state of the work and suggestions as to where future consideration should be given.

6.1 CODE IMPROVEMENT WORK

A significant number of improvements have been made to the Phase3 and ignition code, which allowed consistent predictions to be completed for three new propellant/ingredient models.

Phase3 was improved to allow for the inclusion of phase transitions within the calculated portion of the condensed-phase. The option to apply a penetrating/absorbing heat source (for CO_2 laser applications) was also developed.

Improvements to the ignition code included:

1) replacing the Chemkin software libraries with Cantera libraries;

2) translating the condensed-phase code from Fortran to C, making integration with Cantera and further code development cleaner;

3) fixing inconsistencies in the definition of variables passed between the main program and both internal subroutines and external libraries;

4) verifying the correct application of external software libraries to the code;

5) updating the condensed-phase equations and assumptions to be consistent with Phase3, and changing the convergence criteria to an absolute basis;

6) adding the ability to transition between defined condensed-phase ingredients, allowing each to be described by separate kinetic regimes;

7) adding a robust ramping scheme to handle decomposition kinetics within the condensed-phase for decomposition reactions that increase rapidly at a given start temperature;

8) generalizing the code to allow for multiple ingredients to be modeled, instead of just HMX;

9) adding two sub-models to the code for the application of aluminum to modeled propellants;

10) including a multiple-step algorithm for solving the condensed-phase equations to minimize their time-impact upon the overall simulation.

The work accomplished has made a significant impact upon not only the behavior of the ignition code but upon necessary calculation time as well. The original code would typically diverge for the first several timesteps and had severe problems dealing with restart cases for cookoff simulations that included more than one processor. In addition to these two issues being resolved by the above changes, the improved code runs ~25-30% faster, diverges considerably less often, and has been updated to integrate with a macro-centric Excel spreadsheet that was developed and improved in parallel to the ignition code to graphically visualize the results of a given simulation.

The culmination of the work associated with code development has resulted in a robust, transient, CFD code that has the ability to model multiple propellants/ingredients with detailed gas-phase kinetic mechanisms, moving melt interfaces, and ingredient transitions for describing various phases and/or kinetic regimes of a given propellant/ingredient. The code can be used to model either enclosed or bare-face propellants and their response to an externally-applied heat source. It has no reliance upon the acquisition of any external software licenses or costs to use.

As it currently stands, the ignition code still has a few limitations that should be addressed by future work. Gas-phase mechanisms that result in steep temperature profiles near the surface require a high level of mesh refinement, which has been seen to be time prohibitive due to the very small time step necessary to keep accuracy. The solution of the gas-phase equations does not currently support an accurate approximation of the conservation equations for a non-uniform mesh. It was also observed while working with the ignition code that cases containing more than about 100 gas-phase nodes had significant convergence issues. The largest problem, however, dealt with the very large wall-clock time necessary to complete simulations that included the AP/HTPB and AP/HTPB/Al models (three to five times longer), since the number of species in the gas-phase mechanisms of those models was much higher than the single ingredient models.

A potential solution to a number of these issues would be to apply an operator-splitting method, which employs a hybrid implicit-explicit approach to solve the individual conservation equations using schemes that are particularly well-suited to each. Techniques such as those proposed by Najm *et al.*[179,180], Singe and Pope[181] and Pope and Ren[182] that are based on Strang splitting methods use a solution process for transient problems similar to the following:

1) Advance the convection, energy, and a portion of the continuity equations by a half time step according to an explicit, predictor-corrector method;

2) Advance the species and remaining portion of the continuity equations by a full time step according to a semi-implicit, stiff-equation solution method, or table lookup;

3) Advance the convection, energy, and the same portion (as in step 1) of the continuity equations by a second half step according to the explicit, predictor-corrector method.

Making use of these methods would reduce the computational time necessary for overall solution by decreasing the time spent using the time-expensive, implicit, non-linear methods that are currently employed by the code for all conservation equations. Applying new solution techniques such as these to the ignition code were not of primary concern during the current work and would have required a relatively large amount of effort, yet the need for such a future improvement of the ignition code, based upon the results of the current work, seems to be justified.

6.2 STEADY-STATE WORK

The steady-state models associated with the current work included those for AP as a monopropellant and AP/HTPB propellant. Since the AP/HTPB/Al propellant model was based exclusively upon the AP/HTPB model, it will not be treated separately here.

6.2.1 AP MODEL

Several significant improvements were made to the AP model, which included reverting to an older gas-phase mechanism and employing a newly-developed condensed-phase mechanism based on the experimental observations and measurements of several sources. The new AP model describes burning rate (± 10%), temperature sensitivity (within data scatter), surface temperature (within data scatter), and melt-layer thickness (within the observed range) at pressures ranging from 300 to 1200 psi, and also laser-augmented burning rate (± 50% for all data and ± 20% for the most recent data) over an applied heat flux range of 20 to 400 cal/cm^2/s.

There was significant improvement over the results of the original AP model, which were quite different from the data in regard to the predicted melt-layer thickness (-95%) and laser-augmented burning rate (+100%), and additionally over the updated version of the Gross AP model, which additionally predicted a temperature sensitivity much higher than the data (+90%). Improving the AP model in this way has allowed for confidence to be gained in both the steady-state description of the results and the application of the AP model to the ignition code.

There is still a shortage of experimental data to help fully describe the necessary inputs of the steady-state AP model (melt temperature, thermal properties above 513 K, temperature variance of laser-absorption parameter), and so several reasonable assumptions were made, based upon experimental observations where possible. Additional experimental data that would be most helpful toward accurately describing the AP model in the future include an accurate melting temperature for crystalline AP and an accurate thermal conductivity for temperatures above the solid-phase transition temperature of 513 K. Additionally, having an idea of how the absorptivity of crystalline AP might change with temperature would be of primary benefit to further model development.

Validation of the AP model completed as part of this work has resulted in a model that predicts a much larger data set than previous models and can now be confidently applied to both steady-state deflagration and transient ignition simulations.

6.2.2 AP/HTPB MODEL

Relatively few changes were made to the AP/HTPB model as a whole. The model was extended to include the AP84/HTPB16 formulation by extrapolation of the decomposition reactions from the AP75/HTPB25 and AP80/HTPB20 formulations of the AP/HTPB model. The

changes to the AP/HTPB model comprised focusing the condensed-phase description to a singular decomposition pathway and then altering the condensed-phase kinetics to accurately predict burning rate while still accurately predicting final species fractions and final flame temperature. Burning rate predictions for the current AP/HTPB model are accurate (± 50%) over a pressure range of 50 to 300 psi, being low for lower pressures and high for higher pressures. Deviations at high pressure are probably due to diffusion-flame appearance, with which this research was not focused, and those at low pressure are assumed to be a result of the highly-endothermic condensed-phase decomposition used in the current model. These are both characteristics of the model that have been carried over from the previous version. Surface temperature predictions are at the low end of the data scatter. Predicted temperature sensitivity and laser-augmented burning rate are fairly poor, with predictions showing both low values and shallow trends for each. Both of these characteristics are also consistent with the previous model. Comparison of model results to experimental data suggested that the condensed-phase heat release should be exothermic for fine AP/HTPB propellants, which the model was developed to predict. Based on the results of the current AP model work, developing an AP/HTPB model with exothermic condensed-phase decomposition should be able to allow for the accurate prediction of the data sets that the current model fails to predict: temperature sensitivity, laser-augmented burning rate, and low-pressure steady-state burning rate.

6.3 IGNITION WORK

Once the steady-state models were validated against experimental data, or deemed to be sufficiently accurate for the purposes of the current work, the numerical inputs for the steady-state models were applied to a transient ignition code to predict propellant/ingredient times to

ignition over a wide range of heat fluxes. This process was accomplished for both the AP and AP/HTPB models for laser-driven ignition events, and for the AP/HTPB/Al model for both laser-driven ignition and cookoff events.

The current AP model performed very well when applied to the ignition code in predicting times to ignition (± 10%). Attempts to further validate the steady-state model using the ignition modeling results were inconclusive due to the limited range of AP ignition data. Thus, a range of possible values for three input variables within the AP model (melting temperature, thermal conductivity above 513 K, and laser absorption parameter above 513 K) was developed such that each set could result in the near-identical description of both steady-state and ignition data. This set of input variables will allow for the model to be compared to additional AP ignition data, as they become available. The assumption made regarding negligible sub-melt decomposition within the AP model is consistent with AP ignition at the relatively high heat fluxes to which the predictions were compared.

The current AP/HTPB and AP/HTPB/Al models described ignition data across a wide range of fluxes, bounding the data for time to surface temperature of 513 K (assumed first decomposition) and 735 K (assumed ignition), but were unable to predict the trends of go/no-go times. Go/no-go predictions, however, are much more difficult to predict as they require a very accurate representataion of the kinetics and heat release associated with the deflagration of the propellant/ingredient. Predictions from the current AP/HTPB and AP/HTPB/Al propellant models are based upon the current Phase3 assumption that no sub-melt decomposition occurs prior to ignition.

An aluminum reflection model was applied to the AP/HTPB/Al propellant ignition predictions based on a uniform scatter of reflective aluminum particles and calculations made by

a Mie particle code. The accuracy of the aluminum reflective model is unknown. A more rigorous solution of the radiative transfer equation, as it pertains to the solid-phase distribution of aluminum particles throughout the semi-transparent solid, would allow for the current model to be evaluated, although such an effort was beyond the scope of the current work. The accuracy of applying the Maxwell approximation of determining the effective thermal conductivity of AP/HTPB/Al propellants is unknown but deemed sufficient. Modeling results suggest that the modeled thermal conductivity of an AP/HTPB/Al propellant is too low, with the contribution of the AP/HTPB being slightly too high and the effect of added aluminum being too small. Additional experimental and/or theoretical work toward understanding the impact of aluminum on the thermal properties of propellants to which it has been added would be helpful.

6.4 COOKOFF WORK

The results of the current AP/HTPB/Al cookoff work were very enlightening. Cookoff predictions of AP/HTPB/Al propellants were good, with comparisons being slightly lower than comparable experimental data (± 25%). Reported experimental ignition events occurred with surface temperatures that were significantly lower than the assumed melt temperature of the current model (735 K), and thus occurred before any condensed-phase decomposition within the model. This emphasized the need for a significant change to the current AP/HTPB and AP/HTPB/Al models, and also to the prior way of thinking when dealing with models for propellants/ingredients such as these. Assumptions used for one propellant/ingredient are usually not valid when modeling another propellant/ingredient and must instead be defined for each. The assumption used in Phase3 that there is no significant sub-melt decomposition within the solid-phase, an idea verified by observations for nitramines like RDX and HMX, does not seem to be

valid for AP/HTPB propellants. The progress necessary for determining a more valid AP/HTPB/Al model for cookoff seems to be dependent upon the primary need for a model that is better at first describing the steady-state data for non-aluminized AP/HTPB propellants, before it can be applied to ignition/cookoff simulations.

APPENDICES

APPENDIX A

The tables below are populated with the five descriptors of the condensed-phase portion of the propellant/ingredient models used in the current work for the Design of Experiment. Input parameters for the sub-studies included:

1) Pre-exponential of the condensed-phase decomposition reaction
2) Value of heat release(-)/absorption(+) due to condensed-phase decomposition
3) Value of heat flux at the surface of the propellant

Parameter 2 was varied using a sublimation decomposition reaction for the condensed phase (Equation 27), and then varying the heat of formation of AP and/or HTPB so that the calculated heat of reaction at the melt temperature (in Mathcad) was equal to the value of Parameter 2 in the table. This process resulted in calculated heats of reaction that were close but not identical to the defined levels of heat release, as Mathcad only used a single temperature to calculate this value while Phase3 calculations occur over a range of temperature between the melt temperature and the surface temperature.

The values selected for the three input parameters were chosen after several inital DoE studies. In these initial studies, optimal solutions converged to points that were at the upper range of the inputs. After widening the input ranges several times and shifting them according to the results of each case, an optimal range of input parameters was arrived upon. Those ranges are presented in the tables below.

Predictions of the condensed-phase portion of the model used as optimization parameters in the sub-study included:

1) steady-state burning rate,

2) temperature sensitivity,

for model predictions at 68 atm (1000 psi). Temperature sensitivity calculations were made between initial temperatures of 298 K and 323 K using Equation 29:

$$\sigma_p = \frac{\ln\left(r_2 / r_1\right)}{T_2 - T_1} \tag{29}$$

(Note: the impact of the gas-phase chemistry on the surface heat flux at 323 K is not taken into account for these calculations (only the condensed-phase portion of the model was used to make the calculations). Although this difference is probably small, the analysis detailed here can only be considered as approximate due to this fact.

Table A1 – Setup for Design of Experiment of current AP model

Run	CP PreExp	CP dHrxn	SurfHeatFlux	BurnRate	TempSens
1	$2.51\cdot10^{10}$	120	400	0.13667	$5.791\cdot10^{-4}$
2	$5.00\cdot10^{10}$	-120	5000	3.25285	$1.227\cdot10^{-3}$
3	$2.51\cdot10^{10}$	120	2700	0.84852	$6.127\cdot10^{-4}$
4	$1.00\cdot10^{8}$	360	5000	0.79203	$4.695\cdot10^{-3}$
5	$1.00\cdot10^{8}$	-120	5000	2.09567	$7.644\cdot10^{-4}$
6	$2.51\cdot10^{10}$	120	5000	1.52050	$5.800\cdot10^{-4}$
7	$1.00\cdot10^{8}$	120	2700	0.70786	$4.798\cdot10^{-4}$
8	$2.51\cdot10^{10}$	-120	2700	1.81264	$1.262\cdot10^{-3}$
9	$2.51\cdot10^{10}$	360	2700	0.55695	$4.069\cdot10^{-4}$
10	$5.00\cdot10^{10}$	120	2700	0.86276	$6.287\cdot10^{-4}$
11	$5.00\cdot10^{10}$	360	400	0.08770	$2.589\cdot10^{-4}$
12	$5.00\cdot10^{10}$	360	5000	1.02249	$3.990\cdot10^{-4}$
13	$1.00\cdot10^{8}$	360	400	0.08030	$2.827\cdot10^{-4}$
14	$1.00\cdot10^{8}$	-120	400	0.24208	$1.196\cdot10^{-3}$
15	$2.51\cdot10^{10}$	120	2700	0.84852	$6.127\cdot10^{-4}$
16	$5.00\cdot10^{10}$	-120	400	0.33713	$1.719\cdot10^{-3}$

Table A2 – DoE results for current AP model

CP Pre-exp	$1.76 \cdot 10^{9}$
CP dHrxn	196.36
SHF	4080
BurnRate	0.83
TempSens	$1.96 \cdot 10^{-3}$

Table A3 – Setup for Design of Experiment of current AP/HTPB model

Run	CP PreExp	CP dHrxn	SurfHeatFlux	BurnRate	TempSens
1	$1.00 \cdot 10^{13}$	300	200	0.674	$6.67 \cdot 10^{-3}$
2	$1.00 \cdot 10^{13}$	100	200	0.247	$2.57 \cdot 10^{-3}$
3	$1.00 \cdot 10^{13}$	100	600	0.731	$2.34 \cdot 10^{-3}$
4	$5.05 \cdot 10^{12}$	300	400	1.259	$6.07 \cdot 10^{-3}$
5	$5.05 \cdot 10^{12}$	200	600	1.036	$3.24 \cdot 10^{-3}$
6	$1.00 \cdot 10^{11}$	300	600	1.130	$3.29 \cdot 10^{-3}$
7	$1.00 \cdot 10^{13}$	300	600	1.870	$5.94 \cdot 10^{-3}$
8	$1.00 \cdot 10^{11}$	300	200	0.494	$4.36 \cdot 10^{-3}$
9	$5.05 \cdot 10^{12}$	100	400	0.487	$2.55 \cdot 10^{-3}$
10	$5.05 \cdot 10^{12}$	200	200	0.359	$3.78 \cdot 10^{-3}$
11	$1.00 \cdot 10^{11}$	100	600	0.600	$1.81 \cdot 10^{-3}$
12	$1.00 \cdot 10^{11}$	100	200	0.228	$2.19 \cdot 10^{-3}$
13	$5.05 \cdot 10^{12}$	200	400	0.707	$3.46 \cdot 10^{-3}$
14	$1.00 \cdot 10^{13}$	200	400	0.715	$3.61 \cdot 10^{-3}$
15	$5.05 \cdot 10^{12}$	200	400	0.707	$3.46 \cdot 10^{-3}$
16	$1.00 \cdot 10^{11}$	200	400	0.562	$2.69 \cdot 10^{-3}$

Table A4 – DoE results for current AP75/HTPB25 model

CP Pre-exp	$5.1 \cdot 10^{12}$
CP dHrxn	-190.0
SHF	370.0
BurnRate	0.605
TempSens	$3.50 \cdot 10^{-3}$

APPENDIX B

Proposed condensed-phase decomposition reactions used during development trials for the steady-state AP model are listed in the following three tables. The first reaction listed in each table (Trial #0) is Gross's original condensed-phase decomposition reaction.

Table B1 – One condensed-phase reaction, original Gross[17] gas-phase mechanism

Trial	AP	NO	N2O	N2	NO2	NH3	NH2	O2	H2O	OH	HCL	CLOH	CL2	HCLO4	CLO4	CLO3	CLO2	CLO	CL
0	10	0	0	3	0	4	0	7	13	0	1	0	1	1	0	3	0	0	3
1	10	0	0	3	0	4	0	7	13	0	1	0	1	1	0	3	0	0	3
2	10	0	2	1	0	4	0	6	13	0	1	0	1	1	0	3	0	0	3
3	20	4	2	2	0	8	0	11	26	0	2	0	2	2	0	6	0	0	6
4	20	4	2	2	0	8	0	10	24	0	2	3	1	3	0	5	0	0	5
5	23	4	2	2	0	11	0	10	24	0	2	3	1	6	0	5	0	0	5
6	23	4	2	2	0	11	0	9	24	0	0	5	1	6	0	5	0	0	5
7	23	4	2	2	0	11	0	12	24	0	0	5	0	6	0	3	0	0	9
8	23	3	2	2	1	11	0	14	24	0	0	5	0	6	0	0	1	2	9
9	29	3	2	2	1	17	0	18	26	0	0	5	0	8	0	0	3	4	9
10	29	3	2	2	1	17	0	15	26	0	0	5	0	8	0	0	6	4	6
11	33	3	2	2	1	21	0	12	26	0	0	5	0	12	0	0	9	4	3
12	34	3	2	2	1	22	0	12	24	0	0	9	0	13	0	0	8	4	0
13	34	5	2	2	1	20	0	6	28	0	0	9	0	11	0	6	8	0	0
14	34	5	2	2	1	20	0	9	26	0	0	13	0	11	0	6	4	0	0
15	34	6	1	3	0	20	0	11	26	0	4	9	0	11	2	4	4	0	0
16	20	5	1	2	1	8	0	10	26	0	2	0	2	2	0	6	0	0	6
17	34	6	1	3	0	20	0	25	26	0	4	9	0	11	0	0	0	0	10
18	38	2	1	3	4	24	0	29	30	0	0	9	0	11	0	0	0	0	18
19	38	0	1	3	5	25	0	30	31	0	0	10	0	5	5	0	0	0	18
20	42	0	1	3	6	28	0	26	37	0	0	10	0	0	14	0	0	0	18
21	50	0	2	3	8	32	0	38	46	0	0	12	0	0	12	0	0	0	26
22	54	0	2	3	12	32	0	34	46	16	0	12	0	0	12	0	0	0	30
23	38	0	1	3	5	25	0	30	31	0	0	10	0	5	5	0	0	0	18
24	38	0	1	3	0	0	30	30	41	0	0	10	0	0	10	0	0	0	18
25	38	0	1	3	1	29	0	30	25	0	0	10	0	5	5	0	7	0	11
26	40	0	1	3	1	31	0	18	28	0	0	11	0	0	17	0	7	0	5
27	52	0	1	3	1	43	0	20	34	0	0	11	0	0	19	0	22	0	0
28	34	6	1	3	0	20	0	25	26	0	4	9	0	11	0	0	0	0	10
29	34	0	4	3	0	20	0	23	26	0	0	12	0	12	0	0	0	0	10
30	34	0	2	3	4	20	0	20	26	0	0	12	0	12	0	0	0	0	10

Table B2 – One condensed-phase reaction, updated Gross gas-phase mechanism

Trial	AP	NO	N2O	N2	NO2	NH3	NH2	O2	H2O	OH	HCL	CLOH	CL2	HCLO4	CLO4	CLO3	CLO2	CLO	CL
0	10	0	0	3	0	4	0	7	13	0	1	0	1	1	0	3	0	0	3
1	34	0	2	3	5	19	0	9	27	0	0	9	0	16	0	0	3	0	6
2	37	0	2	3	6	21	0	8	30	0	0	6	0	19	0	0	3	0	9
3	41	0	2	3	6	25	0	12	32	0	0	8	0	17	0	0	9	0	7
4	41	1	2	3	6	24	0	9	30	0	0	11	0	21	0	0	3	0	6
5	39	2	2	3	4	23	0	12	29	0	0	11	0	18	0	0	4	0	6
6	39	4	2	3	2	23	0	13	29	0	0	11	3	18	0	0	4	0	0
7	36	6	2	3	0	20	0	13	27	0	1	11	3	18	0	0	0	0	0
8	35	6	2	3	0	19	0	14	26	0	4	10	2	17	0	0	0	0	0
9	34	5	2	3	1	18	0	14	25	0	6	10	1	16	0	0	0	0	0
10	34	5	2	3	1	18	0	14	25	0	6	10	1	16	0	0	0	0	0
11	38	9	2	3	1	18	0	6	30	0	10	5	0	23	0	0	0	0	0
12	46	14	2	3	0	22	0	6	36	0	16	0	0	30	0	0	0	0	0

Trials presented in Table B3 included two condensed-phase reactions, with 70% moving through the sublimation pathway (Equation 4) and the remaining 30% being defined in Table B3, while using the gas-phase mechanism proposed by Ermolin.

Table B3 – Two condensed-phase reactions, Ermolin[35] gas-phase mechanism

Trial	AP	NO	N2O	N2	NO2	NH3	NH2	HNO	O2	H2O	OH	HCL	CLOH	CL2	HCLO4	CLO4	CLO3	CLO2	CLO	CL
0	10	0	0	3	0	4	0	0	7	13	0	1	0	1	1	0	3	0	0	3
1	10	0	0	3	0	4	0	0	8	13	0	0	2	1	0	0	3	0	0	3
2	10	2	2	0	0	4	0	0	6	13	0	0	2	1	0	0	3	0	0	3
3	8	1	2	0	1	2	0	0	5	12	0	0	2	1	0	0	1	0	0	3
4	6	2	2	0	0	0	0	0	3	10	0	0	4	1	0	0	0	0	0	0
5	6	4	1	0	0	0	0	0	2	9	0	0	6	0	0	0	0	0	0	0
6	10	4	1	0	0	4	0	0	8	9	0	0	10	0	0	0	0	0	0	0
7	10	4	1	0	0	2	0	2	4	11	2	0	8	0	0	0	0	2	0	0

APPENDIX C

Ermolin's gas-phase mechanism for AP combustion is printed below in Cantera's "cti" format, using units of cm, mol, sec, K, and activation energy in cal/mol, with kinetic parameters listed in brackets: pre-exponential, temperature exponent, and activation energy, respectively. Additionally, as the mechanism predicted inaccurate final products for NO, N2, and O2, Gross's gas-phase NO-elimination reaction was included into this version of Ermolin's mechanism for this work. Gross's elimination reaction is the final reaction listed.

```
reaction(  "CLO3 <=> CLO + O2",  [1.70000E+10, 0.5, 0])
reaction(  "OCLO + NO <=> CLO + NO2",  [4.00000E+11, 0, 0])
reaction(  "OCLO + CL <=> CLO + CLO",  [5.00000E+13, 0, 6000])
three_body_reaction( "NOCL + M <=> NO + CL + M",  [2.00000E+17, 0, 37700])
reaction(  "CLO + CLO <=> CL2 + O2",  [1.00000E+11, 0, 0])
reaction(  "CLO + O <=> CL + O2",  [6.60000E+13, 0, 440])
reaction(  "CLO + NO <=> CL + NO2",  [1.40000E+13, 0, 311])
reaction(  "CLO + NH3 <=> NH2 + CLOH",  [6.00000E+11, 0.5, 6400])
reaction(  "CL + HO2 <=> HCL + O2",  [1.80000E+13, 0, 0])
reaction(  "HCL + O <=> OH + CL",  [2.30000E+11, 0.64, 900])
reaction(  "OH + HCL <=> H2O + CL",  [5.00000E+11, 0, 750])
three_body_reaction( "CL + O2 + M <=> OCLO + M",  [1.60000E+10, 0, 5200])
three_body_reaction( "CL + CL + M <=> CL2 + M",  [7.20000E+14, 0, -1800])
reaction(  "CLOH + O <=> HCL + O2",  [1.20000E+14, 0, 0])
reaction(  "O2 + HNO <=> NO2 + OH",  [1.50000E+13, 0, 10000])
reaction(  "NH2 + O2 <=> HNO + OH",  [3.00000E+09, 0, 0])
```

```
reaction(  "NO + HO2 <=> NO2 + OH",  [2.10000E+12, 0, 480])

reaction(  "O + NO2 <=> NO + O2",  [1.00000E+13, 0, 600])

reaction(  "HNO + HNO <=> H2O + N2O",  [3.95000E+12, 0, 5000])

reaction(  "O2 + HNO <=> NO + HO2",  [8.00000E+09, 0.75, 3465])

reaction(  "NH2 + NO <=> N2 + H2O",  [6.20000E+15, -1.25, 0])

reaction(  "CLOH + OH <=> CLO + H2O",  [1.80000E+13, 0, 0])

reaction(  "NH3 + CL <=> NH2 + HCL",  [1.00000E+12, 0.5, 100])

reaction(  "OH + HNO <=> H2O + NO",  [1.20000E+11, 0.5, 2000])

reaction(  "HCLO4 <=> OH + CLO3",  [1.00000E+11, 0, 39100])

reaction(  "NO + CL2 <=> CL + NOCL",  [2.70000E+12, 0, 19900])

reaction(  "CLOH + CLO <=> CL2 + HO2",  [1.00000E+11, 0, 10000])

reaction(  "HCLO4 + HNO <=> CLO3 + NO + H2O",  [3.50000E+13, 0, 6000])

reaction(  "NH2 + CLO <=> HNO + HCL",  [2.50000E+12, 0, 0])

reaction(  "NO2 + NO2 <=> O2 + NO + NO",  [1.00000E+14, 0, 25000])

reaction(  "N2O + CL <=> CLO + N2",  [1.20000E+14, 0, 33500])

reaction(  "N2 + HO2 <=> NO + HNO",  [2.70000E+10, 0.5, 41800])

reaction(  "NH3 + OH <=> NH2 + H2O",  [1.00000E+11, 0.68, 1100])

reaction(  "HCLO4 + HNO <=> OCLO + NO2 + H2O",  [2.00000E+13, 0, 6000])

reaction(  "OH + OH <=> H2O + O",  [6.00000E+08, 1.3, 0])

reaction(  "NH2 + NO2 <=> N2O + H2O",  [4.50000E+11, 0, 0])

reaction(  "NH2 + HNO <=> NH3 + NO",  [5.00000E+11, 0.5, 1000])

reaction(  "OH + N2O <=> N2 + HO2",  [2.00000E+11, 0, 10000])

three_body_reaction( "N2O + M <=> N2 + O + M",  [1.60000E+14, 0, 51600])
```

```
reaction(  "NH2 + NO2 <=> HNO + HNO",  [5.00000E+12, 0, 0])
reaction(  "CLOH + HCL <=> H2O + CL2",  [2.00000E+12, 0, 10000])
reaction(  "HCLO4 + NH2 <=> H2O + OCLO + HNO",  [1.00000E+12, 0, 0])
reaction(  "HCLO4 + NH2 <=> CLOH + HNO + HO2",  [1.00000E+11, 0, 0])
reaction(  "HCLO4 + NO <=> HO2 + CLO + NO2",  [1.00000E+13, 0, 10000])
reaction(  "CLOH + HNO <=> H2O + NOCL",  [3.00000E+12, 0, 0])
reaction(  "OCLO + OCLO <=> CLO3 + CLO",  [1.80000E+13, 0, 18000])
reaction(  "NOCL + CLO <=> NO2 + CL2",  [1.50000E+12, 0, 0])
reaction(  "CLO + HNO <=> HCL + NO2",  [3.00000E+12, 0, 0])
reaction(  "HCL + HO2 <=> CLO + H2O",  [3.00000E+12, 0, 0])
reaction(  "H + NO2 <=> OH + NO",  [3.47000E+14, 0, 1480])
reaction(  "NH2 + NO <=> NNH + OH",  [6.40000E+15, -1.25, 0])
reaction(  "NNH + NO <=> HNO + N2",  [5.00000E+13, 0, 0])
reaction(  "NH2 + NO <=> N2 + OH + H",  [6.30000E+19, -2.5, 1900])
reaction(  "CL + CLOO <=> CLO + CLO",  [4.80000E+12, 0, 0])
three_body_reaction( "CL + O2 + M <=> CLOO + M",  [9.70000E+14, 0, 0])
reaction(  "CLOH + CLO <=> CLOO + HCL",  [4.00000E+10, 0, 0])
reaction(  "NH2 + OH <=> H2O + NH",  [4.00000E+06, 2, 1000])
reaction(  "NH2 + NH2 <=> NH3 + NH",  [5.00000E+13, 0, 10000])
reaction(  "NH + NO <=> N2 + OH",  [1.00000E+13, 0, 0])
reaction(  "NH + NO <=> N2 + O + H",  [2.30000E+13, 0, 0])
reaction(  "CL + NH2 <=> HCL + NH",  [5.00000E+10, 0.5, 0])
reaction(  "OCLO + NH <=> CLO + HNO",  [1.00000E+14, 0, 0])
```

```
reaction(  "HCLO4 + NH <=> OH + OCLO + HNO",  [1.00000E+14, 0, 0])
reaction(  "OH + H2 <=> H2O + H",  [1.17000E+09, 1.3, 3626])
reaction(  "N + NO2 <=> NO + NO",  [1.00000E+14, 0, 0])
reaction(  "N + N2O <=> NO + N2",  [5.00000E+13, 0, 0])
reaction(  "NH + OH <=> N + H2O",  [5.00000E+11, 0.5, 2000])
reaction(  "NH + OH <=> NO + H2",  [1.60000E+12, 0.6, 1500])
reaction(  "NH + NH2 <=> NH3 + N",  [1.00000E+13, 0, 2000])
reaction(  "NH + NH2 <=> N2H2 + H",  [5.00000E+13, 0, 0])
reaction(  "NH2 + NH2 <=> N2H2 + H2",  [5.00000E+11, 0, 0])
reaction(  "HO2 + HO2 <=> H2O2 + O2",  [2.00000E+12, 0, 0])
three_body_reaction( "H2O2 + M <=> OH + OH + M",  [1.30000E+17, 0, 45500])
reaction(  "H2O2 + OH <=> H2O + HO2",  [1.00000E+13, 0, 1800])
reaction(  "N2H2 + NO <=> N2O + NH2",  [3.00000E+12, 0, 0])
reaction(  "HCL + H <=> H2 + CL",  [7.94000E+12, 0, 3400])
reaction(  "CLOH + H <=> CLO + H2",  [6.00000E+12, 0, 0])
reaction(  "CLOH + NH <=> NOCL + H2",  [1.00000E+13, 0, 0])
reaction(  "HCLO4 + NH <=> CLO3 + N + H2O",  [1.00000E+14, 0, 11000])
reaction(  "NO + NO <=> N2 + O2",  [5.00000E+20, 0, 75506])
```

APPENDIX D

This appendix contains the published reactions of M.C. Lin *et al.* that were either added to, or updated within, Gross's gas-phase mechanism as part of the current work. Gross's original mechanism can be found in already-published work. The reactions are all listed in Cantera's "cti" format. A single species, CLNH2, was added to the mechanism as part of this update.

```
falloff_reaction( "HCLO4 (+ M) => OH + CLO3 (+ M)",
        kf = [1.45000E+17, 0, 52655],
        kf0   = [1.69000E+55, -11.2, 58453.6])

falloff_reaction( "O + CLO2 (+ M) => CLO3 (+ M)",
        kf = [7.05000E+13, -0.039, -101.3],
        kf0   = [2.54000E+28, -4.46, 431.2])

reaction(  "OH + CLO2 <=> HCLO3",  [1.07000E+04, 2.25, -4172.7],
        options = ["duplicate"])

falloff_reaction( "CL + O2 (+ M) => CLOO (+ M)",
        kf = [4.00000E+13, 0.004, 15.9],
        kf0   = [8.63000E+27, -4.92, 1226])

falloff_reaction( "O + CLO (+ M) => CLO2 (+ M)",
        kf = [2.61000E+13, -0.03, -85.4],
        kf0   = [3.12000E+27, -4.1, 834.5])

reaction(  "CL + CLO4 <=> CLO + CLO3",  [4.85000E+13, 0.158, 97.4])

reaction(  "NH2 + HNO => NH3 + NO",  [5.87000E+02, 2.95, -3469.3],

reaction(  "NH3 + NO => NH2 + HNO",  [1.46000E+03, 3.12, 54404.1])

reaction(  "NH2 + HNO <=> NH3 + NO",  [7.83000E-08, 5.29, -468.9],
        options = ["duplicate"])

reaction(  "NH2 + HNO <=> NH3 + NO",  [1.49000E-12, 6.41, -1818.1],
        options = ["duplicate"])

falloff_reaction( "NH2 + HNO (+ M) <=> NH3 + NO (+ M)",
        kf = [8.37000E+13, 0.22, 51.7],
        kf0   = [2.32000E+53, -8.13, 2859.3])
```

```
reaction(  "NH2 + HNO <=> H + H2NNO",  [2.43000E+05, 2.15, 759])

reaction(  "NH2 + HONO <=> OH + H2NNO",  [5.33000E+03, 2.28, 7981.8])

reaction(  "NH2 + HONO => NH3 + NO2",  [3.17000E+02, 2.83, -3572.6],
        options = ["duplicate"])

reaction(  "NH2 + HONO => NH3 + NO2",  [2.96000E-09, 6, 2366.5],
        options = ["duplicate"])

reaction(  "NH3 + NO2 => NH2 + HONO",  [2.69000E-01, 4.02, 23247.9],
        options = ["duplicate"])

reaction(  "NH3 + NO2 => NH2 + HONO",  [4.24000E-10, 6.48, 27023.2],
        options = ["duplicate"])

falloff_reaction( "NH2 + HNO3 (+ M) <=> NH3 + NO3 (+ M)",
        kf = [3.03000E+14, -0.28, -536.5],
        kf0   = [4.13000E+37, -4.38, 993.5])

reaction(  "NH2 + HNO3 => NH3 + NO3",  [3.48000E+01, 3.2, -111.3])

reaction(  "NH3 + NO3 => NH2 + HNO3",  [4.06000E+00, 3.57, 1689])

reaction(  "NH2 + HNO3 <=> H2NO + HONO",  [8.85000E+01, 2.96, 24440.1],
        options = ["duplicate"])

reaction(  "NH2 + HNO3 <=> H2NO + HONO",  [1.73000E+08, 1.17, 29558.6],
        options = ["duplicate"])

reaction(  "H + HCLO4 <=> H2 + CLO4",  [6.44000E+06, 1.97, 14876.7])

reaction(  "H + HCLO4 <=> OH + HCLO3",  [3.66000E+07, 1.96, 15357.5])

reaction(  "OH + HCLO4 <=> H2O + CLO4",  [2.38000E+01, 3.3, 1847.9])

reaction(  "CL + HCLO4 <=> HCL + CLO4",  [1.05000E+08, 1.63, 22184.9])

reaction(  "CL + HCLO4 <=> CLOH + CLO3",  [8.01000E+11, 0.67, 19190.4])

reaction(  "CLOH + CLO => CL2O + OH",  [1.38000E+07, 1.77, 18650])

reaction(  "CLOH + CLO2 <=> HCLO2 + CLO",  [6.50000E+02, 2.48, 23180.3])

reaction(  "CLOH + CLO3 <=> HCLO3 + CLO",  [2.34000E-06, 5.45, 7683.7])
```

```
reaction(  "CLOH + CLO4 <=> HCLO4 + CLO",  [8.13000E+05, 1.73, -2020.8])

reaction(  "CL2O + OH => CLOH + CLO",  [3.89000E+08, 1.39, -824.6])

reaction(  "CLOH + CLOH => CL2O + H2O",  [6.80000E+01, 3.03, 23220.1],
        options = ["duplicate"])

reaction(  "CLOH + CLOH <=> CL2O + H2O",  [2.40000E+01, 3.06, 22397.5],
        options = ["duplicate"])

reaction(  "CLOH + HONO <=> CLNO2 + H2O",  [8.13000E+01, 2.86, 2791.7],
        options = ["duplicate"])

reaction(  "CLOH + HONO <=> CLNO2 + H2O",  [3.24000E+03, 2.56, 11727.3],
        options = ["duplicate"])

reaction(  "CLOH + HNO <=> CL + NO + H2O",  [3.48000E+02, 3.06, 6068.3])

reaction(  "CL2O + H2O => CLOH + CLOH",  [7.29000E+02, 2.82, 26228.4],
        options = ["duplicate"])

falloff_reaction( "CLONO2 (+ M) => CLO + NO2 (+ M)",
        kf = [4.59000E+23, -2.43, 26699.3],
        kf0   = [3.66000E+47, -6.54, 27446.4])

falloff_reaction( "CLO + NO2 (+ M) => CLONO2 (+ M)",
        kf = [2.01000E+17, -1.48, 35.8],
        kf0   = [1.16000E+31, -5.54, 763])

reaction(  "CL + NO3 <=> CLO + NO2",  [7.17000E+14, -0.6, -115.2])

reaction(  "CLO + NO <=> CL + NO2",  [8.61000E+14, -0.83, -182.8])

falloff_reaction( "CLNO2 (+ M) <=> CL + NO2 (+ M)",
        kf = [7.25000E+19, -1.89, 33530.6],
        kf0   = [1.51000E+62, -6.8, 36578.7])

reaction(  "O + HCL <=> OH + CL",  [5.58000E+00, 3.67, 2046.6])

reaction(  "OH + CLO <=> HCLO2",  [3.17000E+15, -1.03, 79.5])

reaction(  "HO2 + CLO2 <=> HCLO4",  [5.06000E+44, -13.5, 1249.8])

reaction(  "HO2 + CLO2 => OH + CLO3",  [8.43000E+09, 0.93, 29244.7])
```

```
falloff_reaction( "CLONO2 (+ M) => CLO + NO2 (+ M)",
        kf = [4.59000E+23, -2.43, 26699.3],
        kf0   = [3.66000E+47, -6.54, 27446.4])

falloff_reaction( "CL + NH2 (+ M) <=> CLNH2 (+ M)",
        kf = [7.22000E+13, 0.196, 32],
        kf0   = [1.28000E+31, -4.76, 1165])
```

REFERENCES

[1] Creighton, J. R., "The Variation of the Ignition Temperature of Solid Explosives as a Function of Heating Rate,"*JANNAF Propulsion Systems Hazards Subcommittee Meeting, CPIA No. 599*, pgs. 473-482, (1993).

[2] Raun, R.L., Butcher, A.G., Caldwell, D.J. and Beckstead, M.W., "An Approach for Predicting Cookoff Reaction Time and Reaction Severity", *1992 JANNAF Propulsion Systems Hazards Meeting*, Vol. I, CPIA No. 582, pgs. 407-504, (1992).

[3] Meredith, K. V. and Beckstead M. W., "Fast Cookoff Modeling of HMX", *39th JANNAF Combustion Meeting. Colorado Springs, CO*, pgs. 1-22, (2003).

[4] Kuo, K. K., and Lu, Y. C., "Modeling of Pysicochemical Processes of Burning RDX Monopropellants," *30th JANNAF Combustion Meeting*, CPIA #606, Vol. 2, pgs. 235-257, (1993).

[5] Hanson-Parr, D. M., and Parr, T. P., "RDX Laser Assisted Flame Structure," *Proceedings of the 31st JANNAF Combustion Meeting*, Vol. II, CPIA Publication 620, pgs. 407-423, (1994).

[6] Melius, C. F., and Binkley, J. S., "Thermochemistry of the Decomposition of Nitramines in the Gas Phase," *21st Symposium (Int'l) on Comubstion*, The Combustion Institute, pgs. 1953-1963, (1986).

[7] Jeppson, M. B., Beckstead, M.W. and Jing, Q., "A Kinetic Model for the Premixed Combustion of a Fine AP/HTPB Composite Propellant", *35th JANNAF Combustion Meeting*, (1998).

[8] Washburn, E., and Beckstead, M. W., "Modeling Mutilphase Effects in the Combustion of HMX and RDX," Journal of Propulsion and Power, Vol. 22, No. 5, pgs. 938-946, (2006).

[9] Beckstead, M. W., Puduppakkam, K., Thakre, P., and Yang, V., "Modeling of combustion and ingiitnio of solid-propellant ingredients," Progress in Energy and combustion Science, Vol 33, pgs. 497-551, (2007).

[10] Manelis, G.B. and Strunin, V.A., "The Mechanism of Ammonium Perchlorate Burning," *Combustion and Flame*, Vol. 17, pgs. 69-77, (1971).

[11] Miller, M.S., "In Search of an Idealized Model of Homogeneous Solid Propellant Combustion," *Combustion and Flame*, Vol. 46, pgs. 51-73, (1982).

[12] Merzhanov, A.G., "The Theory of Stable Homogeneous Combustion of Condensed Substances," *Combustion and Flame*, Vol. 13, No. 2, pgs. 143-156, (1969).

[13] Guirao, C. and Williams, F.A., "A Model for Ammonium Perchlorate Deflagration between 20 and 100 atm," *AIAA Journal*, Vol. 9, No. 7, pgs. 1345-1356, (1971).

[14] Beckstead, M.W., Derr, R.L., and Price, C.F., "The Combustion of Solid Monopropellants and Composite Propellants," *Proceedings of the Combustion Institute*, Vol. 13, pgs. 1047-1056, (1971).

[15] Beckstead, M. W., and Puduppakkam, K. V., and Yang, V., "Modeling and Simulation of Combustion of Solid Propellant Ingredients Using Detailed Chemical Kinetics," *49th AIAA Joint Propulsion Conference and Exhibit*, AIAA-2004-4036, (2004).

[16] Davidson, J. E. and Beckstead, M. W., "A Three-Phase Model of HMX Combustion," *26th Symposium (Int'l) on Combustion*, pgs. 1989-1996, (1996).

[17] Gross, M. L., Shurtz, R. C., Hawkins, M. G., Beckstead, M. W., and Hecker, W. C., "Development of an Updated Model for Monopropellant AP Combustion: Methodology and Results," 41st JANNAF Combustion Meeting, pgs. 1-13, (2006).

[18] Kee, R. J., Grcar, J. F., Smooke, M.D., and Miller, J. A., "A Fortran Program for Modeling Steady Laminar One-Dimensional Premixed Flames, " *Sandia Report SAND85-8240*, UC-401, Apr (1992).

[19] Brown, P. N., Byrne, G. D., and Hindmarsh, A. C., "VODE: A Variable Coefficient ODE Solver," SIAM J. Sci. Stat. Comput., 10, pgs. 1038-1051, (1989).

[20] Vyazovkin, S., and Wight, C. A., "Kinetics of Thermal Decomposition of Cubic Ammonium Perchlorate," *Chem. Mater.*, Vol. 11, No. 11, pgs. 3386–3393, (1999).

[21] Lang, A. J., and Vyazovkin, S., "Effect of pressure and sample type on decomposition of ammonium perchlorate," *Combustion and Flame*, Vol 145, pgs. 779-790, (2006).

[22] Galwey, A. K., and Mohamed, M. A., "The Low Temperature Thermal Decomposition of Ammonium Perchlorate: Nitryl Perchlorate as the Reaction Intermediate," *Proceedings of the Royal Society of London, Series A, Mathematical and Physical Sciences*, Vol. 296, No. 1811, pgs. 425-440, Dec (1984).

[23] Boldyrev, V. V., "Thermal decomposition of ammonium perchlorate," *Thermochimica Acta*, Vol 443, pgs. 1-36, (2006).

[24] Behrens, R., and Minier, L., "The Thermal Decomposition Behavior of Ammonium Perchlorate and of an Ammonium-Perchlorate-Base Composite Propellant," *33rd JANNAF Combustion Subcommittee Meeting,* Monterey, CA, November (1996).

[25] Kraeutle, K. J., "The Thermal Decomposition of Orthorhombic Ammonium Perchlorate Single Crystals," *Journal of Physical Chemistry*, Vol. 74, No. 6, pgs. 1350-1356, March (1970).

[26] Kraeutle, K. J., Atwood, A. I., and Curran, P. O., "The Partial Decomposition and Sublimation of Propellant Grade Ammonium Perchlorate: Effect of Temperature, Time, and Particle Size," *Propulsion Systems Hazards Meeting*, CPIA 681, Vol. 1, pgs. 45-56, (1998).

[27] Watt Jr., D. M., and Petersen, E. E., "Relationship between the Limiting Pressure and the Solid Temperature for the Deflagration of Ammonium Perchlorate," *The Journal of Chemical Physics*, Vol. 50, No. 5, pgs. 2196-2198, March (1969).

[28] Boggs, T. L., "Deflagration Rate, Surface Structure, and Subsurface Profile of Self-Deflagrating Single Crystals of Ammonium Perchlorate," *AIAA Journal*, Vol. 8, No. 5, pgs. 867-873, (1970).

[29] Atwood, A. I., Boggs, T. L., Curran, P. O., Parr, T. P., Hanson-Parr, D. M., Price, C. F., and Wiknich, J., "Burning Rate of Solid Propellant Ingredients, Part 1: Pressure and Initial Temperature Effects," *Journal of Propulsion and Power*, Vol. 15, No. 6, pgs. 740-747, Nov-Dec (1999).

[30] Beckstead, M. W., and Hightower, J. D., "Surface Temperature of Deflagrating Ammonium Perchlorate Crystals," AIAA Journal, Vol. 5, No. 10, pgs. 1785-1790, Oct (1967).

[31] Cordes, H. F., "An Estimate of the Melting Point of Ammonium Perchlorate," AIAA Journal, Vol. 7, No. 6, pgs. 1193-1195, June (1969).

[32] Foltz, M. F., and Maienschein, J. L., "Ammonium perchlorate phase transitions to 256 GPa and 700 K in a diamond anvil cell," Materials Letters, Vol 24, Iss 6, pgs. 407-414, (1995).

[33] Ermolin, N.E., Korobeinichev, O.P., Tereshchenko, A.G., and Fomin, V.M., "Measurement of the Concentration Profiles of Reacting Components and Temperature in an Ammonium Perchlorate Flame," *Combustion, Explosion, and Shock Waves*, Vol. 18, pgs. 36-38, (1982).

[34] Korobeinichev, O. P., "Dynamic Flame Probe Mass Spectrometry and Condensed-System Decomposition," *Combustion, Explosion, and Shockwave,* Vol. 23, No. 5, pgs. 64-76, (1987).

[35] Ermolin, N. E., Korobeinichev, O. P., Terechchenko, A. G., and Fomin, V. M., "Kinetic Calculations and Mechanism Determination from Chemical Reactions in an Ammonium Perchlorate Flame," *Combustion, Explosion, and Shockwave,* Vol. 18, No. 2, pgs. 61-70, (1982).

[36] Price, C., Boggs, T., and Derr, R., "Modeling of Solid Monopropellant Deflagration," *AIAA 16th Aerospace Sciences Meeting*, Huntsville, AL, Jan 16th-18th, pgs. 1-12, (1978).

[37] Price, C. F., Boggs, T. L., and Derr, R. L., "The Steady-State Combustion Behavior of Ammonium Perchlorate and HMX," *17th Aerospace Sciences Meeting*, New Orleans, LA, Jan 15th-17th, pgs. 1-14, (1979).

[38] Ermolin, N.E., Korobeinichev, O.P., Tereshchenko, A.G., and Fomin, V.M., "Kinetic Calculations and Mechanism Definitions for Reactions in an Ammonium Perchlorate Flame," *Combustion, Explosion, and Shock Waves*, Vol. 18, pgs. 180-188, (1982).

[39] Nahari, H.K., Mukunda, H.S., and Jain, V.K. "A Model of Combustion Monopropellants (AP) with Complex Gas Phase Kinetics," *Proceedings of the Combustion Institute*, Vol. 20, pgs. 2073-2082, (1984).

[40] Ermolin, N.E., "Model for Chemical Reaction Kinetics in Perchloric Acid – Ammonia Flames," *Combustion, Explosion, and Shock Waves*, Vol. 31, No. 5, pgs. 555-565, (1995).

[41] Jing, Q., Beckstead, M. W., and Jeppson, M., "Influence of AP Solid Phase Decomposition of Temperature Profile and Sensitivity," *AIAA 36th Aerospace Sciences Meeting & Exhibit*, AIAA-98-0448, (1998).

[42] Tanaka, M., and Beckstead, M. W., "A Three-Phase Model of Ammonium Perchlorate," *AIRR 96-2888*, (1996).

[43] Sheshadri, T. S., and Jain, V. K., "Propellant Gas Phase Chemical Kinetics," *Propellants, Explosives, and Pyrotechnics*, 14, pgs. 193-198, (1989).

[44] Beckstead, M. W., Tanaka, M., Jing, Q., and Jeppson, M. B., "An Ammonium Perchlorate Model Based on a Detail Kinetic Mechanism," *33rd JANNAF Combustion Meeting*, Monterey, CA, pgs. 1-14, (1996).

[45] Ermolin, N. E., Korobeinichev, O. P., Tereshchenko, Al, G., and Fomin, V. M., "Kinetic Calculations and Mechanism Definiton for Reaction in an Ammonium Perchlorate Flame," *Combustion, Explosion, and Shock Wave*, Vol. 18, No. 2, pgs. 61-70, (1982).

[46] Ermolin, N. E., Korobeinichev, O. P., Tereshchenko, A. G., and Fomin, V. M., "Simulation of Kinetics and Chemical Reaction Mechanism of Ammonium Perchlorate Burning," *Sov. J. Chem. Phys.*, Vol. 1, No. 12, pgs. 2872-2883, (1984).

[47] Parr, T., and Hanson-Parr, D., "Thermal Properties Measurements of Solid Rocket Propellant Oxidizers and Binder Materials as a Function of Temperature," 34th JANNAF Combustion Meeting, Vol. III, CPIA #662, pgs. 379-404, (1997).

[48] Shoemaker, R. L., Stark, J. A., and Taylor, R. E., "Thermophysical Properties of Propellants," *High Temperatures-High Pressures, ETPC Proceedings*, Vol. 17, pgs. 429-435, (1985).

[49] Liau, Y. C., Yang, V., Lin M. C., and Park, J., "Analysis of Ammonium Dinitramide (ADN) Combustion with Detailed Chemistry," 35th JANNAF Combustion Meeting, CPIA No. 691, pgs. 13-30, (1999).

[50] Korobeinichev, O. P., Bolshova, T. A., and Paletsky, A. A., "Modeling the Chemical Reaction of Ammonium Dinitramide (ADN) in a Flame," Combustion and Flame, Vol. 126, pgs. 1516-1523, (2001).

[51] Ramakrishna, P. A., Paul, P. J., and Mukunda, H. S., "Revisiting the Modeling of Ammonium-Perchlorate Combustion: Development of an Unsteady Model," *Journal of Propulsion and Power*, Vol. 22, No. 3, pgs. 661-668, (2006).

[52] Rahman, S., Giovangigli, V., and Borie, V., "Application of Continuation Techniques to Pressure and Initial Temperature Sensitivity Coefficient Calculation in Ammonium Perchlorate Flames," *46th AIAA/ASME/SAE/ASEE Joint Propulsion Conference & Exhibit*, Nashville, TN, July (2010).

[53] Beckstead, M. W., "An Overview of Combustion Mechanisms and Flame Structures of Advanced Solid Propellants," *AIAA 2000-3325*, pgs. 267-286, (2000).

[54] Ermolin, N. E., Korobeinichev, O. P., Fomin, V. M., and Chernov, A. A., "Study of Flame Structure for Mixed Solid Fuels Based on Ammonium Perchlorate and Polybutadiene Rubber," *Combustion, Explosion, and Shockwave,* Vol. 28, No. 4, pgs. 59-65, (1992).

[55] Ermolin, N. E., "Kinetic Perameters of Overall Gas-Phase Reactions for Propellants Based on Ammonium Perchlorate and Polybutadiene Binder," *Combustion, Explosion, and Shockwave,* Vol. 29, No. 4, pgs. 97-104, (1993).

[56] Chorpening, B. T., G. M. Knott, and M. Q. Brewster, "Flame Structure and Burning Rate of Ammonium Perchlorate/Hydroxyl-Terminated Polybutadiene Propellant Sandwiches," *Proceedings of The Combustion Institute,* 28:1, pgs. 847-853, (2000).

[57] Knott, G. M. and M. Q. Brewster, "Modeling the Combustion of Propellant Sandwiches," *Combustion Science and Technology*, 174, pgs. 61-90, (2002).

[58] Meyer, R., "Explosives," *3rd ed. VCH Publishers*, New York, pg. 357, (1986).

[59] Arisawa, H., and Brill, T. B., "Flash Pyrolysis of Hydroxyl-Terminated Polybutadiene (HTPB) I: Analysis and Implications of the Gaseous Products," *Combustion and Flame*, Vol. 106, pgs. 131-143, (1996).

[60] Stephens, H. L., "Physical Constants of Poly(butadiene)," *Polymer Handbook, 3rd Ed.*, John Wiley & Sons, New York, (1989).

[61] Foster, R. L., and Miller, R. R., "The Burn Rate Temperature Sensitivity of Aluminized and Non-Aluminized HTPB Propellants," *1980 JANNAF Propulsion Meeting*, CPIA #315, Vol. 4, pgs. 667-693, (1981).

[62] Tanner, M. W., "Multidimensional modeling of Solid Propellant Burning Rates and Aluminum Agglomeration and One-Dimensional Modeling of RDX/GAP and AP/HTPB." *PhD Dissertation, Brigham Young University*, (2008).

[63] Foster, R. L., Condon, J. A., and Miller, R. R., "Low Exponent Technology," *Hercules Report, AFRPL-TR-81-95*, Hercules Inc., Air Force Rocket Propulsion Laboratory, Edwards AFB, CA, (1982).

[64] JANNAF Thermochemical Tables, 3rd Edition, Journal of Physical and chemical Reference Data, Vol. 14, (1985).

[65] Atwood, A. I., Ford, K. P., Bui, D. T., Curran, P. O., and Lyle, T., "Radiant Ignition Studies of Ammonium Perchlorate Based Propellants," *2nd EUCASS*, Brussels, Belgium, July (2007).

[66] Hermance, C. E., "Solid-Propellant Ignition Theories and Experiments," *Fundamentals of Solid Propellant Combustion*, Vol. 90, pgs. 239-304, (1984).

[67] Vilyunov, V. N., and Zarko, V. E., *Ignition of Solids*, Vol. 60, Elsevier, (1989).

[68] Vilyunov, V. N., Vorozhtsov, A. B., Borovskoi, I. G., and Shelupanov, A. A., "Ignition of Condensed Material," *Combustion, Explosion & Shockwave*, Vol. 24, No. 3, pgs. 39-41, (1988).

[69] Dik, I. G., Zurer, A. B., and Knyazeva, A. G., "Ignition of Condensed Material by a Heat Flux Pulse Across an Opaque Shield Having a High Thermal Conductivity," *Combustion, Explosion & Shock Waves*, Vol. 25, No. 6, pgs. 3-9, (1989).

[70] Knyazeva, A. G. and Dik, I. G., "Ignition of a Hot Sheet of Condensed Material Through an Inert Shield," *Combustion, Explosion & Shock Waves*, Vol. 26, No. 2, pgs. 8-18, (1990).

[71] Zarko, V. E., "Stability of Ignition of Condensed Substances," *Combustion, Explosion, and Shockwave,* Vol. 26, No. 6, pgs. 3-16, (1990).

[72] Colombier, R., and Pollet, M., "Solid Rocket Motor Ignition Overpressure Prediction", *27th Joint Propulsion Conference, Sacramento, CA*, (1991).

[73] Wooldridge, R. C., and Netzer, D. W., "Ignition and Flammability Characteristics of Solid Fuel Ramjets", *Journal of Propulsion*, Vol. 7, No. 5, pgs. 846-848, (1991).

[74] Gehris, R. D. and Price, C. F., "Ignition Modeling Program," *29th JANNAF Combustion Meeting*, Vol. IV, CPIA #595, pgs. 129-137, (1992).

[75] Lee, L. S., and Borgardt, F. G., "Ignition Transietn Phenomenology – A Programmatic Overview", *29th JANNAF Combustion Meeting, CPIA #595*, Vol. 4, pgs. 103-127, (1992).

[76] Tsai, C. Y., Reneau, L. R., and Schulze, P. A., "Numerical Simulation of Ignition Transients in Solid Rocket Motor", *30th JANNAF Combustion Meeting, Monterey, CA*, (1993).

[77] Eagar, M. A., Luke, G. D., and Stockham, L. W., "Ignition Transient Modelling for the Space Shuttle Advanced Solid Rocket Motor", *29th Joint Propulsion Conference and Exhibit*, Monterey, CA, (1993).

[78] Dik, I. G., and Selikhovkin, A. M., "Calculation of Ignition Parameters and the Transition to Compustion in a Heterogeneous System," *Combustion, Explosion, and Shockwave,* Vol. 29, No. 3, pgs. 124-129, (1993).

[79] Knyazeva, A. H., and Zarko, V. E., "Numerical Simulation of Transients in the Ignition of Two-component Propellants by Intense Heat Fluxes," *Combustion, Explosion, and Shockwave,* Vol. 29, No. 3, pgs. 16-20, (1993).

[80] Zarko, V. E., and Knyazeva, A. H., "Simulation of Ignition Transients for Two-component Solid Propellants under Irradiation, " *AIAA Journal*, Paper 94-0790, (1993).

[81] Huang, T. H., Thynell, S. T., and Kuo, K. K., "Partially Confined Hot Fragment Conductive Ignition: Part I-Modeling," *30th JANNAF Combustion Mtg.*, Vol. I, CPIA No. 606, pgs. 387-400, (1993).

[82] Yang, V. and Liau, Y. C., "A Time-Accurate Analysis of RDX Monopropellant Combustion with Detailed Chemistry," *32nd JANNAF Combustion Mtg.*, Vol. I, CPIA No. 631, pgs. 57-68, (1995).

[83] Liau, Y. C. and Yang, V., "Analysis of RDX Monopropellant Combustion with Two-Phase Subsurface Reactions," *J. Propulsion & Power*, Vol. 11, No. 4, pgs. 729-739, (1995).

[84] Liau, Y. C., Kim, E. S., and Yang, V., "A Comprehensive Analysis of Laser-Induced Ignition of RDX Monopropellant," *Combustion and Flame*, 126(3), pgs. 1680-1698, (2001).

[85] Atwood, A. I., Curran, P. O., Price, C. F., and Wiknich, J., "Burning Rate, Radiant Ignition and Global Kinetics of Cyclotrimethylene Trinitramine (RDX)," *32nd JANNAF Combustion Mtg. & Propellant Hazards Mtg*, Vol. I, CPIA No. 638, pgs. 149-159, (1995).

[86] Parr, T., and Hanson-Parr, D., "RDX Ignition Flame Structure," *27th Symposium (Int'l) on Combustion*, The Combustion Institute, pgs. 2301-2308, (1998).

[87] Atwood, A. I., Price, C. F., Boggs, T. L., Curran, P. O., and Zwierzchowski, N. G., "Ignition and Combustion Properties of Ammonium Perchlorate," *1990 JANNAF PSHS Meeting*, Laurel, Maryland, March (1990).

[88] Atwood, A. I., Price, C. F., and Boggs, T. L., "Ignitability Measurements of Solid Propellants," *Proceedings of the 22nd Annual Conference of ICT*, Karlsruhe, Germany, (1991).

[89] Waeshe, R. H. W., and Wenograd, J., "Calculation of Solid-Propellant Burning Rates from condensed-phase Decomposition Kinetics," *Combustion, Explosion, and Shock Waves*, Vol. 36, No. 1, pgs. 138-148, (2000).

[90] Jojic, I., and Brewster, M. Q., "Condensed-phase Chemical Interaction between Ammonium Perchlorate and Hydroxy-terminated Polybutadiene," *Journal of Propulsion and Power*, Vol. 14, No. 4, pgs. 575-576, (1998).

[91] Shannon, L. J., "Composite Solid-Propellant Ignition by Radiant Energy," *AIAA Journal*, Vol. 8, No. 2, pgs. 346-353, (1970).

[92] Sofue, T., and Iwama, A., "Ignition of Composite Propellant at Sub-atmospheric Pressures by means of a Carbon Dioxide Laser," *Propellants and Explosives*, Vol. 4, pgs. 98-106, (1979).

[93] Ahmad S. R., and Russell D. A., "Studies into Laser Ignition of Unconfined Propellants," *Propellants, Explosives, Pyrotechnics*, Vol. 26, pgs. 235-245, (2001).

[94] Cain, J., and Brewster, M. Q., "Radiative Ignition of Fine-Ammonium Perchlorate Composite Propellants," *Propellants, Explosives, Pyrotechnics*, Vol. 31, No. 4, pgs. 278-284, (2006).

[95] Meredith, K. V., and Beckstead, M. W., "Laser-Induced Ignition Modeling of HMX", 2003 JANNAF Combustion Meeting, Boulder, CO, pgs. 1-22, (2003).

[96] Brill, T. B., "Multiphase Chemistry Considerations at the Surface of Burning Nitramine Monopropellants," *J. Propulsion & Power*, Vol. 11, No. 4, pgs. 740-751, (1995).

[97] Kubota, N., "Survey of Rocket Propellant and Their Combustion Characteristics," *Fundamentals of Solid-Propellant Combustion*, Progress in Astronautics and Aeronautics, Vol. 90, pgs. 1-52, (1984).

[98] Hall, P. G., "Thermal Decomposition and Phase Transitions in Solid NItramines," *Transactions of the Faraday Society*, Vol. 2, pgs. 79-102, (1971).

[99] Isbell, R. A. and Brewster, M. Q., "Optical Properties of RDX and HMX," *Material Research Society Symposium Proceedings*, 418, edited by Brill, T. B. *et al.*, pgs. 850-90, (1996).

[100] Liau, Y. C. and Lyman, J. L., "Modeling Laser-Induced Ignition of Nitramine Propellants with Condensed and Gas-Phase Absorption," *Combust. Sci. and Tech.* Vol. 174, No. 3, pgs. 141-171, (2002).

[101] Erikson, W. W. and Beckstead, M. W., "Modeling Pressure and Heat Flux Responses of Nitramine Monopropellants with Detailed Chemistry," Vol. AIAA 99-2498, (1999).

[102] Balay, S., Gropp, W. D., McInnes, L. C., and Smith, B. F., "PETSc Home Page," *http://www.mcs.anl.gov/petsc/petsc-as*, (1998).

[103] Kee, R. J., Rupley, F. M., and Miller, J. A., SAND87-8215B, Sandia National Laboratories, (1992).

[104] Ali, A. N., Son, S. F., Asay, B. W., Sander, R. K., and Brewster, M. Q., "Laser Ignition of High Explosives," *36th JANNAF Combust. Subcomm. Mtg*. Vol. I, CPIA No. 691, pgs. 51-67, (1999).

[105] Creighton, J. R., "The Variation of the Ignition Temperature of Solid Explosives as a Function of Heating Rate," *JANNAF Propulsion Systems Hazards Subcommittee Meeting, CPIA No. 599*, pgs. 473-482, (1993).

[106] Hobbs, M. L., Baer, M. R., and Gross, R. J., "Modeling ignition chemistry," *JANNAF Systems Hazards Meeting*, pgs. 1-10, (1993).

[107] Baer, M. R., Gross, R. J., Gartling, D. K., and Hobbs, M. L., "Multidimensional Thermal-Chemical Cookoff Modeling," *1994 JANNAF Propulsion Systems Hazards Meeting*, CPIA No. 615, pgs. 323-332, (1994).

[108] Erikson, W. W., and Schmitt, R. G., "Coupled Thermal-Chemical-Mechanical Modeling of Validation Cookoff Experiments", *50th JANNAF Propulsion meeting, Salt Lake City, Utah*, (2001).

[109] Erikson, W. W., and Schmitt, R. G., "Pre- and Post-ignition Modeling of Validation Cookoff Experiments", *38th JANNAF CS, 26th APS, 20th PSHS, and 2nd MSS Joint Meeting, Destin, FL*, (2002).

[110] Erikson, W. W., and Schmitt, R. G., "Modeling Thermal Decomposition and Deflagration in Small- and Munition-Scale Navy Coook-off Experiments", *21st JANNAF PSHS Meeting*, CD-ROM ONLY, (2003).

[111] Atwood, A. I., Curran, P. O. Erikson, W. W., Heimdahl, O. E. R., McClelland, M. A., and Rattanapote, M. K., "Full-Scale Cookoff Model Validation Experiments", *21st JANNAF PSHS Meeting*, CD-ROM ONLY, December (2003).

[112] Beckstead, M. W. and Hendershot, R. J., "Calculated Conditions for Fast Cookoff," *36th JANNAF Combustion Meeting*, CPIA #691, Vol I, pgs. 123-132, (1999).

[113] Ciro, W., Eddings, E. G., and Sarofim, A., "Thermal Behavior of a High-Energy Material Immersed in a Fire," *Proceedings of the Third Joint Meeting of the U.S. Sections of the Combustion Institute,* Chicago, IL, (2003).

[114] Ford, K. P, Davis, N. C., Farmer, A. D., Washburn, E. B., Atwood, A. I., Wilson, K. J., Abshire, J. P., Shewmaker, M. L., Goedert, Z. P., Wheeler, C. J., Curran, P. O., and Covino, J., "Subscale External Fire/Fast Cookoff Testing Results," *2008 DDESB Seminar Proceedings*, (2009).

[115] Wilson, E., Gross, M., Washburn, E., *et al.*, "Cookoff Results of Sub-scale Hazard Division 1.3 Propellant Samples," *34th DoD Explosive Safety Board Seminar*, Portland, Oregon, pgs. 1-46, (2010).

[116] Washburn, E., Walpole, M., Ford, K., Wilson, E., Atwood, A., Bowman, H., Boggs, T., Homer, V., Sawyer, L., and Covino, J., "Ignition of Energetic materials from Heat Fluxes Found in Hazard Situations," *33nd Explosives Safety Seminar*, Palm Springs, CA, August 12-14, (2008).

[117] Reaction Design, *www.reactiondesign.com*, (2003).

[118] Goodwin, D. G., *www.cantera.org*, California Institute of Technology, (2006).

[119] Behrens Jr., R., and Bulusu, S., "Thermal Decomposition of Energetic Materials. 3. Temporal Behaviors of the Rates of Formation of the Gaseous Pyrolysis Products from Condensed-

Phase Decomposition of 1,3,5-Trinitrohexahydro-s-triazine," *Journal of Physical Chemistry*, Vol. 96, pgs. 8877-8891, (1992).

[120] Maxwell, J. C., "A Treatise on Electricity and Magnetism," Vol. 1, 3rd ed., *Oxford University Press*, (1904).

[121] Bohren, C. F., and Huffman, D. R., "Absorption and Scattering of Light by Small Particles," *John Wiley & Sons, Inc.*, (1983).

[122] http://code.google.com/p/scatterlib, (2011)

[123] Parr, T., and Hanson-Parr, D., "Thermal Properties Measurements of Solid Rocket Propellant Oxidizers and Binder Materials as a Function of Temperature," *34th JANNAF Combustion Meeting*, Vol. 3, CPIA #662, pgs. 379-404, (1997).

[124] Zhu, R. S., and Lin, M. C., "Towards Reliable Prediction of Kinetics and Mechanisms for Elementary Reactions: Key Combustion Initiation Processes of Ammonium Perchlorate", *Energetic Materials, Part 2, Detonation and Combustion*, P. Politzer and J. S. Murray, eds. chp. 11, pgs. 373-443, Elsevier Science Pub., (2003).

[125] Lin, M. C., *http://chemistry.emory.edu/faculty/lin/pub.htm*, Department of Chemistry, Emory University, (2011).

[126] Levy, J. B., and Friedman, R.,"Further Studies of Pure Ammonium Perchlorate Deflagration," *International Symposium on Combustion*, Vol. 8, No. 1, pgs. 663-672, (1961).

[127] Hertzberg, M., "The Combustion of Pure and Composite Propellants. The Expansion and Application of Laminar Flame Theory to Heterogeneous Solid Propellants," *Oxidation and Combustion Reviews*, Vol. 5, pgs. 1-81, (1971).

[128] Pellett, G. L., "Ammonium Perchlorate Gasification and Combustion at High Heating Rates and Low Pressures," *International Symposium on Combustion*, Vol. 14, Iss 1, pgs. 1317-1330, (1973).

[129] Schroeder, T. B., and Brewster, M. Q., "Steady and Unsteady Laser Augmented Combustion of Ammonium Perchlorate and Atmospheric Conditions," *30th JANNAF Combustion Meeting*, Vol. 1, CPIA No. 6, pgs. 327-336, (1993).

[130] Tereshchenko, A. G., and Korobeinichev, O. P., "Correctness of Mass-Spectrometric Probe Measurements when Investigating the Flame Structure of Condensed Systems," *Combustion, Explosion, and Shock Waves*, Vol. 18, No. 6, pgs. 39-45, (1982).

[131] Vyazovkin, S., and Wight, C. A., "Kinetics of Thermal Decomposition of Cubic Ammonium Perchlorate," *Chemistry of Materials*, Vol. 11, pgs. 3386-3393, (1999).

[132] Brill, T. B., Brush, P. J., and Patil, D. G., "Thermal Decomposition of Energetic Materials 60. Major Reaction Stages of a Simulated Burning Surface of NH_4ClO_4," *Combustion and Flame*, Vol. 94, pgs. 70-76, (1993).

[133] Korobeinichev, O. P., "Dynamic Flame Probe Mass Spectrometry and Condensed-System Decomposition," *Combustion, Explosion, and Shock Waves*, Vol. 23, No. 5, pgs. 64-76, (1987).

[134] Ermolin, N. E., Korobeinichev, O. P., Tereshchenko, A. G., and Fomin, V. M., "Simulation of Kinetics and Chemical Reaction Mechanism of Ammonium Perchlorate Burning," *Soviet Journal of Chemical Physics*, Vol. 1, Iss. 12, pgs. 2872-2883, (1984).

[135] JMP 9.0, *<www.jmp.com>*, SAS Institute Inc., (2009).

[136] Zhu, R., and Lin M. C., "Mechansim and Kinetics for Ammonium Perchlorate Sublimation: A First Principles Study," *Journal of Physical Chemistry C*, Vol 112, pgs. 14481-14485, (2008).

[137] Longuet, B., and Gillard, P., "Experimental Investigation of the Heterogeneous Kinetic Process of the Low Thermal Decomposition of Ammonium Perchlorate Particles," *Propellants, Explosives, and Pyrotechnics*, Vol. 34, pgs. 59-71, (2009).

[138] Ermolin, N. E., "Model for Chemical Reaction Kinetics in Perchloric Acid – Ammonia Flames," *Combustion, Explosion, and Shock Waves*, Vol. 31, No. 5, pgs. 555-565, (1995).

[139] Powling, J., "Experiments Relating to the Combustion of Ammonium Perchlorate-Based Propellants," *International Symposium on Combustion*, Vol 11, pgs. 447-456, (1967).

[140] Beckstead, M. W., and Hightower, J. D., "Surface Temperature of Deflagrating Ammonium Perchlorate Crystals," *AIAA Journal*, Vol. 5, No. 10, pgs. 1785-1790, (1967).

[141] Bakhman, N. N., Kickin, YU. S., Kolyasov, S. M., and Fogelzang, A. E., "Investigation of the Thermal Sturcture of the Burning Zone in Condensed Mixtures by Fine Thermocouples," *Combustion and Flame*, Vol 26, pgs. 235-247, (1976).

[142] Korobeinichev, O. P., Zenin, A. A., Tereshchenko, A. G., and Puchkov, V. M., "Investigation of the Structure of the Combustion Wave of Mixed Systems Based on APC, PMMA, and a Catalyst using Mass-spectrometric and Thermocouple Methods," *Combustion, Explosion, and Shock Waves*, Vol. 13, No. 3, pgs. 335-342, (1977).

[143] McAlevy III, R. F., Cowan, P. L., Summerfield, M., "The Mechanism of Ignition of Composite Solid Propellants by Hot Gases," *Progress in Astronautics and Rocketry*, Vol. 1, pgs. 623-652, (1960).

[144] Isbell, R. A., and Brewster, M. Q., "Optical Properties of Energetic Materials: RDX, HMX, AP, NC/NG, and HTPB," *Propellants, Explosives, Pyrotechnics*, Vol 23., pgs. 218-224, (1998).

[145] Loner, P. S., and Brewster, M. Q., "On the oscillatory laser-augmented combustion of HMX," *Proceedings of the 34th JANNAF Combustion Subcommittee Meeting*, Vol. 2, CPIA, Pub. 662, pgs. 47-60, (1997).

[146] Hanson-Parr, D., and Parr, T., "RDX Laser-Assisted Flame Structure," *31st JANNAF combustion Meeting*, Vol. 2, CPIA 620, pgs. 407-423, (1994).

[147] Hanson-Parr, D., and Parr, T., "RDX Flame Structure," *25th Symposium (International) on Combustion*, pgs. 1635-1643, (1994).

[148] Korobeinichev, O. P., Chernox, A. A., Emel'yanov, I. D., Ermolin, N. E., and Trofimycheva, T. V., "Investigation of the Kinetics and the Chemical reaction Mechanism in the Flame of a Mixed Compound, Based on Ammonium Perchlorate and Polybutadiene Rubber," *Combustion, Explosion, and Shock Waves*, Vol. 26, No. 3, pgs. 292-300, (1989).

[149] Godai, T. and Shimizu, M., "Pressure exponent of controllable solid rocket propellants," *Proceedings of AIAA/SAE 8th Joint Propulsion Specialist Conference*, AIAA Paper 72-1135, New Orleans, Louisiana, (1972).

[150] Sutton, G. P., "*Rocket Propulsion Elements, Sixth Edition*," John Wiley & Sons., 1992.

[151] Kohga, M., "Burning Characteristics and Thermochemical Behavior of AP/HTPB Composite Propellant Using Coarse and Fine AP Particles," *Propellants, Explosives, and Pyrotechnics*, Vol.36, pgs. 57-64, (2011).

[152] Foster, R. L., Condon, J. A., and Miller R. R., "Low Exponent Technology," *Hercules Report*, *AFRPL-TR-81-95*, Hercules Inc., Air Force Rocket Propulsion Laboratory, Edwards AFB, CA, (1982).

[153] Son, S. F., and Brewster, M. Q., "Radiation-Augmented Combustion of Homogeneous Solids," *Combustion Science and Technology*, Vol. 107, pgs. 127-154, (1995).

[154] Fitzgerald, R. P., and Brewster, M. Q., "Flame and Surface Structure of Laminate Propellants with Coarse and Fine Ammonium Perchlorate," *Combustion and Flame*, Vol. 136, No. 3, pgs. 313-326, (2004).

[155] Rasmussen, B., and Frederick, R. A. Jr., "Nonlinear Hereogeneous Model of Composite Solid-Propellant Combustion," *Journal of Propulsion and Power*, Vol. 18, No. 5, pgs. 1086-1092, (2002).

[156] Bellec, R., Duterque, J., and Lengelle, G., "Modeling of Aluminized Solid Propellants," *ONERA, Technical Report RT 37/7128 EN*, Palaiseau, France, (1996).

[157] Cohen-Nir, E., "Temperature Sensitivity of the Burning Rate of Composite Solid Propellants," *Combustion Science and Technology*, Vol. 9, pgs. 183-194, (1974).

[158] Foster, R.L. and R.R. Miller, "The Burn Rate Temperature Sensitivity of Aluminized and Non-Aluminized HTPB Propellants," *1980 JANNAF Propulsion Meeting*, CPIA #315, Vol. IV, pgs. 667-693, (1981).

[159] Kubota, N., and Miyazaki, S., "Temperature Sensitivity of Burning Rate of Ammonium Perchlorate Propellants," *Propellants, Explosives, Pyrotechnics*, Vol. 12, pgs. 183-187, (1987).

[160] Korobeinichev, N. E., Ermolin, N. E., Chernov, A. A., and Emel'yanov I. D., "Flame Structure, Kinetics and Mechanism of Chemical Reactions in Flames of Mixed Composition Based on Ammonium Perchlorate and Polybutadiene Rubber," *Combustion, Explosion, and Shock Waves*, Vol. 28, No. 4, pgs. 366-371, (1992).

[161] Atwood, A. I., *personal communication*, (2008).

[162] Osman, M. B. S., Dakroury, A. Z., Dessouky, M. T., Kenawy, M. A., and El-Sharkawy, A. A., "Measurement of Thermophysical Properties of Ammonium Salts in the Solid and Molten States," *Journal of Thermal Analysis*, Vol. 46, pgs. 1697-1703, (1996).

[163] Atwood, A. I., Boggs, T. L., Curran, P. O., Parr, T. P., Hanson-Parr, D. M., Price, C. F., and Wiknich, J., "Burning Rate of Solid Propellant Ingredients, Part 1: Pressure and Initial Temperature Effects," *Journal of Propulsion and Power*, Vol. 15, No. 6, pgs. 740-747, Nov-Dec (1999).

[164] Ross, S. D., "Forbidden Transitions in the Infrared Spectra of Some Tetrahedral Anions – I. Perchlorates," *Spectrochimica Acta*, Vol. 18, pgs. 225-228, (1962).

[165] Maycock, J. N., Pai Vernecker, V. R., and Gorzynski Jr., C. S., "Electrical Conductivity of Ammonium Perchlorate," *Solid State Communications*, Vol. 5, pgs. 225-227, (1967).

[166] Owen, G. P., Thomas, J. M., and Williams, J. O., "Electrical Conduction in Ammonium Perchlorate," *Journal of the Chemical Society*, Faraday Transactions 1, Vol. 68, pgs. 2356-2366, (1972).

[167] Jacobs, P. W. M., Lovatt, F. E., and Ng, W. L., "Electrical Conductivity of Pure and Doped Ammonium Perchlorate Crystals," *Canadian Journal of Chemistry*, Vol. 50, No. 19, pgs. 3154-3160, (1972).

[168] Ivashchenko, Yu. S., Sadyrin, A. L., and Pavlenko, V. L., "Electrical Conductivity of the Burning Surface of Ammonium Perchlorate, " *Combustion, Explosion, and Shock Waves*, Vol, 2. No. 4, pgs. 414-416, (1986).

[169] Yang, V., Brill, T. B., and Ren, W. Z., "Flash Pyrolysis of Ammonium Perchlorate-Hydroxyl-Terminated-Polybutadiene Mixtures Including Selected Additives," *Solid Propellant Chemistry, Combustion, and Motor Interior Ballistics*, Chapter 1.1, Progress in Astronautics and Aeronautics, Vol. 185, pgs. 3-32, (2000).

[170] Beckstead, M. W., *personal communication*, (2011).

[171] Eagar, M. A., Luke, G. D., and Stockham, L. W., "Ignition Transient Modeling for the Space Shuttle Advanced Solid Rocket Motor," *29th Joint Propulsion Conference*, AIAA 93-2062, Monterey, CA, pgs. 1-11, (1993).

[172] Jojic, I., and Brewster, M. Q., "Condensed-Phase Chemical Interaction Between Ammonium Perchlorate and Hydroxy-Terminated Polybutadiene," *Journal of Propulsion and Power*, Vol. 14, No. 4, pgs. 575-576, (1998).

[173] Ahmad, S. R., and Russell, D. A., "Studies into Laser Ignition of Unconfined Propellants," *Propellants, Explosives, Pyrotechnics*, Vol. 26, pgs. 235-245, (2001).

[174] Kimura, E., and Oyumi, Y., "Shock ignitability test for azide polymer propellants," *Journal of Energetic Materials*, Vol. 16, pgs. 173–186, (1998).

[175] Zanotti, C., and Galfetti L., "Experimental and Numerical Study of Ignition Transients of Solid Propellants," *Flame structure* (Ed. O.P. Korobeinichev), Novosibirst, Nauka, Vol. 2, pgs. 393-396, (1991).

[176] Atwood, A. I., Price, C. F., and Boggs, T. L., "A Comparison of Radiant Ignition and Ballistic Impact Chamber Results, " *1992 JANNAF PSHS Mtg.*, pgs. 1-17, (1992).

[177] Cocchiaro, J. E., "Subscale Fast Cookoff Testing and Modeling for the Hazard Assessment of Large Rocket Motors," *Chemical Propulsion Information Agency,* CPTR-72, (2001).

[178] Lengelle, G., Bizot, A., Duterque, J., and Amiot, J., "Ignition of Solid Propellants," *Rech. Aerosp.*, Vol. 2, pp. 1-20, (1991).

[179] Najm, H. N., Wyckoff, P. S., and Knio, O. M., "A Semi-implicit Numerical Scheme for Reacting Flow," *Journal of Computational Physics*, Vol. 143, pgs. 381-402, (1998).

[180] Najm, H. N., and Knio, O. M., "Modeling Low Mach Number Reacting Flow with Detailed Chemistry and Transport," *Journal of Scientific Computing*, Vol. 25, Nos. 1&2, pgs. 263-287, (2005).

[181] Singer, M. A., and Pope, S. B., "Exploiting ISAT to solve the reaction-diffusion equation," *Combustion Theory and Modeling*, Vol. 8, pgs. 361-383, (2004).

[182] Pope, S.B., and Ren, Z. "Efficient Implementation of Chemistry in Computational Combustion," *Flow Turbulence Combustion*, Vol. 82, pgs. 437-453, (2009).